

การเพิ่มความเสถียรของฟิล์มบางพอลิไธรีนโดยการเติมโมเลกุลแอมโมเนียมมากกิ่ง
พอลิไธรีนสามแขนและอนุภาคโลหะออกไซด์ระดับนาโนเมตร

นางสาวน้ำผึ้ง ผึ้งไพบูลย์

วิทยานิพนธ์นี้เป็นส่วนหนึ่งของการศึกษาตามหลักสูตรปริญญาวิทยาศาสตรดุษฎีบัณฑิต

สาขาวิชาวัสดุศาสตร์ ภาควิชาวัสดุศาสตร์

คณะวิทยาศาสตร์ จุฬาลงกรณ์มหาวิทยาลัย

ปีการศึกษา 2556

ลิขสิทธิ์ของจุฬาลงกรณ์มหาวิทยาลัย

บทคัดย่อและแฟ้มข้อมูลฉบับเต็มของวิทยานิพนธ์ตั้งแต่ปีการศึกษา 2554 ที่ให้บริการในคลังปัญญาจุฬาฯ (CUIR)

เป็นแฟ้มข้อมูลของนิสิตเจ้าของวิทยานิพนธ์ที่ส่งผ่านทางบัณฑิตวิทยาลัย

The abstract and full text of theses from the academic year 2011 in Chulalongkorn University Intellectual Repository (CUIR)
are the thesis authors' files submitted through the Graduate School.

STABILITY ENHANCEMENT OF POLYSTYRENE THIN FILMS BY ADDING HIGHLY BRANCHED
AROMATIC MOLECULES, THREE-ARM POLYSTYRENE AND METAL OXIDE NANOPARTICLES

Miss Nampueng Pangpaiboon

A Dissertation Submitted in Partial Fulfillment of the Requirements
for the Degree of Doctor of Philosophy Program in Materials Science

Department of Materials Science

Faculty of Science

Chulalongkorn University

Academic Year 2013

Copyright of Chulalongkorn University

Thesis Title	STABILITY ENHANCEMENT OF POLYSTYRENE THIN FILMS BY ADDING HIGHLY BRANCHED AROMATIC MOLECULES, THREE-ARM POLYSTYRENE AND METAL OXIDE NANOPARTICLES
By	Miss Nampueng Pangpaiboon
Field of Study	Materials Science
Thesis Advisor	Assistant Professor Nisanart Traiphol, Ph.D.
Thesis Co-advisor	Assistant Professor Rakchart Traiphol, Ph.D.

Accepted by the Faculty of Science, Chulalongkorn University in Partial Fulfillment of the Requirements for the Doctoral Degree

.....Dean of the Faculty of Science
(Professor Supot Hannongbua, Dr. rer. nat.)

THESIS COMMITTEE

.....Chairman
(Assistant Professor Sirithan Jiemsirilers, Ph.D.)

.....Thesis Advisor
(Assistant Professor Nisanart Traiphol, Ph.D.)

.....Thesis Co-advisor
(Assistant Professor Rakchart Traiphol, Ph.D.)

.....Examiner
(Assistant Professor Kanoktip Boonkerd, Ph.D.)

.....Examiner
(Assistant Professor Rojana Pornprasertsuk, Ph.D.)

.....External Examiner
(Assistant Professor Toemsak Srikhirin, Ph.D.)

น้ำผึ้ง ผังไพบูลย์ : การเพิ่มความเสถียรของฟิล์มบางพอลิสไตรีนโดยการเติมโมเลกุลแโรแมติกมากกิ่ง พอลิสไตรีนสามแขนและอนุภาคโลหะออกไซด์ระดับนาโนเมตร (STABILITY ENHANCEMENT OF POLYSTYRENE THIN FILMS BY ADDING HIGHLY BRANCHED AROMATIC MOLECULES, THREE-ARM POLYSTYRENE AND METAL OXIDE NANOPARTICLES) อ.ที่ปรึกษาวิทยานิพนธ์หลัก : ผศ.ดร.นิศานาถ ไตรผล, อ.ที่ปรึกษาวิทยานิพนธ์ร่วม : ผศ.ดร.รัชชาติ ไตรผล, 105 หน้า

งานวิจัยนี้ศึกษาการเพิ่มความเสถียรของฟิล์มบางพอลิเมอร์โดยการเติม โมเลกุลแโรแมติกมากกิ่ง พอลิสไตรีนสามแขนและอนุภาคโลหะออกไซด์ระดับนาโน สารเติมแต่งที่ใช้ได้แก่ โมเลกุลแโรแมติกมากกิ่งซึ่งสังเคราะห์ขึ้นมาใหม่ โดยประกอบไปด้วยสายโซ่ที่ไม่มีความเป็นขั้วและแกนโครงสร้างที่มีความเป็นขั้ว พอลิสไตรีนสามแขนซึ่งมีสายโซ่กิ่งและค่าพลังงานพื้นผิวใกล้เคียงกับพอลิเมอร์เมทริกซ์ และอนุภาคโลหะออกไซด์ระดับนาโนเมตร คือ ไทเทเนียมไดออกไซด์และซิงก์ออกไซด์ พอลิเมอร์เมทริกซ์ที่ใช้ในงานนี้ได้แก่ พอลิสไตรีนที่มีน้ำหนักโมเลกุลแตกต่างกัน ปฏิกิริยาการยับยั้งการ dewetting สามารถติดตามได้โดยให้ความร้อนแก่ฟิล์มในหม้ออบสุญญากาศที่เวลาแตกต่างกัน จากนั้นศึกษาลักษณะพื้นผิวของฟิล์มโดยใช้กล้องจุลทรรศน์แรงอะตอมและกล้องจุลทรรศน์แบบใช้แสง และคำนวณพื้นที่ที่เกิด dewetting ที่ระยะเวลาในการให้ความร้อนต่างๆ จากการศึกษาพบว่า สารเติมแต่งโมเลกุลแโรแมติกมากกิ่ง พอลิสไตรีนสามแขนและอนุภาคโลหะออกไซด์ระดับนาโนเมตรเพิ่มความเสถียรของฟิล์มบางพอลิสไตรีนได้เป็นอย่างมาก นอกจากนี้ยังพบว่าปริมาณของสารเติมแต่ง น้ำหนักโมเลกุลของพอลิเมอร์เมทริกซ์ และความหนาของฟิล์มมีอิทธิพลต่อความเสถียรของฟิล์ม งานวิจัยนี้ได้อภิปรายถึงกลไกในการยับยั้งการ dewetting ของฟิล์มบางพอลิเมอร์ที่เติมสารเติมแต่งด้วยเช่นกัน

ภาควิชา...วัสดุศาสตร์..... ลายมือชื่อนิสิต.....
 สาขาวิชา...วัสดุศาสตร์..... ลายมือชื่อ อ.ที่ปรึกษาวิทยานิพนธ์หลัก.....
 ปีการศึกษา ...2556..... ลายมือชื่อ อ.ที่ปรึกษาวิทยานิพนธ์ร่วม.....

5173824323: MAJOR MATERIALS SCIENCE

KEY WORD: DEWETTING / FILM STABILITY / POLYMER THIN FILM

NAMPUENG PANGPAIBOON : STABILITY ENHANCEMENT OF POLYSTYRENE THIN FILMS BY ADDING HIGHLY BRANCHED AROMATIC MOLECULES, THREE-ARM POLYSTYRENE AND METAL OXIDE NANOPARTICLES. ADVISOR : ASST.PROF.NISANART TRAIIPHOL, Ph.D., CO-ADVISOR : ASST.PROF.RAKCHAT TRAIIPHOL, Ph.D., 105 pp

This study investigates the increasing of polymeric thin film stability via adding the highly branched aromatic molecules, three-arm polystyrene and metal oxide nanoparticles. The additive include novel synthesized highly branched aromatic molecules consisting of non-polar side chains and polar cores, three-arm polystyrenes with similar branch chain and surface energy to the polymer matrix, and two metal oxide nanoparticles i.e., titanium dioxide and zinc oxide. Polystyrenes with various molecular weight are used as polymer matrix in this study. The dewetting retardation phenomenon is followed by annealing the films in vacuum oven for different periods of time and examining the film morphology evolutions by using atomic force microscope and optical microscope. Then, dewetting area as a function of annealing time is calculated. It is found that the presence of the highly branched aromatic molecules, three-arm polystyrene and the inorganic nanoparticles considerably increase the stability of the polystyrene thin films. In addition, additive concentration, molecular weight of polymer matrix, and film thickness are found to affect stability of thin films. Mechanisms of dewetting suppression in the polymeric thin film containing these additives are also discussed in this research.

Department: ...Materials Science.....Student's Signature.....

Field of Study: ...Materials Science.....Advisor's Signature.....

Academic Year: ...2013.....Co-advisor's Signature.....

ACKNOWLEDGEMENTS

Firstly, I would like to express my sincere thanks to my advisor, Asst. Prof. Dr. Nisanart Traiphol and my co-advisor, Asst. Prof. Dr. Rakchart Traiphol for support and guidance throughout my Ph.D. study at Chulalongkorn University

I would like to thank the chairman, Asst. Prof. Dr. Sirithan Jiemsirilern and other committee members, Asst. Prof. Dr. Kanoktip Boonkerd, Asst. Prof. Dr. Rojana Pornprasertsuk and Asst. Prof. Dr. Toemsak Srihirin for many valuable comments and their perceptive suggestions.

I would like to acknowledge Prof. Dr. Dvora Perahia, who has kindly given me very useful suggestion and valuable opportunity to use necessary reserch facilities in her laboratory at the Department of Chemistry, Clemson University, USA.

I would like to thank Research Unit of Advanced Ceramics, Department of Materials Science, Faculty of Science, Chulalongkorn University, Thailand for the use of the facility, NANOTEC Center of Excellence at Mahidol University, Thailand for supporting the AFM facility.

I would like to gratefully acknowledge the Office of the Higher Education Commission (the program Strategic Scholarships for Frontier Research Network for the Join Ph.D. Program Thai Doctoral degree) for my scholarship. The appreciation extends to National Nanotechnology Center (NANOTEC), the National Science and Technology Development Agency (NTSDA) (Project P-10-10589), and Center of Excellence on Petrochemical and Materials Technology, Chulalongkorn University, Bangkok, Thailand for research fundings.

I would like to thank staff members and my colleagues in Department of Materials Science, Faculty of Science, Chulalongkorn University, Thailand for their support, friendship and encouragement.

Finally, I am eternally grateful to my family and my friends for their support and encouragement throughout my life.

CONTENTS

	Page
ABSTRACT (THAI)	iv
ABSTRACT (ENGLISH)	v
ACKNOWLEDGEMENTS	vi
CONTENTS	vii
LIST OF TABLES	x
LIST OF FIGURES	xi
CHAPTER I INTRODUCTION.....	1
CHAPTER II LITERATURE REVIEW	6
2.1 THEORETICAL BACKGROUND	6
2.1.1 DEWETTING IN POLYMER FILM	6
2.1.2 MECHANISMS OF DEWETTING	8
2.1.3 KINETICS OF DEWETTING	9
2.2 INHIBITION OF DEWETTING.....	10
2.2.1 DEWETTING INHIBITION BY CHEMICAL MODIFICATION	11
2.2.2 DEWETTING INHIBITION BY POLYMER CROSS-LINKING	16
2.2.3 DEWETTING INHIBITION BY ADDITIVE ADDITION.....	18
2.2.4 DEWETTING INHIBITION BY PHASE SEPARATION.....	23
CHAPTER III METHODOLOGY.....	26
3.1 OPTICAL MICROSCOPY	26
3.2 ATOMIC FORCE MICROSCOPY.....	28
3.2.1 CONTACT MODE.....	30
3.2.2 TAPPING MODE.....	30
3.2.3 NON-CONTACT MODE.....	30

	Page
3.3 CONTACT ANGLE AND SURFACE TENSION MEASUREMENT	32
3.3.1 CONTACT ANGLE MEASUREMENT	32
3.3.2 CALCULATION OF SURFACE TENSION	33
3.4 MEASUREMENT OF FILM THICKNESS BY ELLIPSOMETRY	35
3.5 PARTICLE SIZE DISTRIBUTION BY LIGHT SCATTERING	37
3.5.1 STATIC LIGHT SCATTERING	37
3.5.2 DYNAMIC LIGHT SCATTERING	38
3.5.3 ZETA POTENTIAL MEASUREMENT	39
3.6 TRANSMISSION ELECTRON MICROSCOPY	40
CHAPTER IV EXPERIMENTAL PROCEDURE	43
4.1 MATERIALS	43
4.1.1 POLYSTYRENE MATRIX	43
4.1.2 POLYMER ADDITIVES	44
4.1.2.1 HIGHLY BRANCHED AROMATIC MOLECULES	44
4.1.2.2 THREE-ARM POLYSTYRENE ADDITIVES	45
4.1.3 NANOPARTICLE ADDITIVES	46
4.2 THIN FILM PREPARATION	48
4.3 THIN FILM CHARACTERIZATION	49
4.3.1 SURFACE ENERGY	49
4.3.2 SURFACE TOPOGRAPHY	50
4.4 EXPERIMENTAL DIAGRAM	51
CHAPTER V RESULTS AND DISCUSSIONS	52
5.1 HIGHLY BRANCHED AROMATIC MOLECULES	52
5.1.1 EFFECT OF HBA1 IN PS11K FILMS	53
5.1.2 EFFECT OF FILM THICKNESS	58

	Page
5.1.3 EFFECT OF PS MOLECULAR WEIGHT	61
5.1.4 EFFECT OF HBA STRUCTURE	64
5.2 THREE-ARM POLYSTYRENE	67
5.2.1 EFFECT OF TA-PS19 IN PS11K FILMS.....	68
5.2.2 EFFECT OF MOLECULAR WEIGHT OF TA-PS BRANCH	71
5.2.3 EFFECT OF FILM THICKNESS.....	75
5.3 EFFECTS OF NANOPARTICLES.....	80
5.3.1 TiO ₂ NANOPARTICLES	81
5.3.2 ZnO NANOPARTICLES	90
CHAPTER VI CONCLUSIONS	95
REFERENCES	97
BIOGRAPHY.....	105

LIST OF TABLES

	Page
Table 3.1 Probe position, force on tip, advantages and disadvantages of each AFM image modes	31
Table 4.1 Polystyrenes with various molecular weights were used as matrix.....	43
Table 4.2 Film Thickness of each concentration	48
Table 4.3 Contact angles of water and diiodomethane on different surfaces and their solid surface tension components calculated by using simultaneous equation of the Owens-Wendt-Kaelble approach.....	49
Table 5.1 Hole depth and hole width of 7 nm thick PS11K films containing different concentration of HBA1 annealed at 120 °C for 30 min	58
Table 5.2 Hole depth and hole width of 7 nm thick PS33K films containing different concentration of HBA1 annealed at 120 °C for 120 min	62

LIST OF FIGURES

	Page
Figure 1.1 Chemical structures of (a) hyperbranched polymer HBA1, (b) hyperbranched polymer HBA2., and (c) Schematic model of interaction between highly branched aromatic molecules, polystyrene, and substrate.....	3
Figure 1.2 (a) Chemical structure of three-arm polystyrene. (b) Schematic model of interaction between three-arm polystyrene, polystyrene, and substrate	4
Figure 1.3 Schematic model of interaction between nanoparticles, polystyrene, and substrate.....	4
Figure 2.1 The effective interface potential as a function of film thickness,	6
Figure 2.2 Model of three phase contact line, substrate, film, and air	7
Figure 2.3 Illustration of spinodal mechanism.....	8
Figure 2.4 Illustration of heterogeneous nucleation mechanism	9
Figure 2.5 Three states of dewetting process.....	10
Figure 2.6 Schematic model of thin films contains a chain brush at the surface	12
Figure 2.7 Schematic model of interface structures of polystyrene and APTES under various curing and precuring condition	13
Figure 2.8 Schematic model of (a) ω -barium sulfonato polystyrene and (b) α, ω -barium sulfonato polystyrene.....	14
Figure 2.9 Schematic model of surface anchoring of $-\text{CH}_2\text{Cl}$ group on SiO_x/Si surface.....	15

	Page
Figure 2.10 Schematic model of the distribution of $-\text{CH}_2\text{Cl}$ group in 22 and 45 nm thick film	15
Figure 2.11 Optical micrographs of 25 nm films after annealing overnight at 170 °C.....	17
Figure 2.12 Effects of degree of cross-linking to the partially cross-linked film rupture. (A) Optical micrographs show the number of holes when increasing UV exposure time in 45 nm films. (B) Density of holes per unit area (from top to bottom, UV exposure time are 1, 10, 20, 30 and 40 min). (C) Density of holes per unit area as a function of azide conversion	18
Figure 2.13 Optical micrograph of 50 nm films (a) pure polystyrene and (b) polystyrene with fullerene (mass fraction = 0.01).....	19
Figure 2.14 Plot between V_{eff} ($V_{\text{particle}}/V_{\text{PS}}$) vs R ($R_g/R_{\text{particles}}$) for both 10 nm diameter of Au particles and 3 nm diameter of Pd particles in difference molecular weight polystyrene matrices. The inset shows schematic model of filled system (a) $R > 1$ and (b) $R \ll 1$	20
Figure 2.15 (a) AFM scan of holes on the PS surface with silica particles prior to annealing. (b) AFM scan of the same hole after annealing for 24 h. The particle clusters in the rim are now clear	21
Figure 2.16 Optical micrographs of blends of linear polystyrene with nanoparticle. All the films were annealed for > 24 h in vacuum: (a) Pure PS, (b) 1%, (c) 5%, (d) 10%, (e) 15%, and 20% nanoparticles concentration. The length of the scale bars is 100 μm	22

	Page
Figure 2.17 Optical micrographs of PS/PMMA blend films with different PMMA content. (a)-(c) 1.0 wt% with annealing time 20, 50 and 120 min. (d)-(f) 5.0 wt% with annealing time 20, 50 and 120 min. (g)-(i) 10.0 wt% with annealing time.....	24
Figure 2.18 Schematic model of the interaction of P(S-Cl5), P(S-Cl20) and P(S-Cl45) copolymers with SiO _x /Si substrate.....	23
Figure 3.1 The compound light microscope	27
Figure 3.2 Perception of a magnified virtual image of a specimen in the microscope.....	28
Figure 3.3 Schematic view of an atomic force microscope	29
Figure 3.4 Plot of force as a function of probe-sample separation.....	31
Figure 3.5 Illustration of contact angles on a smooth surface	32
Figure 3.6 Demonstration according to droplet shape	33
Figure 3.7 The unbalanced force of liquid molecules at surface causes the surface tension	34
Figure 3.8 Illustration of an ambient-film-substrate optical system. The Incident light is partially reflected and partially transmitted	36
Figure 3.9 Optical system of a static light scattering	37
Figure 3.10 Dynamic light scattering (DLS) layout	38
Figure 3.11 Double layer model and zeta potential measured at the slipping plane	39
Figure 3.12 Optical diagram for zeta potential.....	40
Figure 3.13 The layout of Transmission Electron Microscope	41
Figure 4.1 Chemical structure of PS.....	43
Figure 4.2 Chemical structures of highly branched aromatic molecules	44

	Page
Figure 4.3 Chemical Structure of TA-PS.....	45
Figure 4.4 TEM micrograph of TiO ₂ nanoparticles.....	46
Figure 4.5 TEM micrograph of ZnO nanoparticles.....	46
Figure 4.6 Zeta potential versus pH of ZnO and TiO ₂ nanoparticles dispersed in water	47
Figure 5.1 Optical micrographs of 7 nm thick PS11K films containing different concentration of HBA1 annealed at 120 °C for 60, 150, 360, and 720 min. Size of each image is 60 μm x 60 μm.....	54
Figure 5.2 (a) Dewetting area versus annealing time of 7 nm thick PS11K films annealed at 120 °C. (b) Dewetting area of PS/HBA1 films versus ratio of HBA1.....	56
Figure 5.3 AFM topography images of 7 nm thick PS11K films containing different concentration of HBA1 annealed at 120 °C for 30, 150 and 720 min. Size of the images is 10 μm x 10 μm.....	58
Figure 5.4 Optical micrographs of 23 nm thick PS11K films containing different concentrations of HBA1 annealed at 120 °C for 2, 6, 12 and 24 h. Size of each image is 100 μm x 100 μm.	60
Figure 5.5 Dewetting area versus annealing time of 23 nm thick PS11K films annealed at 120 °C.....	60
Figure 5.6 AFM topography images of 7 nm thick PS33K films containing different concentration of HBA1 annealed at 120 °C for 540, 720 and 2160 min. Size of each image is 10 μm x 10 μm.	62
Figure 5.7 (a) Dewetting area versus annealing time of 7 nm thick PS33K films annealed at 120 °C. (b) Dewetting area versus annealing time of 23 nm thick PS33K films annealed at 165 °C.	63

	Page
Figure 5.8 Dewetting area versus annealing time of 23 nm thick PS11K films containing (a) HBA1 and (b) HBA2 annealed at 120 °C	65
Figure 5.9 Dewetting area versus annealing time of 23 nm thick films	66
Figure 5.10 Optical micrographs of 23 nm thick PS11K films containing different concentrations of TA-PS19 annealed at 120 °C for 12, 36, 60 and 120 h. Size of each image is 100 μm x 100 μm.	69
Figure 5.11 (a) Dewetting area versus annealing time of 23 nm thick PS11K films annealed at 120 °C. (b) Dewetting area of PS/TA-PS19 films versus TA-PS19 concentration.....	70
Figure 5.12 Optical micrographs of 23 nm thick PS33K films containing different concentration of (a) TA-PS19 and (b) TA-PS110 annealed at 165 °C for 30 and 60 min. Size of each image is 100 μm x 100 μm.....	72
Figure 5.13 Dewetting area versus annealing time of 23 nm thick PS33K films annealed at 165 °C.....	74
Figure 5.14 Dewetting area versus annealing time of 23 nm thick PS11K films annealed at 120 °C.....	75
Figure 5.15 Optical micrographs of 7 nm thick PS33K films containing different concentrations of (a) TA-PS19 and (b) TA-PS110 annealed at 115 °C for 120 and 300 min. Size of each image is 50 μm x 50 μm.	76
Figure 5.16 AFM topography images of 7 nm thick PS33K films containing different concentration of TA-PS19 and TA-PS110 annealed at 115 °C for 300 min. Size of the images are 10 μm x 10 μm.	77

	Page
Figure 5.17 Dewetting area versus annealing time of 7 nm thick PS33K films annealed at 115 °C.....	78
Figure 5.18 Optical micrographs illustrate dewetting pattern of PS films containing TiO ₂ nanoparticles at 0-0.02 wt.%. Film thickness is ~30 nm. All films are annealed at 180°C. Image size is 300 μm x 300 μm.....	82
Figure 5.19 The %dewetting area versus annealing time of 30 nm-films	82
Figure 5.20 Optical micrographs illustrate dewetting pattern of PS films containing TiO ₂ nanoparticles at 0-0.02 wt.%. Film thickness is ~100 nm. All films are annealed at 190°C. Image size is 500 μm x 500 μm.....	84
Figure 5.21 The %dewetting area versus annealing time of 100 nm-films.....	84
Figure 5.22 The %dewetting area versus Ratio of TiO ₂ nanoparticles with thickness about (a) 30 nm-films and (b) 100 nm-films.	86
Figure 5.23 AFM topographs of the as-cast films with 0.2 wt.% TiO ₂ (a) 30 nm- films and (b) 100 nm-films. Image size is 10 μm x 10 μm.....	87
Figure 5.24 Optical micrographs illustrate dewetting pattern of PS films containing TiO ₂ nanoparticles at 0-0.02 wt.%. Film thickness is ~265 nm. All films are annealed at 190°C. Image size is 1000 μm x 1000 μm.....	88
Figure 5.25 (a) The %dewetting area versus annealing time of 256 nm-films (b) %dewetting area versus Ratio of TiO ₂ nanoparticles.....	89

Figure 5.26 Optical micrographs illustrate dewetting pattern of PS films containing ZnO nanoparticles at 0 to 0.20 wt.%. Film thickness is ~30 nm. All films are annealed at 180°C. Image size is 300 μm x 300 μm	90
Figure 5.27 (a) The %dewetting area versus annealing time of 30 nm-films (b) %dewetting area versus Ratio of ZnO nanoparticles at different annealing time.	91
Figure 5.28 Optical micrographs illustrate dewetting pattern of PS films containing ZnO nanoparticles at 0-0.02 wt.%. Film thickness is ~100 nm. All films are annealed at 190°C. Image size is 500 μm x 500 μm	93
Figure 5.29 (a) The %dewetting area versus annealing time of 100 nm-films (b) %dewetting area versus Ratio of ZnO nanoparticles.	94

CHAPTER I

INTRODUCTION

Polystyrene thin films have numerous technology applications. These films on solid surface are used as dielectric coating, lithography resisting, electronic packaging, and surfaces lubricating because of a remarkable insulation property of polystyrene. As electronic products become smaller, the thinner coating is required. Polymer thin films need to be stable on the solid substrate in application. However many parameters influence the stability of the films, such as molecular weight, film thickness and temperature [1-5]. By decreasing polymer film thickness or annealing the films at temperature above T_g , the unstable polymer films tend to coalesce and form polymer droplets [6]. In this case, continuous film is destroyed and the film cannot spread over the substrate, this phenomenon is called dewetting behavior.

Many researchers have investigated how to retard the dewetting behaviour of polymer thin films. Several techniques used for inhibit this behaviour based on the two general principles, thermodynamics and kinetics [7]. Thermodynamic strategy aims to change the surface energy while kinetic strategy involves reducing the mobility of the polymer chains. By modifying the interfacial tension between film and substrate, the stability of the polymer thin film is improved. Interface modification technique relies on improving polymer-substrate interactions [8-12]. Several materials containing chemical compositions that are compatible to the polymer thin film are used for modifying the substrate of surface, such as a grafting homopolymer, a random copolymer and a functionalized self-assembled monolayer (SAM) [10, 13-20]. Although substrate modification can extend a strong interfacial interaction, this process is complicated. Moreover, this approach tends to alter the film properties which might be undesirable. An alternative technique of the interface modification is polymer modification. An end-functionalized polymer chain with sticky end group forms polymer brushes on the

substrate [11, 13, 14, 18, 19, 21]. The segregation of the modified polymer to the substrate changes the interface tension, thus suppressing the dewetting behavior. A fascinating strategy to repress dewetting behavior has been presented by Barnes et al. [22]. Addition of a small amount of fullerene into polystyrene and polybutadiene thin films significantly enhances film stability. In recent years, many researchers have investigated the mechanism of this phenomenon and have discovered other nanoparticles that can be used as dewetting inhibitors [23-31].

In this research, the stability of polystyrene thin films with addition of highly branched aromatic molecules, three-arm polystyrene and metal oxide nanoparticles are investigated. All films are annealed at temperatures higher than T_g of the polystyrene for various times. The dewetting behavior and stability of all films are investigated. Topography, roughness and thickness are examined by atomic force microscopy (AFM). Topography and % dewetting area are examined by optical microscopy (OM). Contact angles are measured using a contact angle meter. Chemical structures of highly branched aromatic molecules used in this research are shown in Figure 1.1. These highly branched aromatic molecules behave as anchoring sites or physical cross-linking points for PS chains within the entire film. The mobility of polymer films is expected to reduce. Since the appearance of oxygen atoms and the structure symmetry of the two highly branched aromatic molecules are different, one may also expected the difference in ability to wet substrate. Another hyperbranched polymer additive used in this work is three-arm polystyrenes as shown in Figure 1.2. The entanglement within the mixed films is expected to increase with this hyperbranched polymer and the chain mobility should be reduced, leading to retardation of dewetting behavior. Suppressing the dewetting of the film with nanoparticles is also observed. Titanium dioxide and zinc dioxide nanoparticles are expected to improve stability of the filled-film by pinning contact line effect and changing interfacial interaction between film and substrate as shown in Figure 1.3.

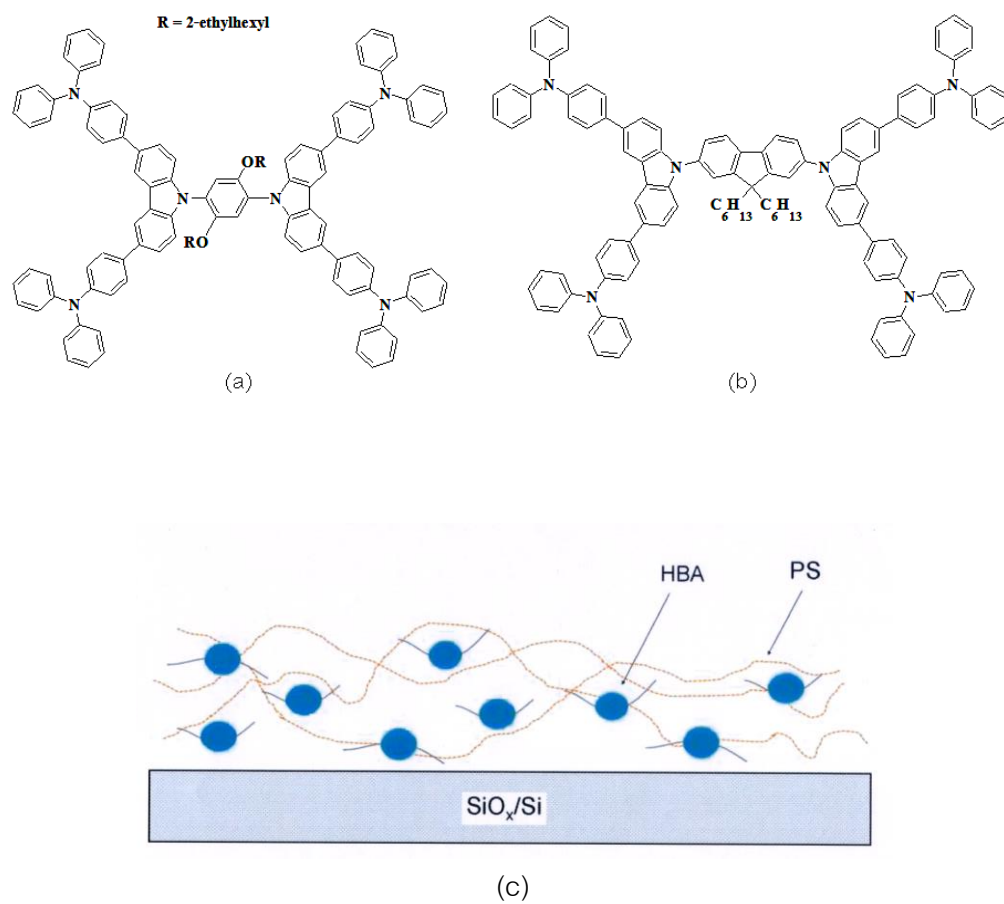
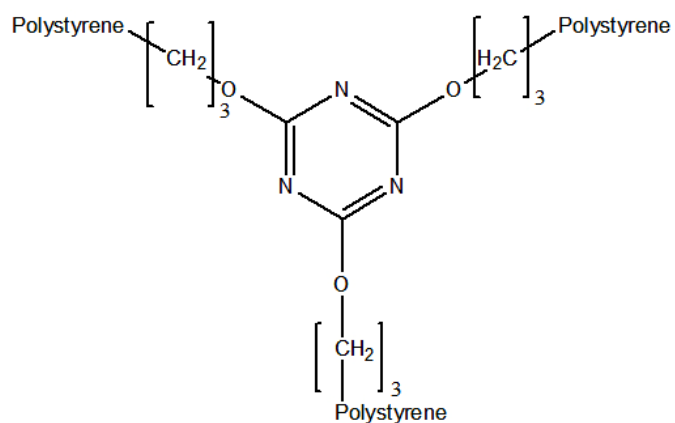
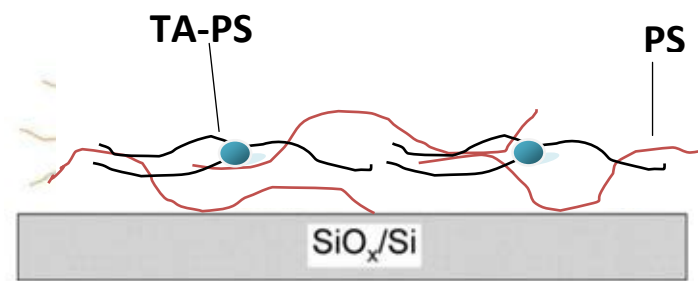


Figure 1.1 Chemical structures of (a) highly branched aromatic molecules HBA1, (b) highly branched aromatic molecules HBA2, and (c) Schematic model of interaction between highly branched aromatic molecules, polystyrene, and substrate



(a)



(b)

Figure 1.2 (a) Chemical structure of three-arm polystyrene. (b) Schematic model of interaction between three-arm polystyrene, polystyrene, and substrate

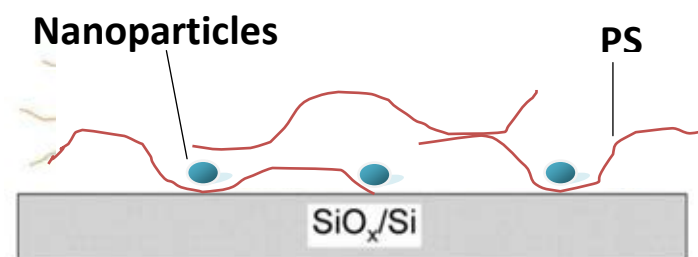


Figure 1.3 Schematic model of interaction between nanoparticles, polystyrene, and substrate

OBJECTIVES OF THIS RESEARCH

1. To study interfacial interaction between pure, mixed and filled polystyrene thin films and inorganic substrate.
2. To investigate methods for suppressing the instability of the polymeric thin films on SiO_x/Si wafer substrate.

CHAPTER II

LITERATURE REVIEW

2.1 THEORETICAL BACKGROUND

2.1.1 DEWETTING IN POLYMER FILM

Stable, metastable and unstable polymer films can be distinguished by the effective interface potential ($\varphi(h)$) [7]. The effective interface potential ($\varphi(h)$) is an excess free energy per unit area which is used for bring two interfaces from infinity to the distance; h . These two interfaces refer to substrate-film and film-air interface. In the other word, distance; h , means the thickness of polymer film. As shown in Figure 2.1 curve (1), curve (2) and curve (3) indicate stable, unstable and metastable film, respectively.

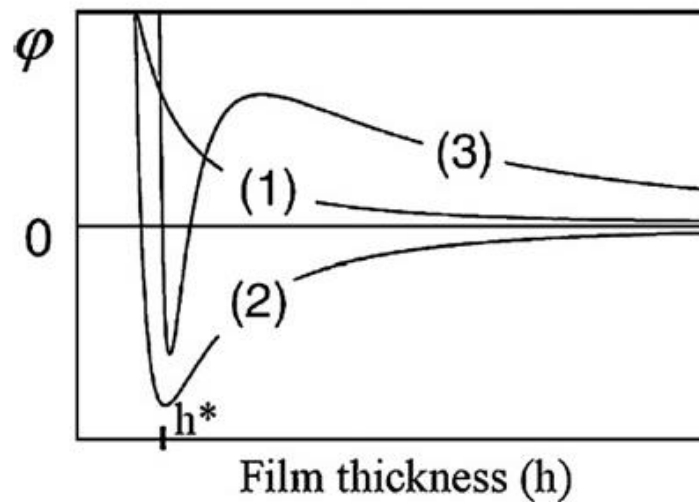


Figure 2.1 The effective interface potential as a function of film thickness, (1) stable film, (2) unstable film and (3) metastable film [32].

Dewetting is a behaviour occurring in unstable or metastable polymer film. This action damages the film and finally transforms the continuous film to polymeric droplets. Dewetting behaviour generally occurs at an interface between organic film and inorganic substrate because of the difference of two materials. The process is driven by the balance of the capillary forces at the three phase contact line, substrate, film and air. Unfavorable interfacial energy between polymer film and metal oxide substrate leads to the separation between film and substrate. Contact angle (θ), surface energy of substrate γ_S , surface energy of film γ_F and interfacial tension between substrate and film γ_{SF} , as shown in Figure 2.2, are related by Young's equation [33].

$$\gamma_S = \gamma_{SF} + \gamma_F \cos\theta \quad (\text{Eq. 2.1})$$

Wetting property of polymer film can be expressed in terms of a spreading coefficient (S) [33].

$$S = \gamma_S - \gamma_F - \gamma_{SF} \quad (\text{Eq. 2.2})$$

If the interfacial tension between film and substrate is higher than the surface energy of substrate, S is negative and dewetting is occurred. Generally, dewetting behavior is an unwanted process in polymer thin film application because dewetting behavior always destroys the required properties of polymer film.

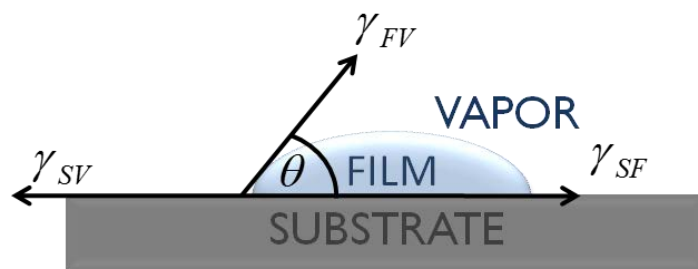


Figure 2.2 Model of three phase contact line, substrate, film, and air

2.1.2 MECHANISMS OF DEWETTING

To clearly understand dewetting process, the mechanisms which induce dewetting behaviour are explained in this section. Dewetting process can begin via two mechanisms, i.e. spinodal mechanism and heterogeneous nucleation mechanism. Spinodal mechanism is caused by the transferring of thermal energy in a wave form [1, 34]. This mechanism occurs in an unstable polymer film. The thermal energy makes the film moving with an appearance of wave. If the thermal energy is high enough, the correlated holes are created, as shown in Figure 2.3.

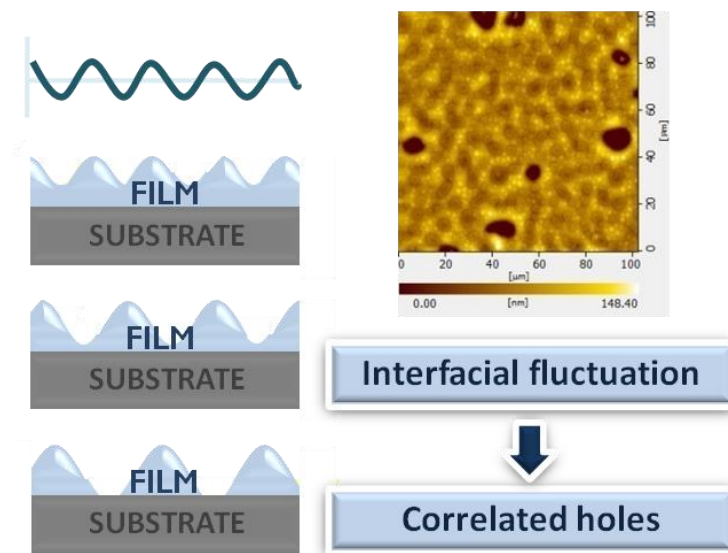


Figure 2.3 Illustration of spinodal mechanism

Heterogeneous nucleation mechanism, as shown in Figure 2.4, is caused by the heterogeneity of surface energy between polymer film and solid substrate and the presence of impurities such as dust particles and/or air bubbles in polymer film. This mechanism refers to metastable film [35, 36]. In this case, the film needs to overcome a potential barrier to reach the lowest energy at $h = h^*$. The $\varphi(h)$ is reduced by an existence of impurities which can produce the dewetting. Heterogeneous nucleation mechanism generates the uncorrelated holes and the impurity performs as an initial of

hole. However, it is difficult to make a distinction between metastable and unstable film because, in experiment, the dewetting can be induced by both mechanisms [2].

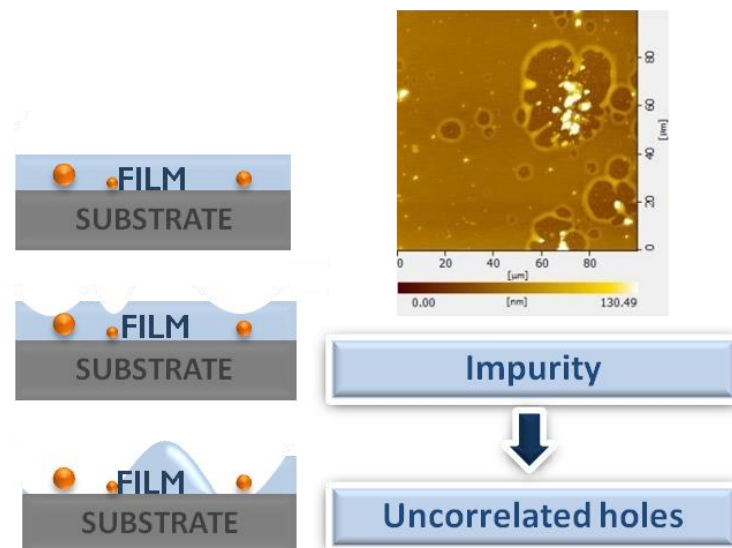


Figure 2.4 Illustration of heterogeneous nucleation mechanism

2.1.3 KINETICS OF DEWETTING

Kinetics of dewetting process is also important to follow dewetting behavior. At normal conditions, below the glass transition temperature of the polymer film (T_g), polymer thin films on non-wettable solid surface does not dewet immediately, it is in a metastable state. Annealing the film above the glass transition temperature, the mobility of polymer molecules is increased. The chains of polymer start to rotate and vibrate to release the residual stress [37-39]. Finally, polymer films undergo a self-destructive process and the dewetting behavior is initiated.

Dewetting behavior can be followed by three steps [11]. The first step is called an early stage. Some small holes can be detected on the continuous film which spreading cover the substrate. After that, small holes grow and coalesce with increasing heating time showing ribbon structure. This step is called an intermediate stage. Further increasing in heating time, unstable ribbon polymer structures are melted and merged

with others. Lastly, polymer droplets are created on the substrate leading to a final stage of dewetting process. The polymer film is then completely dewet. All three steps are shown in Figure 2.5.

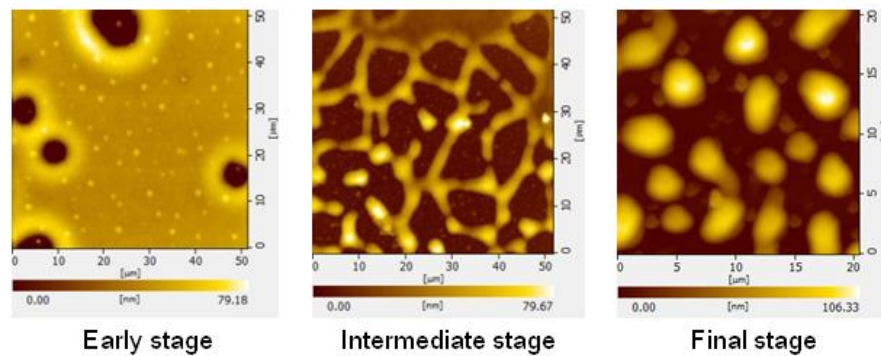


Figure 2.5 Three states of dewetting process

2.2 INHIBITION OF DEWETTING

Polymer thin film need to be stable on the solid substrate in technology application. However, many parameters influence the stability of polymer thin films, such as molecular weight, film thickness and temperature [1-5, 40]. Several researches investigated how to inhibit dewetting behaviour in polymer thin films. All techniques used for preventing this behaviour base on two general principles, thermodynamic and kinetic [7]. Thermodynamic strategy aims to change the surface energy. By increasing the interfacial interaction between film and substrate, the stability of polymer thin film is improved. Moreover, reducing the mobility of the polymer chains can promote the wettability also. This mechanism is based on kinetic strategy.

2.2.1 DEWETTING INHIBITION BY CHEMICAL MODIFICATION

Modifications of substrate surface and polymer structure are applied for stabilizing polymer thin films. Interface modification technique relies on improving polymer-substrate interactions [17, 20, 21, 41, 42]. The material containing some chemical compositions which has high affinity to polymer thin film is used to modify the substrate surface, such as a grafting homopolymer, a random copolymer and a functionalized self-assembled monolayer (SAM) [10, 13-19, 43].

Substrate modifications by using polystyrene brushes have been studied by Yerushalmi-Rozen et al. [21, 44, 45]. The modified-surface substrate was used or polystyrene films with the same composition. Although, this experiment can reduce the difference of surface energy between the film and the substrate, they found that this modification cannot suppress dewetting behavior. Because of the low molecular weight of polystyrene brushes, the formation of an entanglement between polymer films and polymer brushes cannot occur. Polystyrene films were excluded and dewetted on the polystyrene brush layer. This work suggested that the stability of polymer film and modified substrate related to the formation of an entanglement between them. The entanglements prevented the dewetting by breaking the flow of oscillated polymer film, as shown in Figure 2.6. Consequently, only chemical modification of the substrate surface to match with the polymer film is not sufficient to eliminate dewetting behavior. The entanglement between the polymer film and the modified substrate is important also.

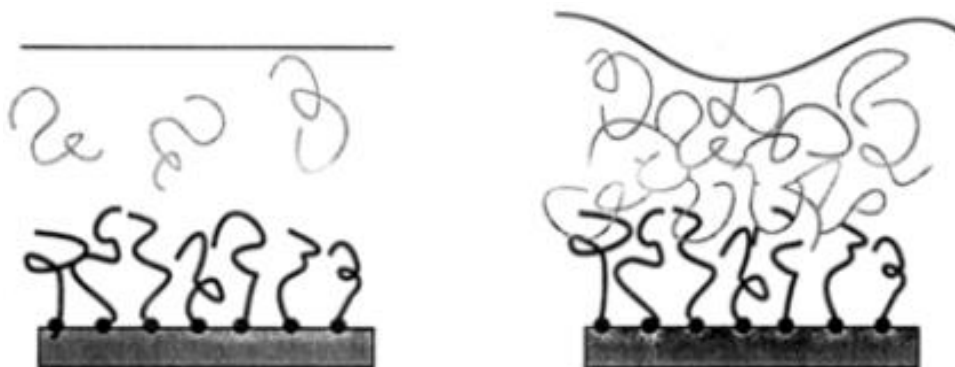


Figure 2.6 Schematic model of thin films contains a chain brush at the surface [44].

Choi et al. [10], investigated the dewetting inhibition of polystyrene film on a modify substrate. A cross-linked 3-amino-propyltriethoxysilane (APTES) was used to modify the surface. They found that, if an APTES possessed a high molecular weight, the cross-linked networks were formed and the dewetting was suppressed. For the lower molecular weight polystyrene chains, the dewetting suppressions were various, as shown in Figure 2.7. Curing the film at room temperature, Figure 2.7 (a), amine groups were bound with non-reacted hydroxyl groups and then polystyrene chains cannot penetrate into the APTES layer. Curing the film at 80 °C or 120 °C, polystyrene chains cross-linked with the APTES molecules and amino groups were extended and penetrated into the polystyrene matrix as shown in Figure 2.7 (b). Precuring at 200 °C, as shown in Figure 2.7 (c), polystyrene chains diffused into the top of APTES layer because the Si-O-Si bonds were formed during precuring step. The dewetting suppression was only observed when curing the film at 80 °C or 120 °C (Figure 2.7 (b)).

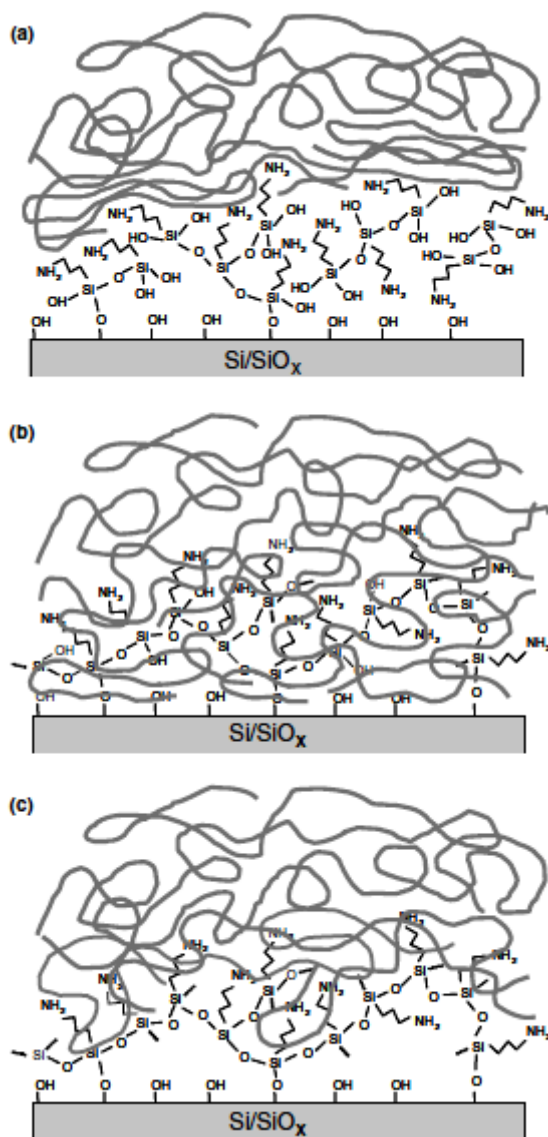


Figure 2.7 Schematic model of interface structures of polystyrene and APTES under various curing and precuring condition [10].

Another chemical modification technique used to inhibit dewetting behavior is polymer modification [8, 11-13]. The modified polymer chain has a sticky end group which attaches to the substrate [14-16, 19, 31, 41]. The segregation of the modified polymer to the substrate changes the interface interaction and the dewetting behavior is suppressed.

Dewetting behavior of end-functionalized polymer film was studied by Henn et al [21]. Two sulfonato polystyrenes, ω -barium and α,ω -barium, showed a strong interaction with the substrate. The short monofunctional chains formed a pack of brush layer on the surface as shown in Figure 2.8 (a). If the monofunctional chain was large enough and the polymers were entangled, dewetting was retarded. Moreover, polymer containing difunctional chains showed no dewetting. The film fluidity was reduced because ionic groups in the film aggregated and formed physical cross-links, which similar to the chain entanglement, as shown in Figure 2.8 (b).

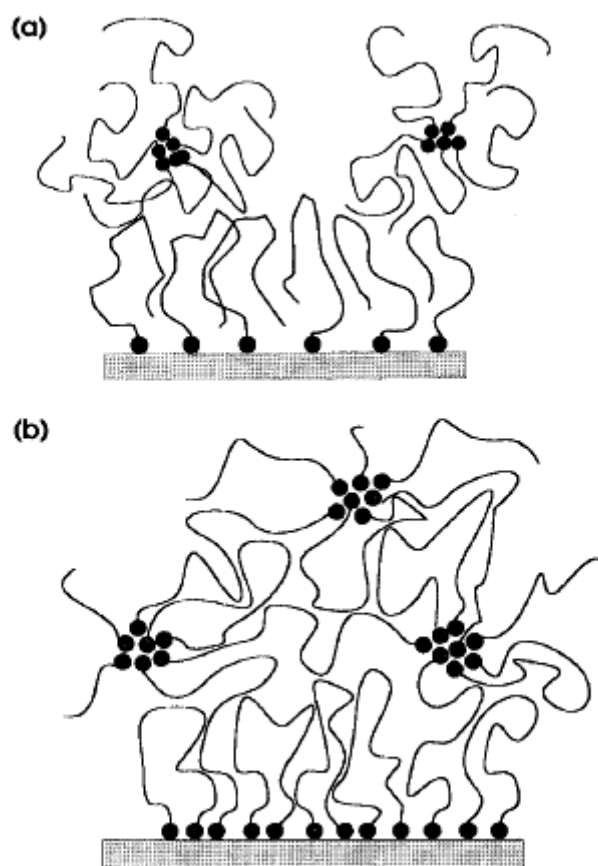


Figure 2.8 Schematic model of (a) ω -barium sulfonato polystyrene and (b) α,ω -barium sulfonato polystyrene [21].

Traiphol [11] has found that addition of a chloromethylstyrene (CIMS) unit only 5 mol% into polystyrene backbone increased stability of the 5 nm-thick film. Addition of the CIMS unit enhanced dipolar and/or acid-base interfacial interactions between the film and SiO_x/Si substrate, as shown in Figure 2.9. Increasing the CIMS mole ratio also increased the film stability. However, the film thickness affected the dewetting inhibition. In thicker film (22 and 45 nm), 5 mol% of the CIMS unit degraded the film stability comparing to pure polystyrene film. Because the dipolar interaction cannot affect in the long-range distance between the CIMS units, the mobility of the thicker film was not reduced. By increasing the concentration of the CIMS units, the distance between the units is shorten, as shown in Figure 2.10. Then, the film stabilities were improved again.

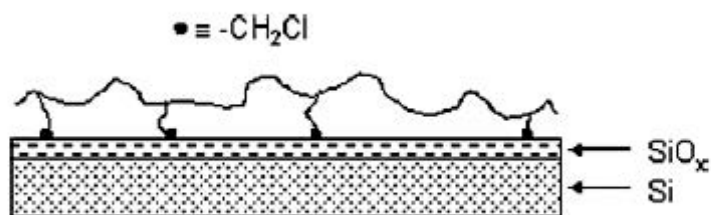


Figure 2.9 Schematic model of surface anchoring of $-\text{CH}_2\text{Cl}$ group on SiO_x/Si surface [11].

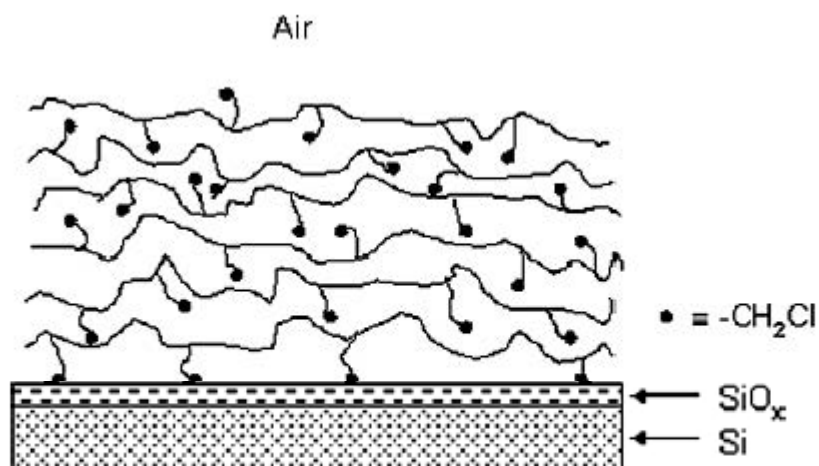


Figure 2.10 Schematic model of the distribution of $-\text{CH}_2\text{Cl}$ group in 22 and 45 nm thick film [11].

The chemical modification technique definitely extends a strong interfacial interaction between film and surface; however, an entanglement between both segments is required to eliminate the dewetting behavior. Every approach has its own advantages and disadvantages. Disadvantage of the modification approach is the presence of phase separation inside the polymer film. Moreover, this technique is complicated and leads to the changing in the film properties which might be undesirable.

2.2.2 DEWETTING INHIBITION BY POLYMER CROSS-LINKING

Addition chemical or physical cross-linker to the polymer film increases macromolecule network. The cross-linking of polymer produces strong interactions between polymers, which reduces film mobility. Viscosity of polymer film increases and then the dewetting process is inhibited corresponding to kinetic strategy. Cross-linking can be created via irradiation [46] or addition of cross-linking agents [46-48].

Carroll et al. have investigated the effects of bifunctional photoactive cross-linker in polystyrene film [47]. The cross-linker contains benzophenone chromophores which can produce cross-linking inside polystyrene film after irradiated with UV light. Then, the film stability is improved, as shown in Figure 2.11.

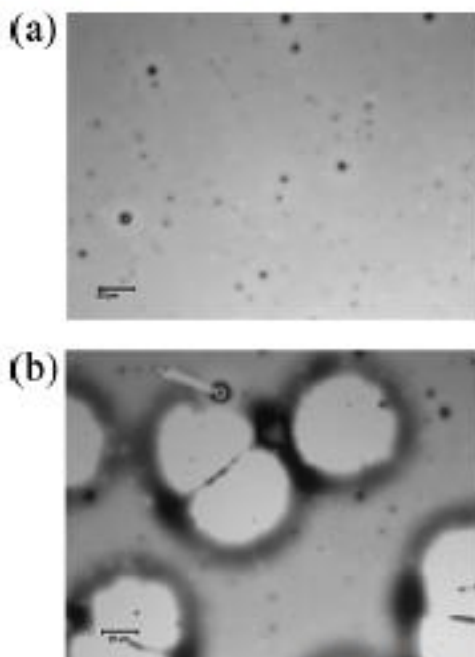


Figure 2.11 Optical micrographs of 25 nm films after annealing overnight at 170 °C (a) irradiated the film containing a ratio of bis-3-benzoyl benzoic acid ethylene glycol to polystyrene of 3:1 and (b) pure polystyrene film [47].

Influence of cross-linking density on the dewetting inhibition of polymer film has been studied by Akhrass et al. [49]. The presence of partial cross-linking with lower molar mass (106 kg/mol) increased the relaxation time. Therefore, the hole density was decreased. They found that the residual stresses inside the films cannot destroy the film which has high probability of un-cross-linking. If highly cross-linking occurred in the film, a rubbery network was then formed. An elastic force in polymer networks reduced the driving force of holes formation. Consequently, cross-linking of lower molar mass can improve film stability in both partial and highly cross-linking, as shown in Figure 2.12. For higher molar mass (2500 kg/mol), the presence of partial cross-linked in the film did not affect the relaxation time. However highly cross-linked film increased the relaxation time. Moreover, the stability of the cross-linked film depended on the film thickness. High degree of cross-linked could not eliminate dewetting in the 20 nm film because the entanglement density decreased in this ultrathin film [50, 51].

Addition of cross-linking network into the film significantly reduces the mobility of the polymer chain. Then, the opening and growth of holes are retarded and the wettability of the films is enhanced. This technique requires a long chain polymer, and the films should be thick enough. In addition, the appearance of cross-linking polymer can alter the desired properties of the polymer films.

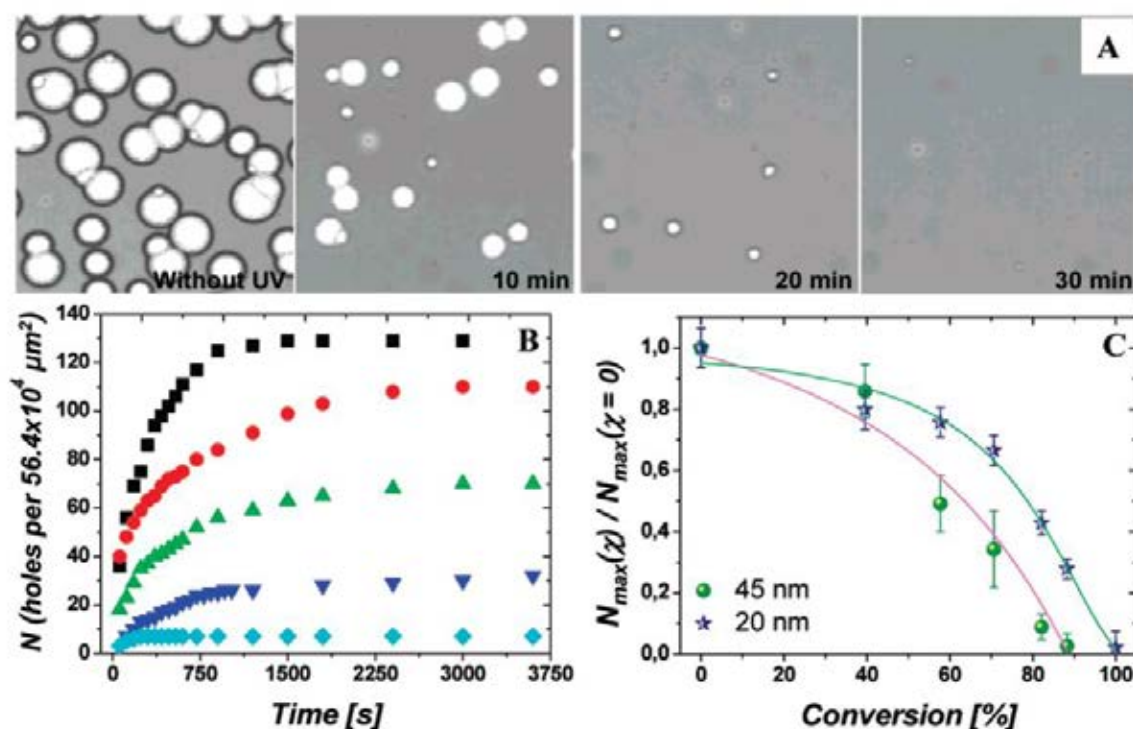


Figure 2.12 Effects of degree of cross-linking to the partially cross-linked film rupture. (A) Optical micrographs show the number of holes when increasing UV exposure time in 45 nm films. (B) Density of holes per unit area (from top to bottom, UV exposure time are 1, 10, 20, 30 and 40 min). (C) Density of holes per unit area as a function of azide conversion [49].

2.2.3 DEWETTING INHIBITION BY ADDITIVE ADDITION

Addition of nanoparticle additive is another technique to improve polymer thin film stability. A fascinating strategy to repress dewetting behavior has been presented by Barnes et al. [43]. Addition of small amounts of C_{60} fullerene nanoparticles into

polystyrene and polybutadiene thin films significantly enhanced the films stability (Figure 2.13). By neutron reflection measurement, they have found the formation of fullerene diffuse layer near solid surface. The fullerene layer created a roughness, which probably contributed to the modified surface similar to the surface modification approach. The immobilized nanoparticles not only formed an enrichment layer but also pinned the contact line of dry region, which arrested the holes growth. Consequently, this technique consisted of two mechanisms for controlling the wetting property. This result is contrary to the conventional knowledge, in which the presence of impurities in polymer films causes dewetting holes. Thus, this method of dewetting suppression is very interesting. Many researchers have investigated the mechanisms of this phenomenon, and have reported the uses of other nanoparticles for dewetting suppression of the polymer films [22-31, 52].

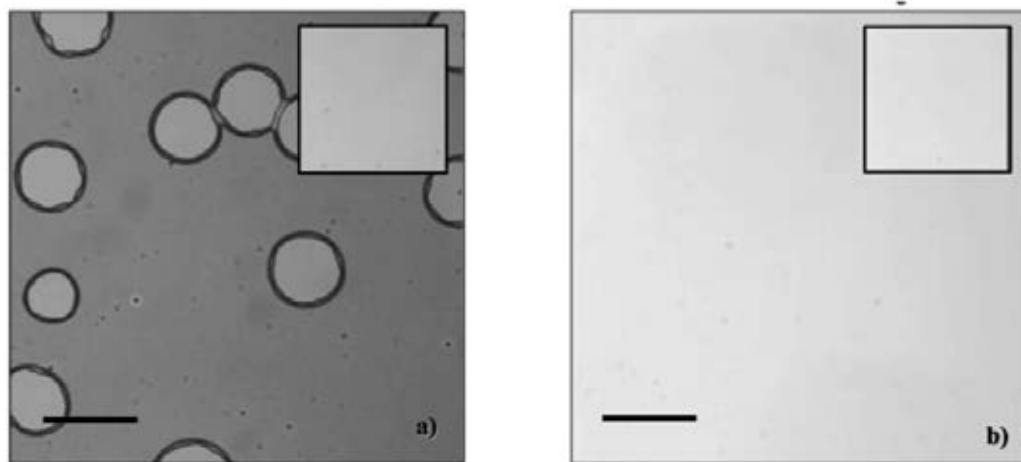


Figure 2.13 Optical micrograph of 50 nm films (a) pure polystyrene and (b) polystyrene with fullerene (mass fraction = 0.01) [22].

Effects of diameter size of C_{18} -functionalized gold (10 nm) and palladium (3 nm) nanoparticles on dewetting dynamics of polystyrene film on poly(methyl methacrylate) substrate were investigated by Xavier et al. [28]. The segregation of particles was not observed at any interfaces. Then, the increasing of viscosity was the only one

mechanism occurring in this system. The dynamics of dewetting were a function of the ratio between the polymer radius of gyration (R_g) and the filler radius (R_{particle}). When the particle diameter was smaller than $R_g/4$, the velocity of the filled system was slower than that of the unfilled system because the particles were fitted in the chain segment (see in Figure 2.14). There was no changes in the overall entropy in the system, thus, the particles can be stable in the film. The viscosity of the films increased and then the velocity of dewetting decreased.

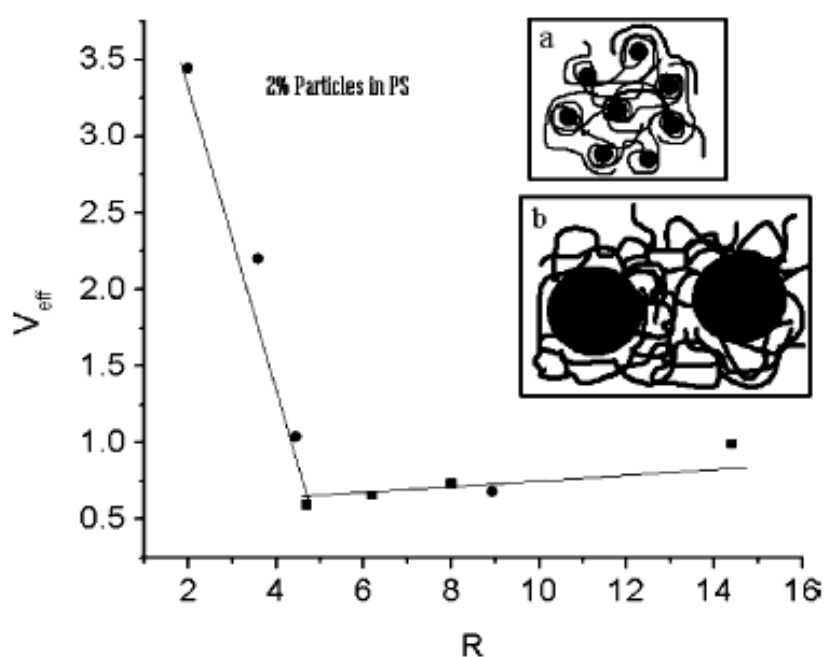


Figure 2.14 Plot between V_{eff} ($V_{\text{particle}}/V_{\text{PS}}$) vs R ($R_g/R_{\text{particles}}$) for both 10 nm diameter of Au particles and 3 nm diameter of Pd particles in difference molecular weight polystyrene matrices. The inset shows schematic model of filled system (a) $R > 1$ and (b) $R \ll 1$

[28].

Formation of nanoparticles enrichment layer is essential to inhibit the dewetting. Films stability is drastically improved when adding nanoparticles at the suitable concentration. The appropriate concentration corresponds to a segregated monolayer of nanoparticles [22]. Each nanoparticles-polymer systems has a critical value of

nanoparticles concentration. Normally, when the concentration is lower than the critical value, dewetting is suppressed. Increasing the concentration decreases the dynamics of dewetting. However, if the concentration is higher than the critical value, the dewetting behavior is enhanced [31]. The mechanisms controlling wetting property in this approach are both contact line pinning and interfacial roughness. The roughness of nanoparticles enrichment layer affects the wetting properties by changing surface energy. Contact line pinning can be observed when holes stop growing with increasing annealing time. The two mechanisms results from kinetic strategy (contact line pinning) and thermodynamic strategy (surface energy changing).

Sharma et. al. reported the unique strategy to control the dewetting rate [53]. The dispersion of small amount of SiO_2 nanoparticle fillers in the PS/PMMA bilayer film was suggested to be a major reason to control the film wettability. Even though the bilayer sample containing SiO_2 fillers presented large holes prior to annealing, heating the samples for up to 32 h produced a negligible change in the size or the number of holes. From the topographical in Figure 2.15, they found that the rim appeared slightly irregular and composed of particle clusters. The clusters migrated to the rim of hole where they pinned the contact line. Further hole growth was prevented and dewetting was arrested. AFM images clearly proved that interfacial pinning was the key to dewetting inhibition.

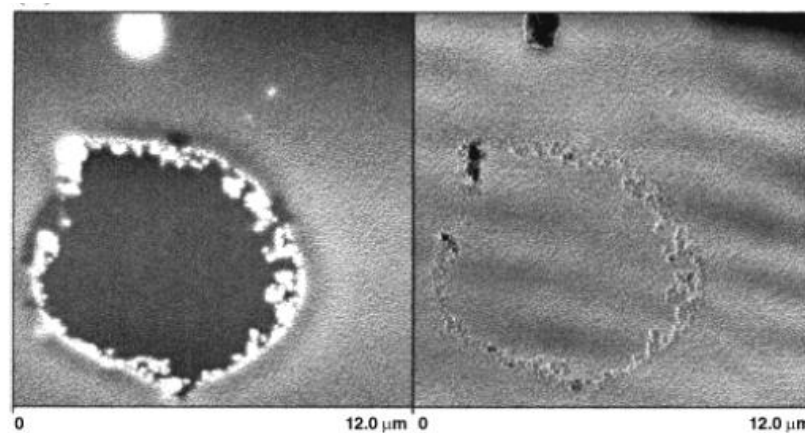


Figure 2.15 AFM scan of the same hole after annealing for 24 h. The particle clusters in the rim are now clear [53]

Addition of polystyrene nanoparticles to thin polystyrene films inhibited and in some cases eliminated dewetting as investigated by Krishnan et al [25]. Neutron reflectivity measurements were used to demonstrate that polystyrene nanoparticles were uniformly distributed in the thin film prior to annealing. After annealing, the nanoparticles were found to separate to the solid substrate. Figure 2.16 showed the optical micrographs of the blend films after annealing for more than 24 h under vacuum. It showed that the dewetting was completely eliminated at around 15-20% weight fraction of polystyrene nanoparticles. An enriched layer of nanoparticles at the substrate surface was reported to play an important role in eliminating dewetting. When molecular weight of nanoparticles decreases, dewetting was not eliminated, but retarded. They concluded that the separated component along the substrate controlled the dewetting kinetics and promoted wetting property of the film.

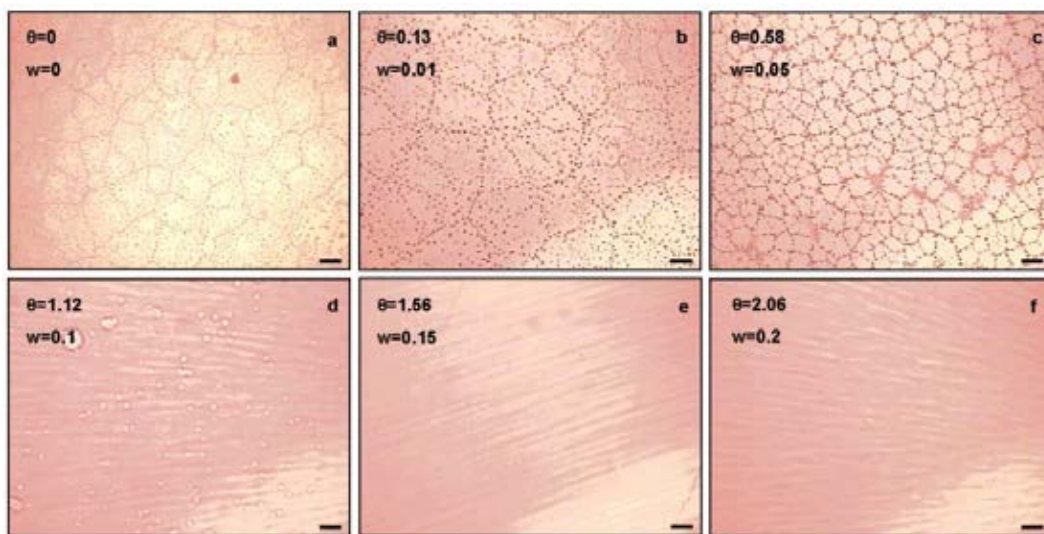


Figure 2.16 Optical micrographs of blends of linear polystyrene with nanoparticle. All the films were annealed for > 24 h in vacuum: (a) Pure PS, (b) 1%, (c) 5%, (d) 10%, (e) 15%, and 20% nanoparticles concentration. The length of the scale bars is 100 μm [25].

Sangjan et al. [56, 57] have found that addition of poly(styrene-*stat*-chloromethylstyrene) into polystyrene promoted the film stability. Dipolar interaction between chloromethylstyrene (CIMS) group and SiO_x/Si substrate led to the segregation of copolymer while the styrene segments of copolymer interacted with polystyrene matrix. The efficiency of dewetting suppression increased with the ratio of polar CIMS groups, which provided higher number of anchoring sites, as shown in Figure 2.17. To suppress dewetting behavior, higher amount of the copolymer with lower ratio of CIMS group is required. However, addition of low ratio of CIMS group copolymer induces the dewetting in thick film.

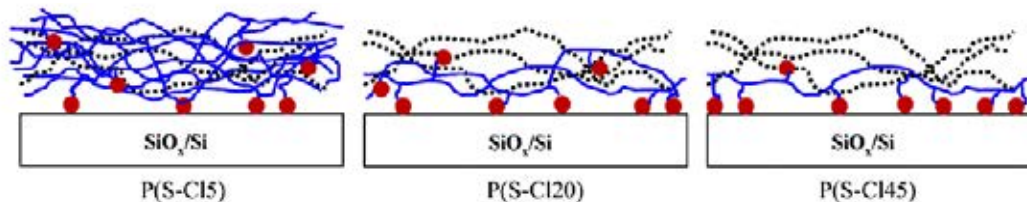


Figure 2.17 Schematic model of the interaction of P(S-CI5), P(S-CI20) and P(S-CI45) copolymers with SiO_x/Si substrate [56, 57].

2.2.4 DEWETTING INHIBITION BY PHASE SEPARATION

Dewetting inhibitions by polymer or nanoparticles segregation to the surface mentioned in the previous approach are driven by phase separation mechanism. Phase separation generally occurs in an unfavourable mixing enthalpy which may cause dewetting. However, phase separation sometimes can be used to directly retard dewetting. The well-known model for investigating dewetting inhibition by phase separation is polystyrene/poly(methyl methacrylate) system. This technique is a simple and low cost method to retard dewetting behavior. As shown in Figure 2.18, Li et al. [54, 55] have found that the preferential segregation of poly(methyl methacrylate) (PMMA) to substrate and forming of PMMA-rich phase layer attributed to the film stabilizing. The

PMMA chains stretched out into the PS rich phase, which increased interfacial tension and decreased the driving force for dewetting.

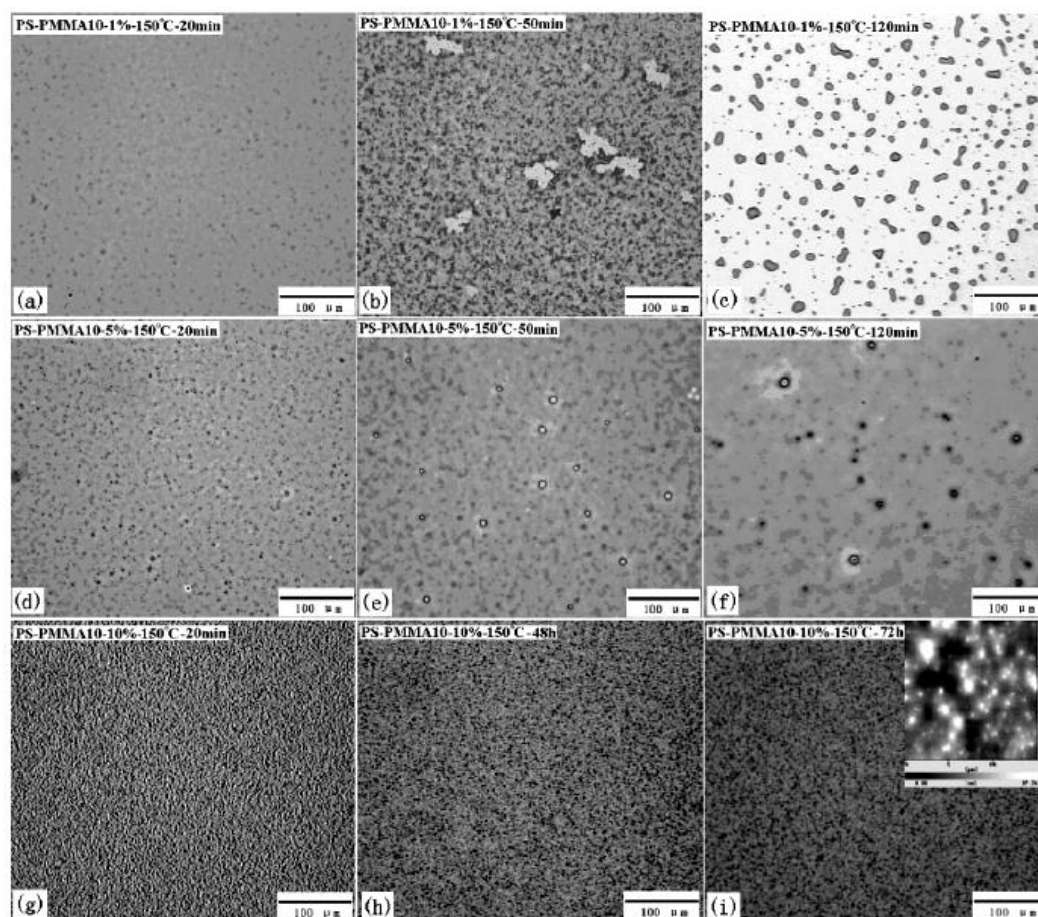


Figure 2.18 Optical micrographs of PS/PMMA blend films with different PMMA content. (a)-(c) 1.0 wt% with annealing time 20, 50 and 120 min. (d)-(f) 5.0 wt% with annealing time 20, 50 and 120 min. (g)-(i) 10.0 wt% with annealing time 20 min, 48 h and 72h [54].

In this research, the stability of polystyrene thin films added by highly branched aromatic molecules, three-arm polystyrene, and metal oxide nanoparticles are investigated. These highly branched aromatic molecules behave as anchoring sites or physical cross-linking points for PS chains within the entire film. The mobility of polymer films are expected to reduce. Since the appearance of oxygen atoms and the structure

symmetry of the two highly branched aromatic molecules are different, one may also expected the difference in ability to wet substrate. Another additive (i.e. three-arm polystyrene) is expected to increase an entanglement in the mixed films because of long branch chain, which has the similar chemical structure as the polymer matrix. The chain mobility should be reduced, leading to retardation of dewetting behavior. Additionally, titanium dioxide and zinc dioxide nanoparticles are expected to improve stability of the filled-film by pinning contact line effect and changing interfacial interaction between the film and the substrate.

CHAPTER III

METHODOLOGY

3.1 OPTICAL MICROSCOPY

Optical microscope (OM) is an instrument using visible light to produce a magnified image of a sample. Objective lenses and eyepiece lenses work together and produce the final magnification of the image (M_{final}) as followed [58];

$$M_{\text{final}} = M_{\text{obj}} \times M_{\text{oc}} \quad (\text{Eq. 3.1})$$

Light from the illuminator are focused by the condenser lens onto the sample, as shown in Figure 3.1 The sample located on optical microscope stage is examined by the objective lenses. The objective lenses collect light diffraction of the sample and form a magnified real image. The eyepiece lenses projects a second real image onto a retina. Brain perceives and interprets the image as a magnified virtual image about 25 cm in front of the eye. For photography, a camera records the intermediate image directly or projects as a real image. Figure 3.2 shows how the image is magnified and is observed by eye.

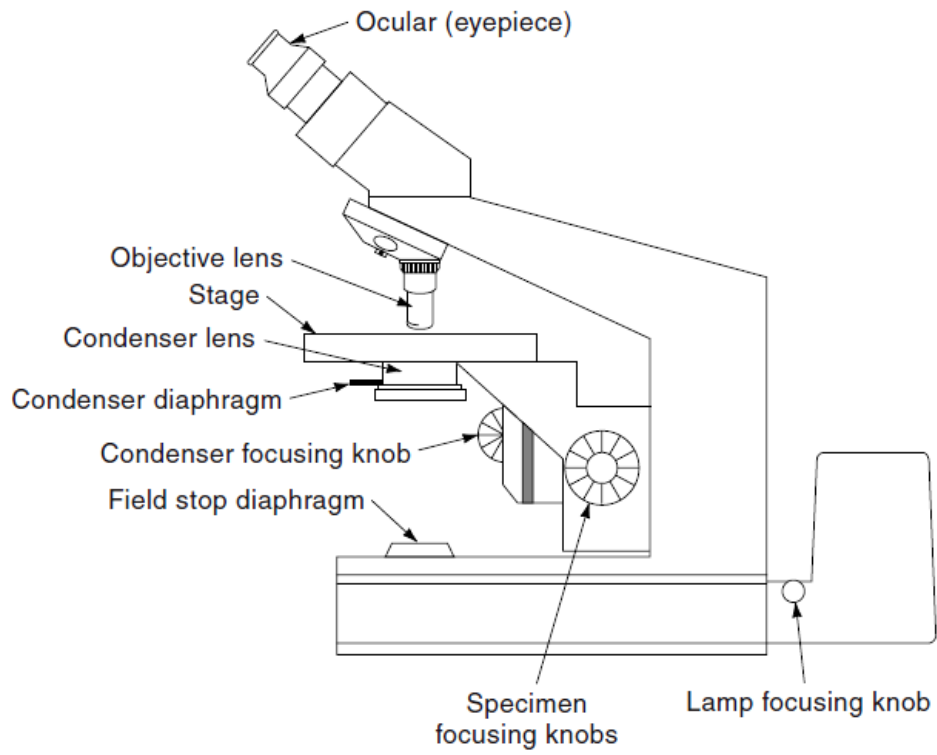


Figure 3.1 The compound light microscope [58]

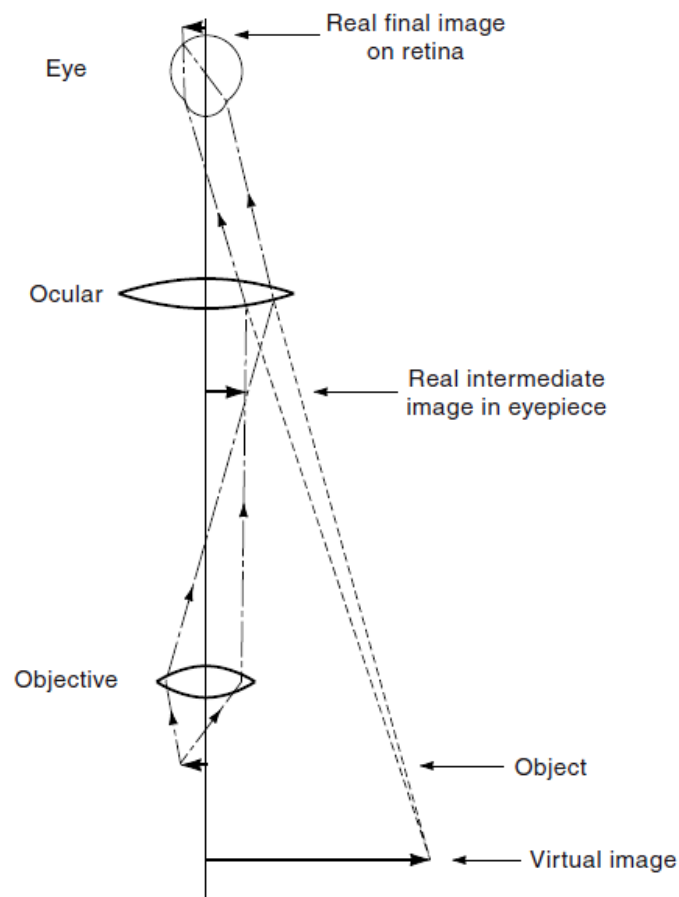


Figure 3.2 Perception of a magnified virtual image of a specimen in the microscope [58]

3.2 ATOMIC FORCE MICROSCOPY

Atomic force microscope (AFM) is an instrument that analyzes and characterizes a sample surface in microscopic level. The surface morphology is illustrated with a very accurate resolution ranging from less than 1 μm to 100 μm . AFM operates by using an extremely sharp tip which comes in contact or in very close to the sample and then scans along a surface. The images are generated by measuring near-field force between the tip and the sample. The near-field force is divided to four types. Firstly, short-range force is interactive force in pair electrons between atoms. It is a chemical bonding formed by sharing electron between two or more atoms. The magnitude of this force depends on distance between atoms. Secondly, Van der Waals force is a weak

dipolar intermolecular interaction. The magnitude of this force depends on the distance between the tip and sample. Next, electrostatic force is the interaction between electric charges on the tip and the sample. It is a long-range force which has a longer interactive distance comparing with the others. The last one is capillary force. This force refers to surface tension of water vapour. Controlling capillary force is important in AFM technique. By decreasing capillary force, the efficiency of AFM measurement is enhanced.

The force sensors in AFM consist of the micrometer-sized cantilever which has an extremely sharp tip located at the end of it. This tip is a couple microns long and less than 10 nm in diameter. The cantilever acts as a spring and has a spring constant which controls force and distance between the tip and the surface of sample. The interaction force can be determined by the deflection of the cantilever tip. Attractive force and repulsive force affect the deflection. As shown in Figure 3.3, the position of reflected beam is recorded and the deflections give information about the height of surface which can be used to generate a topography image.

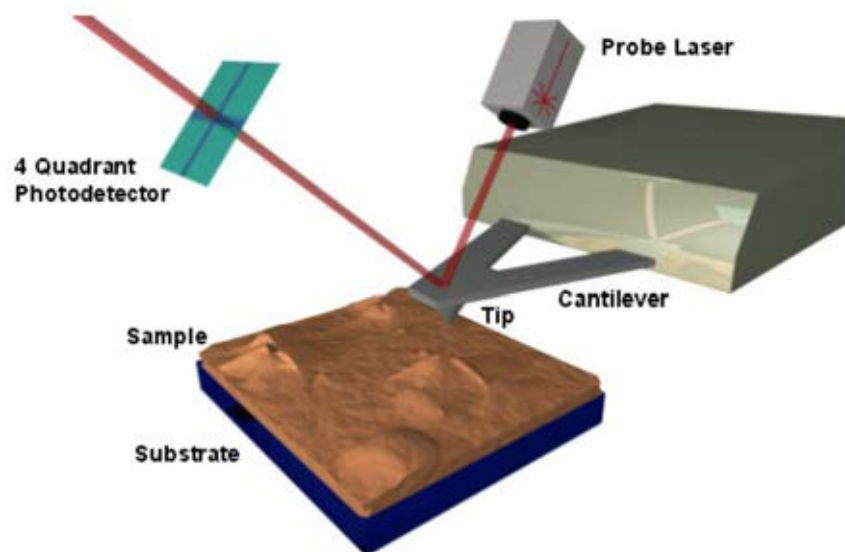


Figure 3.3 Schematic view of an atomic force microscope [59]

As shown in Figure 3.4 and Table 3.1, there are three imaging modes in AFM varied by the probe-sample separation; i.e. contact mode, non-contact mode and tapping mode.

3.2.1 CONTACT MODE

In contact mode, the spring constant of cantilever is less than that of the surface, and the cantilever bends. An image is obtained by maintaining a cantilever deflection. Contact mode is widely used in research because it can scan a small area and has a high speed scan. However, the cantilever tip always contact with the sample surface, which may be destroy a soft sample.

3.2.2 TAPPING MODE

The cantilever is oscillated at its resonant frequency in tapping mode. The tip lightly taps on the sample surface during scanning. When the tip vibrates at high frequency under attractive forces, the tip is closed to the sample, but not touching the surface. An image is obtained by maintain a constant oscillation amplitude. The force between the cantilever tip and sample is very low. Therefore, this mode is used for soft surface materials; e.g. polymers and biological materials.

3.2.3 NON-CONTACT MODE

In non-contact mode, the tip does not contact the sample surface, but it vibrates at high frequency under attractive Van der Waals force. An image is obtained by using a feedback loop to monitor amplitude changing. In this mode, a very low force exerts on the sample.

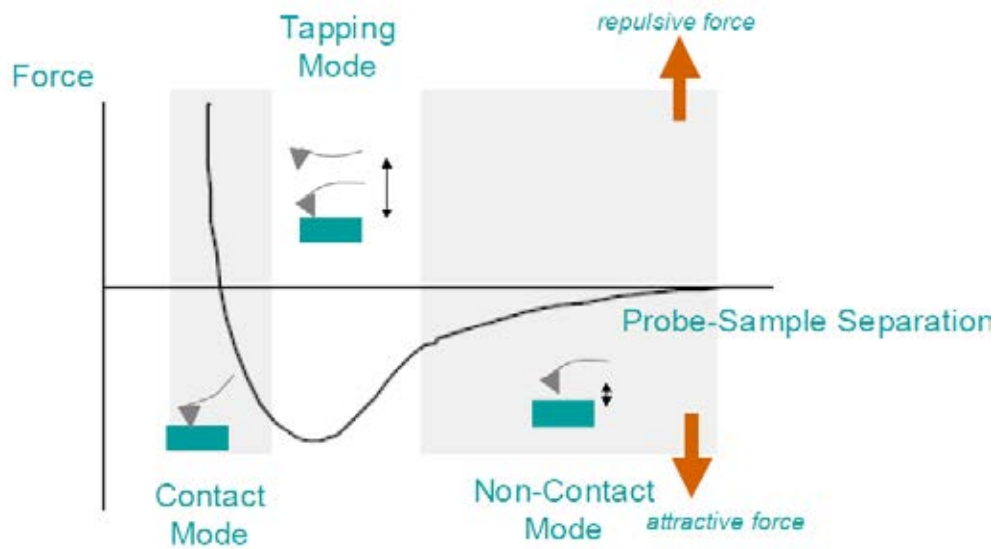


Figure 3.4 Plot of force as a function of probe-sample separation [60]

Table 3.1 Probe position, force on tip, advantages and disadvantages of each AFM image modes

Modes	Probe position	Probe-surface separation	Force on tip	Advantages	Disadvantages
Contact		< 0.5 nm	Repulsive	Fast scanning, good for rough samples and used in friction analysis	Damage or deform soft samples
Tapping		0.5 – 2 nm	Tapping	High resolution of samples and good for easily damaged samples	Slow scanning
Non-contact		0.1 – 10 nm	Attractive	Very low force exerted on the sample, extended probe lifetime.	Lower resolution and need ultra-high vacuum to get the best image

3.3 CONTACT ANGLE AND SURFACE TENSION MEASUREMENT

Analyzing surface energy and interfacial tension between materials are important in scientific research. Unfortunately, thermodynamic interactions are not directly measured. However, these interactions can be determined by studying surface property of materials. A series of liquid droplets, which are formed on the substrate, can estimate the surface tension by measuring the contact angle.

3.3.1 CONTACT ANGLE MEASUREMENT

Contact angle can be defined by an angle at the intersection between liquid-solid and liquid-air interfaces. Figure 3.5 shows the three-phase contact line (the interfaces of solid, liquid and air). If the contact angle is less than 90° , the surface wetting is favourable and liquid will spread over the surface. When the contact angle is greater than 90° , the surface wetting is unfavourable, thus liquid will reduce its contact with the surface and form a droplet.

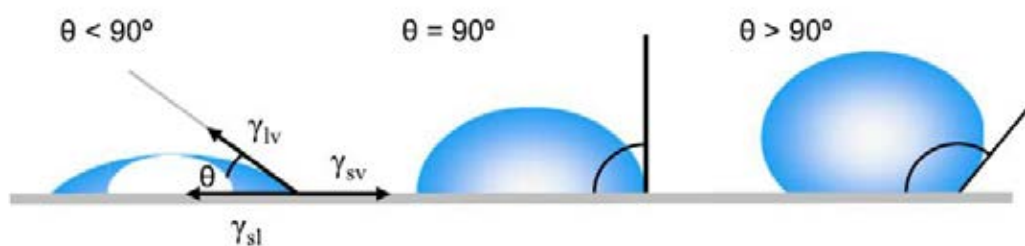


Figure 3.5 Illustration of contact angles on a smooth surface [61]

The most widely used technique to measure the contact angle is a direct estimation of tangent angle of a liquid droplet at the three-phase contact point. Telescope-goniometer is used to evaluate the contact angle of a liquid drop resting on the solid surface. The equipment consists of a stage to mount a substrate sample, a

micropipette to form a liquid droplet, an illumination source and a telescope with a protractor scale. The tangent of the sessile drop profile is simply aligned at the contact point with the surface. The contact angle can be read by the protractor through the eyepiece. The contact angle is calculated by diameter and height of the droplet, which is assumed to be part of a sphere, as shown in Eq. 3.2 and Figure 3.6 [61].

$$\frac{\theta}{2} = \tan^{-1}\left(\frac{h}{d}\right) \quad (\text{Eq. 3.2})$$

The advantages of this method are its simplicity and only a small amount of liquid is required. This method yields accurate results with an extremely small droplet.

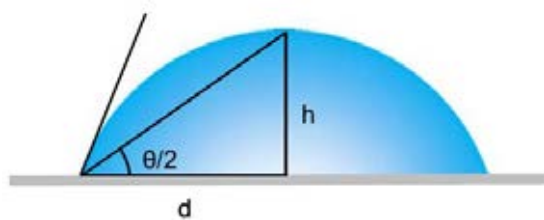


Figure 3.6 Demonstration according to Eq. 3.2 [61]

3.3.2 CALCULATION OF SURFACE TENSION

In pure liquid, molecules in a bulk are forced equally in every direction by neighboring molecules. A net force of each molecule is zero. However, some molecules which are located at the surface do not have neighboring molecules to balance a net force. Then, these molecules are pulled inward and created an internal force, as shown in Figure 3.7. The intermolecular force that contract the surface is called surface tension.



Figure 3.7 The unbalanced force of liquid molecules at surface causes the surface tension

Fowkes' method and, later, Owens and Wendt's method (or geometric-mean method) were used to calculate the surface tension by dividing the surface tension in two components; dispersive component and polar component [62, 63]. Fowkes proposed the dispersion component of the work of cohesion as

$$W_a^d = 2\sqrt{\gamma_{SV}^d \gamma_{LV}^d} \quad (\text{Eq. 3.3})$$

where γ_{LV} is the liquid surface tension and γ_{SV} is the solid surface tension. The interfacial tension between liquid and solid substrate interacting by London dispersion forces alone can be given as

$$\gamma_{SL} = \gamma_{SV} + \gamma_{LV} - 2\sqrt{\gamma_{SV}^d \gamma_{LV}^d} \quad (\text{Eq. 3.4})$$

By combining Fowkes' equation with Young's equation (Eq. 3.2), The Young-Fowkes equation is obtained as expressed in

$$\gamma_{LV} \cos\theta = -\gamma_{LV} + W_a^d \quad (\text{Eq. 3.5})$$

A new surface free energy expression proposed by Owen and Wendt can be represented by

$$W_a = 2\left(\sqrt{\gamma_{SV}^d \gamma_{LV}^d} + \sqrt{\gamma_{SV}^p \gamma_{LV}^p}\right) \quad (\text{Eq. 3.6})$$

When combined with Young-Fowkes equation, one obtained

$$\gamma_{LV}(1 + \cos\theta) = 2\left(\sqrt{\gamma_{SV}^d \gamma_{LV}^d} + \sqrt{\gamma_{SV}^p \gamma_{LV}^p}\right) \quad (\text{Eq. 3.7})$$

Therefore, the total free surface energy is sum of the two components as shown in

$$\gamma_{SV} = \gamma_{SV}^d + \gamma_{SV}^p \quad (\text{Eq. 3.8})$$

Owens and Wendt selected only two liquids (polar and non-polar liquids to form droplets on the surface and measured the contact angle. The recommended liquids were methylene iodine (or diiodomethane) and water, which represent a non-polar and a polar component, respectively. In our study, surface energy of the substrate can be calculated by using Eq. 3.7. Contact angle (θ) of diiodomethane and water are measured. The liquid tension values of water ($\gamma_{water} = 72.7 \text{ mJ/m}^2$, $\gamma_{water}^d = 21.8 \text{ mJ/m}^2$, $\gamma_{water}^h = 50.9 \text{ mJ/m}^2$) and diiodomethane ($\gamma_{diiodomethane} = 50.0 \text{ mJ/m}^2$, $\gamma_{diiodomethane}^d = 0 \text{ mJ/m}^2$) were used in this study [62].

3.4 MEASUREMENT OF FILM THICKNESS BY ELLIPSOMETRY

Ellipsometry is a measurement technique to obtain optical properties of a sample material by using the reflected light. Knowledge of the linearly polarized light is utilized. At an oblique sample, the linearly light incidences to a surface and changes polarization state when it reflect. Then, the incident light is polarized. Ellipsometry can be used to characterize composition, roughness and other properties of sample. Ellipsometry is also used to measure the thickness of thin film, which is located on top of a substrate. A schemetic of ellipsometry in Figure 3.8 shows that the incident light is partially reflected and partially transmitted the surface.

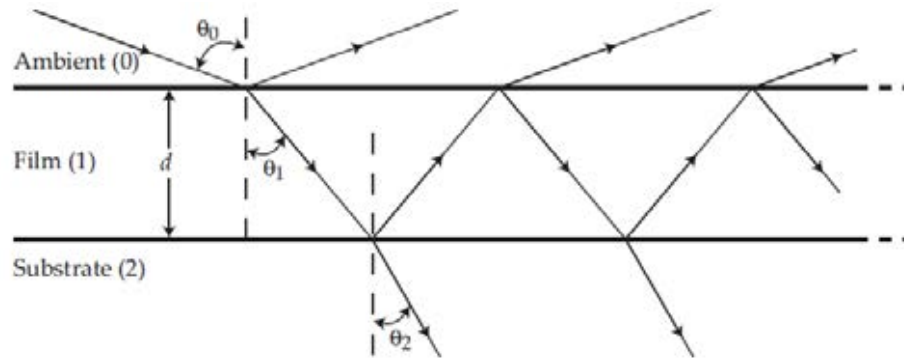


Figure 3.8 Illustration of an ambient-film-substrate optical system.

The Incident light is partially reflected and partially transmitted [64].

Ellipsometry measures the change of polarization upon reflection or transmission and compares it with a model. By analyzing the reflected light, we can obtain the information of materials. If we know the refractive indexes of film and substrate, the thickness of the film can be calculated by using the Fresnel formula [65].

$$\beta = \frac{2\pi}{\lambda} n_f d_f \quad (\text{Eq. 3.9})$$

λ is the wavelength, n_f is the refractive index of film and d_f is the thickness of thin film. β is the phase thickness of the film and is given by

$$r = \frac{r_1 + r_2 \exp(-2i\beta)}{1 + r_1 r_2 \exp(-2i\beta)} \quad (\text{Eq. 3.10})$$

where r_i is the amplitude reflectance at the i th interface. This technique widely used to investigate a thin film thickness (less than a nanometer to several micrometers).

3.5 PARTICLE SIZE DISTRIBUTION BY LIGHT SCATTERING

Measurement of particle size distribution in a solution is based on the principle of the intensity of light scattered. There are two types of the light scattering techniques; static light scattering and dynamic light scattering.

3.5.1 STATIC LIGHT SCATTERING

Static light scattering (SLS) is the technique that extracts particle size information from intensity of the scattering pattern at various angles [66]. When a group of particle is irradiated with a laser beam, the scattered pattern is generated spatially, as shown in Figure 3.9. The intensity of scattered light at different angles depends on the particle size. If a particle is large comparing with the wavelength of light, the light can scatter from different parts of particle and can lead to destructive interference. The destructive interference reduces the intensity of the scattered light. Therefore, the large particle scattering diagram shows that the back scattering intensity is much less than the forward scattering intensity.

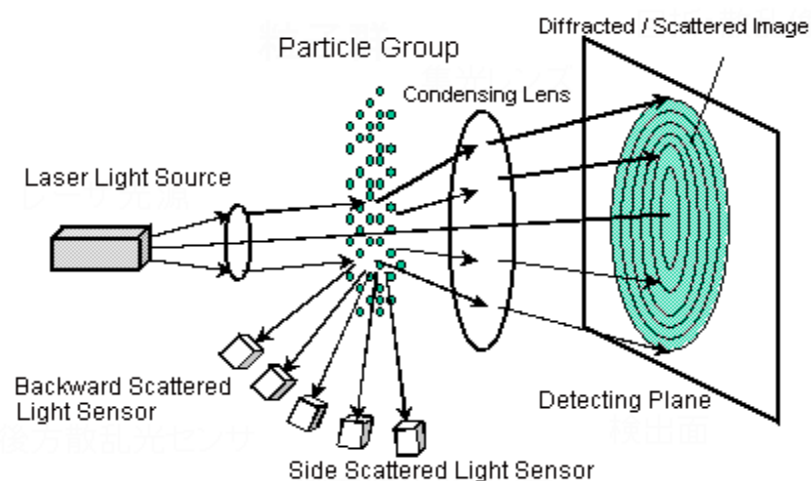


Figure 3.9 Optical system of a static light scattering [67]

3.5.2 DYNAMIC LIGHT SCATTERING (DLS)

Dynamic light scattering (DLS) is the technique that measures Brownian motion which relates to the size of the particles. This measurement is concerned with time fluctuations in intensity due to the motions of particles. The laser light illuminates the sample in the cell, as shown in Figure 3.10. Detectors collect the scattered light signal. The random changes of the light scattering intensity, which are due to the random position of the particles, can be used to determine particle size in a suspension.

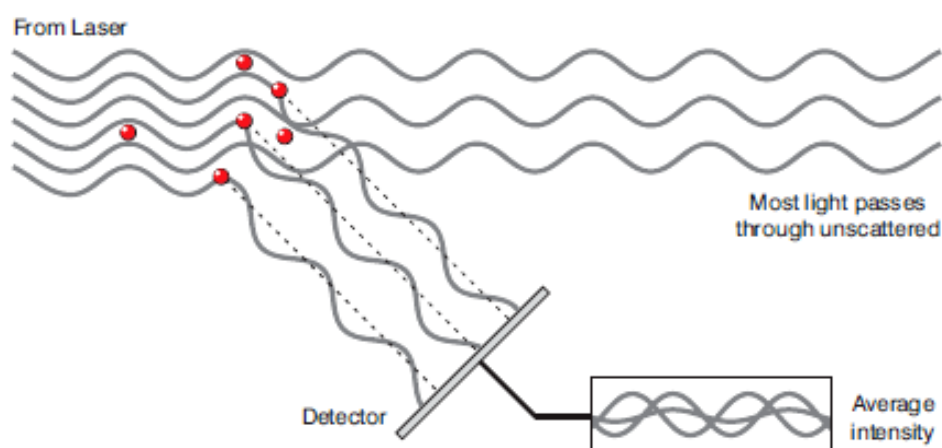


Figure 3.10 Dynamic light scattering (DLS) layout [68]

Brownian motion is the movement of particles caused by the random collision between liquid molecules surrounding the particles. The particle size can be defined by the Stokes-Einstein equation.

$$D_h = \frac{k_B T}{3\pi\eta D_t} \quad (\text{Eq. 3.11})$$

Where: D_h is the particle size, k_B is the Boltzmann's constant, T is the temperature, η is the dynamic viscosity and D_t is the translational diffusion coefficient. From the equation. The relationship between particles size and particle viscosity is obtained. The important of Brownian motion for dynamic light scattering is that smaller particles move faster than larger particles.

3.5.3 ZETA POTENTIAL MEASUREMENT

Zeta potential relates to charge at particle surface in a specific liquid medium. The zeta potential value of surface is generally use for understanding and predicting an interaction between particles in solution. The charge affects an ionic environment in the region nearby the surface of particle. This ionic environment is described by using a double layer model. The stern layer of ions strongly attached close to the particle surface and the diffuse layer of ions is further away from the particle surface. However, the diffuse layer still attracts to the particle, thus the ions move with the particle. The slipping plane, as shown in Figure 3.11, is the boundary between the electric double layer and the ions in the solution. The zeta potential is the charge measured at the slipping plane.

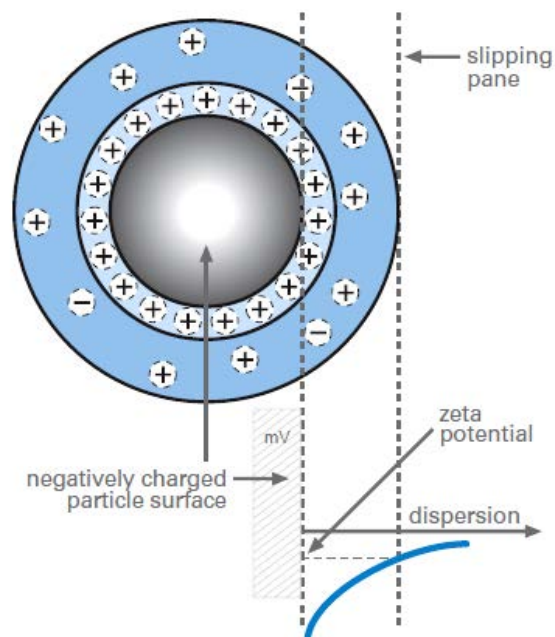


Figure 3.11 Double layer model and zeta potential measured at the slipping plane [69]

To measure the zeta potential, using electrophoresis technique, two electrodes are inserted into a cell containing a small quantity of solution. When the electric field is applied, the particles move to either anode or cathode depending on their surface charge. The direction of the particle motion indicates whether the surface is positively or negatively charged. Moreover, the speed of the particle motion can be used to calculate the magnitude of the charge.

Figure 3.12 shows the optical setup for measuring zeta potential utilizing light scattering technique. The laser light illuminates the particles and, therefore, the particles scatter the light. The scattering beam is mixed with a second beam in order to extract the frequency shift in the scattering light. The magnitude of the frequency shift is used to determine the particle velocity.

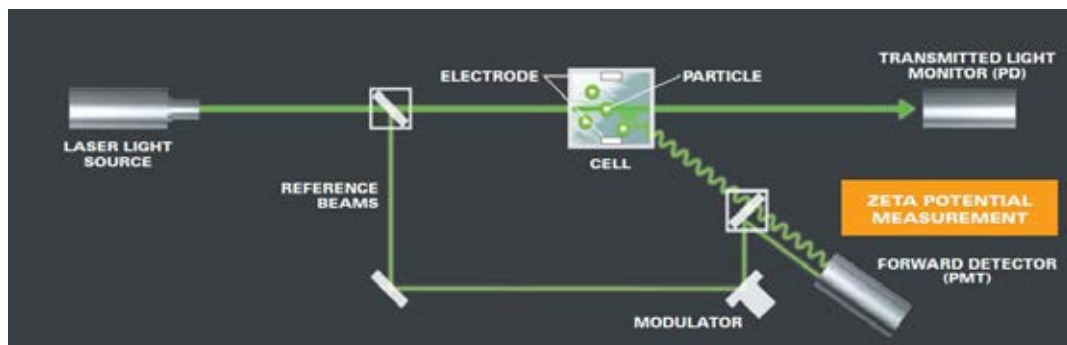


Figure 3.12 Optical diagram for zeta potential [69]

3.6 TRANSMISSION ELECTRON MICROSCOPY

Transmission electron microscopy (TEM) is a technique using electron beam transmits and interacts with an ultra-thin specimen. TEM operates much like an optical microscope, but it uses electrons instead of visible light [70]. This instrument generates material microstructure images with high magnification and high resolution. The important components of transmission electron microscope are electron source, condenser lenses, objective lenses, projector lenses and specimen stage, similar to optical microscope, as shown in Figure 3.13. Since electrons are used instead of light,

this microscope needs additional features such as vacuum environment which is used to prevent the collision between high energy electrons and air molecules.

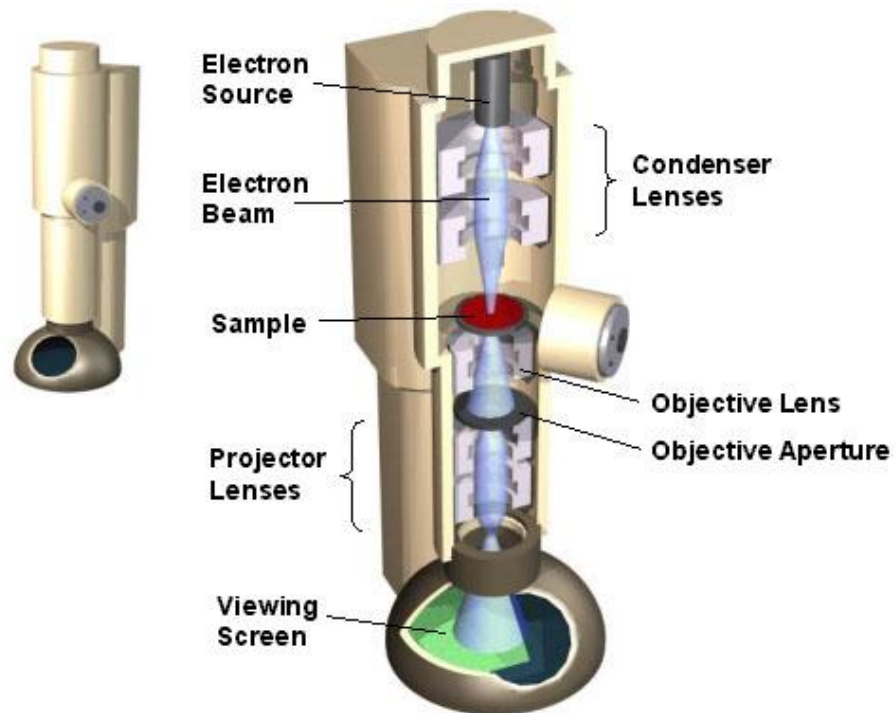


Figure 3.13 The layout of Transmission Electron Microscope [59]

In TEM system, electron beam with high energy is generated by an electron gun. Since an image resolution is determined by electron energy, the resolution of an image depends on the acceleration voltage. Electron gun is composed of the three main part, cathode, anode and Wehnelt electrode. Electrons are emitted from cathode and accelerated by an electric field to anode. Wehnelt electrode, which is placed between cathode and anode, is biased a few hundred volts negative in order to stabilize the electron beam. Glass lenses are not suitable for using in TEM because glass does not focus the electron beam. Magnetic force is used in this case because a magnetic field affect electron charge and then electron beam can be focused. Subsequently, all lenses

in transmission electron microscope are electromagnetic. A thin foil must be used as a specimen of TEM because it allows electron transmission. The thin specimen is mounted in a specimen holder while operating the instrument. Electrons which are collimated from the lenses pass through the sample. The resulting patterns of electron transmission and absorption are magnified on a viewing screen.

CHAPTER IV

EXPERIMENTAL PROCEDURE

4.1 MATERIALS

4.1.1 POLYSTYRENE MATRIX

Polystyrenes (PS) with narrow size distribution listed in Table 4.1 were used as polymer matrix in our study. Chemical structure of PS is shown in Figure 4.1. All PS were purchased from Polymer Source Inc. (Canada).

Table 4.1 Polystyrenes with various molecular weights were used as matrix.

Polystyrene	M_w (g/mol)	M_n (g/mol)	M_w/M_n
PS11K	11,900	11,500	1.04
PS33K	34,300	33,000	1.04
PS52K	55,500	52,000	1.07

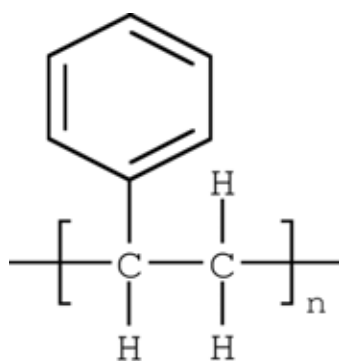


Figure 4.1 Chemical structure of PS

4.1.2 POLYMER ADDITIVES

4.1.2.1 HIGHLY BRANCHED AROMATIC MOLECULES

Two structures of highly branched aromatic molecules (HBA) used in this study, HBA1 and HBA2 were synthesized by Promarak V. [71]. The chemical structures of HBAs are shown in Figure 4.2. The concentrations of HBAs additives in PS matrix were 0, 0.5, 1, 2 and 5 wt.%.

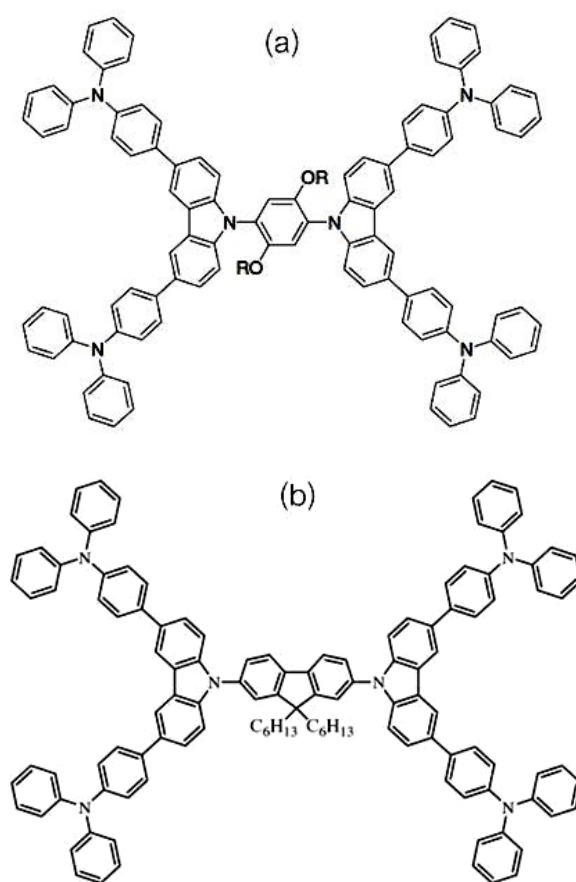


Figure 4.2 Chemical structures of highly branched aromatic molecules

(a) HBA1 and (b) HBA2

4.1.2.2 THREE-ARM POLYSTYRENE ADDITIVES

Two different chain lengths of three-arm polystyrene (TA-PS) used in this study are TA-PS19 (M_n of branch = 18,900 g/mol, $M_w/M_n = 1.09$) and TA-PS110 (M_n of branch = 109,800 g/mol, $M_w/M_n = 1.09$) (Polymer Source Inc. (Canada)). The concentrations of TA-PS additives in PS matrix were varied from 0 – 100 wt.%. The chemical structure of TA-PS is shown in Figure 4.3.

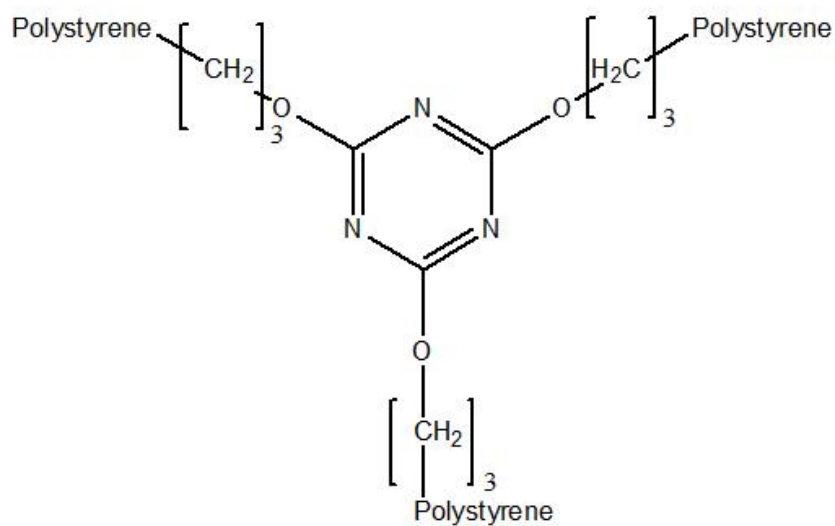


Figure 4.3 Chemical Structure of TA-PS

4.1.3 NANOPARTICLE ADDITIVES

Titanium dioxide (TiO_2) and zinc oxide (ZnO) with diameter sizes < 25 and < 20 nm, respectively, were used in this experiment. The nanoparticles were purchased from Sigma-aldrich. TEM (JEM-2100, JEOL Ltd., Japan) micrographs of TiO_2 nanoparticles and ZnO nanoparticles are shown in Figure 4.4 and Figure 4.5. Suspensions of both nanoparticles in toluene were prepared by using ethanol as a dispersant. Nanoparticles suspensions were mixed with PS at the concentrations of 0.05, 0.10 and 0.20 wt.%.

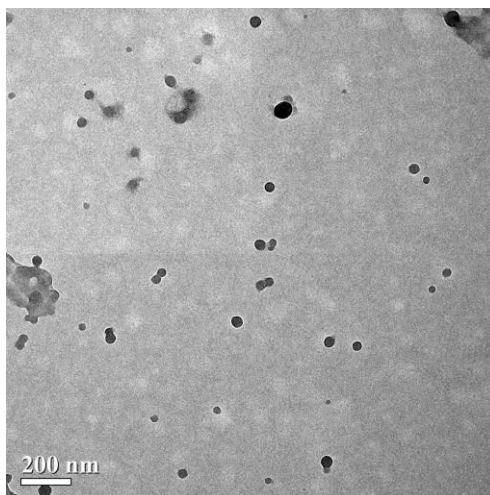


Figure 4.4 TEM micrograph of TiO_2 nanoparticles

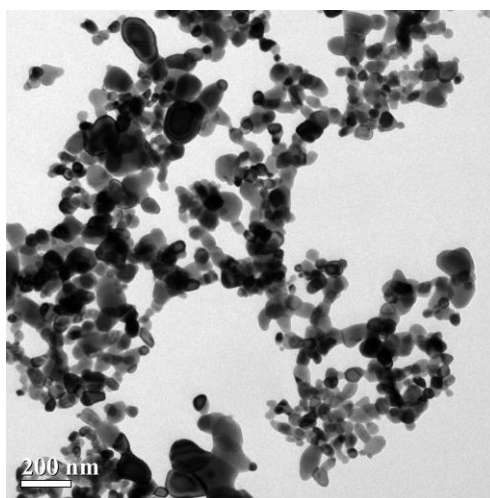


Figure 4.5 TEM micrograph of ZnO nanoparticles

TiO₂ and ZnO nanoparticles possess the difference in surface properties. This could affect their ability to suppress dewetting and cause variation in improvement of polymer film stability. Surface properties of TiO₂ and ZnO nanoparticles are studied using electrophoresis (Brookhaven, ZetaPaLs). Suspensions of TiO₂ and ZnO nanoparticles in deionized water are prepared at various pHs. Zeta potential of TiO₂ and ZnO nanoparticles are measured. The plot between zeta potential and pH of suspension is shown in Figure 4.6.

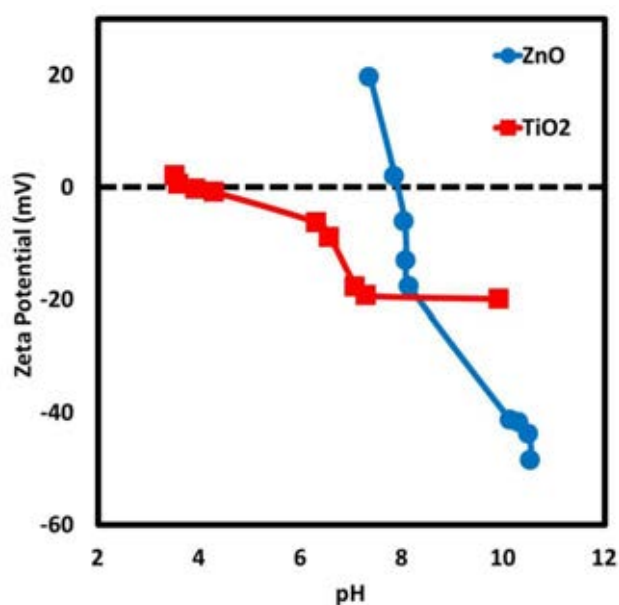


Figure 4.6 Zeta potential versus pH of ZnO and TiO₂ nanoparticles dispersed in water (● ZnO and ■ TiO₂).

4.2 THIN FILM PREPARATION

Cleaned silicon wafers (SiO_x/Si) were used as substrates in our experiments. Silicon substrates were soaked in a 7:3 v/v solution of conc. H_2SO_4 and 30% H_2O_2 at about 80°C for 1 h. The substrates were rinsed with deionized water for several times and were dried by pressurized nitrogen gas. Freshly cleaned substrates were used for coating of polymer thin films. Since all substrates were cleaned by using the same conditions, compositions on the substrate surface were expected to be the same.

Thin films on SiO_x/Si were prepared by spin casting from 0.1 – 5.0 wt.% solutions in toluene (yielding thicknesses of about 7 - 265 nm, respectively, as shown in Table 4.2). Three samples were prepared for each condition. The spinning rate was kept constant at 1000 rpm for 10 s. The film thickness was measured by ellipsometry (Gaertner Scientific Corporation) and atomic force microscopy (AFM, SPI3800N Nanoscope II, Seiko Instrument Inc., Japan). For AFM technique, needles (Hypodermic needle regular wall, NIPRO) with diameter of 0.4 mm and length of 25 mm were immersed in toluene and used to make a scratch on the polymer thin film. The surface analysis software was used to measure film thickness by scanning a scratch in straight line. The differential in vertical axis was determined as film thickness.

Table 4.2 Film Thickness of each concentration

Concentration of PS in toluene (wt.%)	Thickness (nm)
0.1	~ 7
0.3	~ 23
0.5	~ 30
2.0	~ 100
5.0	~ 265

4.3 THIN FILM CHARACTERIZATION

4.3.1 SURFACE ENERGY

In this study, surface energies of PS, HBAs, TA-PS and SiO_x/Si were measured following the Owens–Wendt–Kaelble approach by using (Eq. 3.7), and shown in Table 4.3. Contact angles (θ) of diiodomethane and water were measured on each surface by using goniometer (CAM-PLUS Tanteq, U.S. Patent, USA). The amount of solvents in the droplets was controlled to be the same by using a syringe. Averaged values of contact angles obtained from at least 5 measurements were used in the calculation of surface energies. The surface energies of PS and SiO_x/Si were consistent with the literature values [9].

Table 4.3 Contact angles of water and diiodomethane on different surfaces and their solid surface tension components calculated by using simultaneous equation of the Owens-Wendt-Kaelble approach

Type of surfaces	θ_{water}	$\theta_{diiodomethane}$	$\gamma_s^d (mJ/m^2)$	$\gamma_s^h (mJ/m^2)$	$\gamma_s (mJ/m^2)$
Silicon	46±1	39±1	39.6±0.6	20.6±0.3	60.2±0.9
Polystyrene	94±2	21±2	46.8±0.5	0.1±0.1	46.9±0.6
HBA1	91±6	29±4	43.8±1.8	0.7±1.0	44.5±2.8
HBA2	93±4	29±4	43.9±1.6	0.9±0.9	44.8±2.5
TA-PS19	92±2	23±2	46.0±0.7	0.2±0.1	46.2±0.8
TA-PS110	91±2	24±2	45.7±0.6	0.3±0.2	46.0±0.8

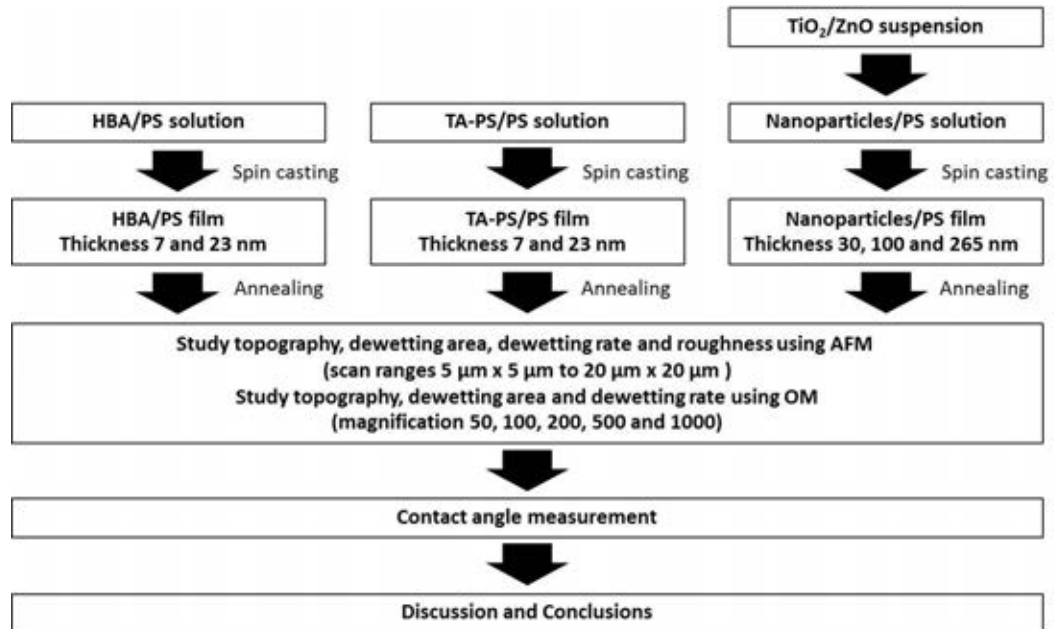
4.3.2 SURFACE TOPOGRAPHY

AFM and optical microscopy (OM, OLYMPUS PX 60M equipped with digital camera OLYMPUS model DP12) were used to study the surface topography of polymer film. AFM operating in a dynamic contact mode provided three dimensional images of sample which represented the topography of the sample. Spring constant of the Si_3N_4 cantilever was about 20 N/m. The AFM measurements were performed under ambient conditions. Scan sizes were varied from about 5×5 to $25 \times 25 \mu\text{m}^2$. Moreover, surface topography was examined by OM. With lower magnification of OM, the technique could investigate the surface by the larger area. Optical micrographs were recorded under reflectance mode with the magnification of 50X - 1000X.

The dewetting behaviors of polymer thin films were induced by annealing the samples in a vacuum oven for different periods of time at 115 - 190 °C depending on their thickness. These annealing temperatures were above the glass transition temperature (T_g) of the PS film [11]. The annealed films were quenched to room temperature. Global structure of the films at different annealing time was investigated using OM. The evolution of local structure upon the annealing was followed by AFM. Hole diameter and hole depth were determined, then dewetting area and roughness were analyzed by using AFM software. The dewetting areas were measured by using commercial graphical analysis software, Adobe Photoshop program. The percentage of dewetting area was calculated by using the following equation;

$$\text{dewetting area (\%)} = (\text{dewetting area} \div \text{total area}) \times 100 \quad (\text{Eq. 4.1})$$

4.4 EXPERIMENTAL DIAGRAM



CHAPTER V

RESULTS AND DISCUSSIONS

5.1 HIGHLY BRANCHED AROMATIC MOLECULES

In this section, we introduce a new class of highly branched aromatic molecules (HBAs) as dewetting inhibitors of PS ultrathin films. Chemical structures of these HBAs shown in Figure 1.1 are rather different from the dendrimers and HBPs used in the previous studies [25, 72]. They constitute of high number of aromatic cores with alkoxy or alkyl chains attached to the center. Although the nitrogen and oxygen heteroatoms are present in the HBAs, their surface energies are comparable to that of PS films (see Table 4.3) The aromatic groups and alkyl chains are expected to provide favourable interactions with phenyl group and aliphatic chain of PS, respectively. Therefore, these HBAs behave as anchoring sites or physical cross-linking points for PS chains within the entire film. The effects of film thickness, PS molecular weight, and HBA structure are investigated in details.

Samples of PS and HBAs are prepared by spin-casting from 1 wt.% solutions, which provides relatively thick films. All films are left in vacuum oven at room temperature for several hours to allow complete evaporation of toluene solvent. Droplets of water or diiodomethane are deposited on top of each film. Averaged contact angles of these solvents on all films are used to calculate surface energies according to Owens-Wendt-Kaelble approach [73]. The obtained results are shown in Table 4.3. The HBA1 and HBA2 exhibit surface energies comparable to that of the PS. The slight increase of polar component is within error bars of the measurements. Therefore, the HBAs are expected to distribute randomly within the entire PS films as illustrated in Figure 1.1. Since the molecules of HBAs constitute aromatic and alkyl moieties, we believe that the $\pi - \pi$ and dispersive interactions contribute to intermolecular forces

between these molecules and PS chains. However it is not trivial to prove the existence of these interactions. Chemical structures at center position of HBA1 and HBA2 are also different. This may cause the variation of dewetting behaviors from the two systems. We note that the concentration of HBAs is limited at 5 wt.% to avoid the effect of phase separation. The absence of phase separation within all PS films is, in fact, confirmed by AFM measurements.

5.1.1 EFFECT OF HBA1 IN PS11K FILMS

In the first section, we demonstrate the improvement of PS film stability upon addition of HBA1 into the system. PS11K films with thicknesses of about 7 and 23 nm are used while the concentration of HBA1 ranges from 0 to 5 wt.%. AFM measurements of all non-annealed films reveal smooth surface with no holes. OM images also show homogeneous films. To minimize experimental errors, all films are annealed at the same time in vacuum oven. The annealing temperature is 120 °C, which is above the glass transition temperature (T_g) of PS11K [11]. The glass transition of HBA1 occurs at 121 °C [71]. Therefore, this annealing condition allows segmental movement of PS chains. The segmental movement of HBA1 may also occur at this condition because the molecules are diluted in the PS matrix. Figure 5.1 shows morphological change of the 7 nm thick films upon increasing the annealing time. The annealing of pure PS11K film for 60 min leads to the formation of large holes and polymer droplets. Total film breakup occurs when the annealing time reaches 90 min. At final stage of the dewetting, the polymeric film transforms into hemispherical droplets, which randomly distribute the SiO_x/Si substrate.

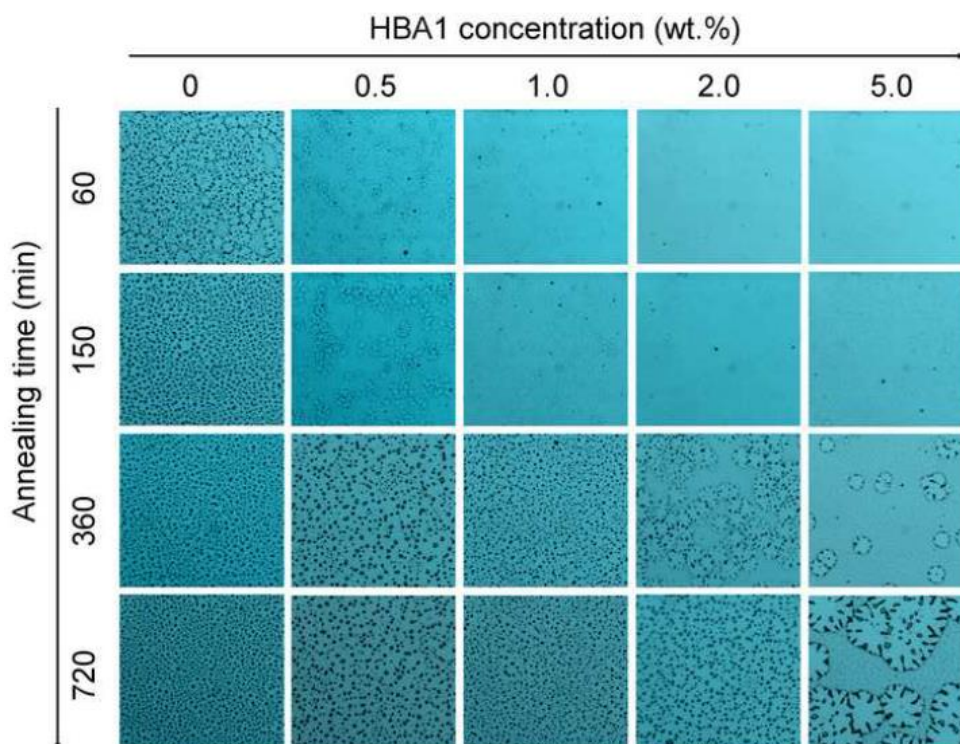


Figure 5.1 Optical micrographs of 7 nm thick PS11K films containing different concentrations of HBA1 annealed at 120 °C for 60, 150, 360, and 720 min. Size of each image is 60 μm x 60 μm .

Dewetting rate of the 7 nm thick PS11K film is suppressed significantly when a small amount of HBA1 is added into the system. The annealing of PS11K film containing only 0.5 wt.% of HBA1 for 150 min still does not cause total dewetting. The formation of some holes is observed, corresponding to an intermediate stage of the dewetting. At this condition, dewetting area of the film is about 50% (see Figure 5.2 (a)). The increase of HBA1 concentration to 1 wt.% causes the drop of dewetting area to about 20%. We do not detect any holes in the PS11K films containing 2 and 5 wt.% of the HBA1. The growth of some holes is observed in these films when the annealing time is increased to 360 and 720 min. These results indicate that thermal stability of the 7 nm thick PS11K film systematically increases upon addition of HBA1 into the system. The plots between dewetting area versus annealing time in Figure 5.2 (a) clearly demonstrates our major finding. Slopes of the plots reflect dewetting rates of each system. It is obvious that the

PS11K film containing 5 wt.% of HBA1 is much more stable than pure PS11K film. The annealing of this film for 12 h causes about 40 % of dewetting area while total dewetting of pure PS11K film occurs at 1.5 h. Figure 5.2 (b) shows systematic decrease of dewetting area upon increasing HBA1 concentration, indicating that the HBA1 is an efficient dewetting inhibitor. We note that the dewetting mechanism of PS films is not affected by the existence of HBA1 molecules. In general, the dewetting process can take place via spinodal and heterogeneous nucleation mechanisms, arising from interfacial thermal fluctuation or the heterogeneity of substrate surface energy, respectively [74-76]. The spinodal one leads to the formation of correlated holes while the heterogeneous nucleation yields random hole distribution. Since the position of holes detected in all systems is random (see Figure 5.1), dewetting process of the PS films takes place via a heterogeneous nucleation mechanism. The observation of fingering pattern in the film containing 5 wt.% HBA1 arises from the increase of film viscosity. Similar result was observed by Reiter [3] where the fingering pattern was detected upon increasing molecular weight of PS (i.e. increase of film viscosity).

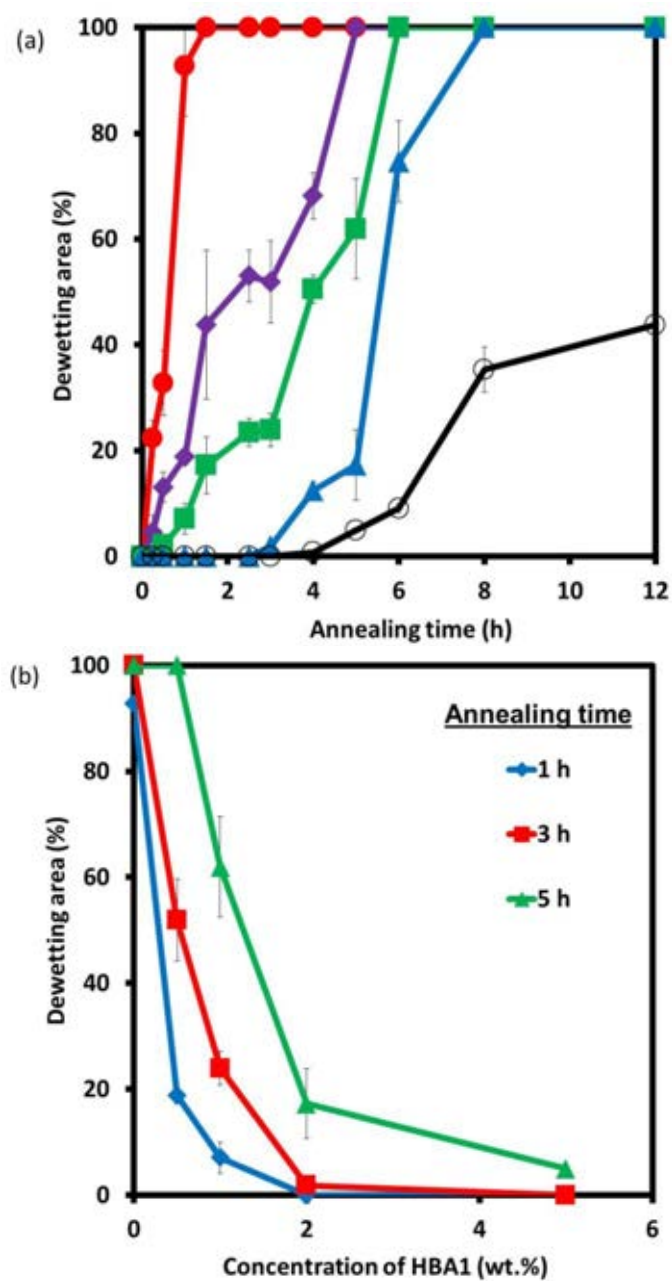


Figure 5.2 (a) Dewetting area versus annealing time of 7 nm thick PS11K films annealed at 120 °C. Concentrations of HBA1 are (●) 0 wt.%, (◆) 0.5 wt.%, (■) 1.0 wt.%, (▲) 2.0 wt.%, and (○) 5.0 wt.%. (b) Dewetting area of PS/HBA1 films versus ratio of HBA1.

The evolution of film morphologies in local scale is followed by AFM as shown in Figure 5.3. The formation of small holes is detected in all films at 30 min of the annealing, which corresponds to an early stage of the dewetting. Depth and diameter of these holes systematically decrease upon increasing the HBA1 concentration. The increase of annealing time leads to the expansion of holes, which eventually merge into each other to form polygonal structure. In final stage of dewetting, the polygons disintegrate into hemispherical droplets. At equilibrium state, the contact angles of these polymeric droplets on solid substrate vary with interfacial tension [73]. Table 5.1 clearly shows that hole expansion systematically decreases upon increasing HBA1 concentration. At 150 min of the annealing, different dewetting stages are observed depending on HBA1 concentration within the film. Interestingly, we observe the formation of many circular hills in the films containing 2 and 5 wt.% of HBA1. These circular hills are observable by OM as well. This cannot be attributed to phase separation of HBA1 because of its relatively low concentration. We suggest that HBA1 molecules behave as anchoring sites or physical cross-linking points for PS chains within the film. At this condition, the HBA1 molecules pull PS chains into each other, resulting in the formation of circular hills. Some holes are still observed within the films. An increase of annealing time to 720 min transforms the film into polymeric droplets. To reach equilibrium state of the droplets, the annealing time is further increased to 24 h. Contact angles of each droplet are measured by utilizing line profile analysis of AFM images. We do not detect any significant variation of the contact angles measured from each system. This result indicates that the interfacial interaction is hardly affected by the addition of HBA1. The increase of viscosity, arising from physical cross-linking between PS chains and HBA1 molecules, is believed to be major reason for the improvement of film stability. Our hypothesis is similar to the sulfonated polystyrene system where the existence of physical cross-linking results in the increase of bulk viscosity and hence the improvement of film stability [13]. Unfortunately, we cannot measure bulk viscosity of our system because it requires relatively large amount of HBA1. To obtain sufficient amount for the experiment, one needs several synthetic batches of the HBA1 [71].

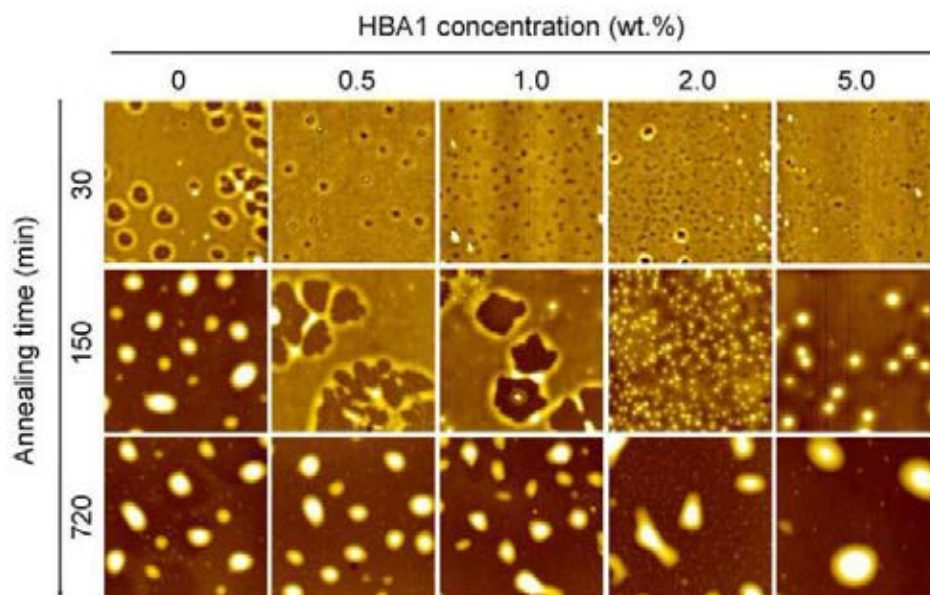


Figure 5.3 AFM topography images of 7 nm thick PS11K films containing different concentration of HBA1 annealed at 120 °C for 30, 150 and 720 min. Size of the images is 10 μm x 10 μm .

Table 5.1 Hole depth and hole width of 7 nm-PS11K films containing different concentration of HBA1 annealed at 120 °C for 30 min

HBA1 conc.	0 wt.%	0.5 wt.%	1.0 wt.%	2.0 wt.%	5.0 wt.%
Hole depth (nm)	2.92 ± 0.27	1.81 ± 0.20	1.79 ± 0.09	1.40 ± 0.13	1.20 ± 0.10
Hole width (nm)	904.5 ± 132.7	286.8 ± 26.1	239.9 ± 42.8	200.6 ± 59.2	179.6 ± 10.0

5.1.2 EFFECT OF FILM THICKNESS

In the previous studies of our research group, it was observed that the presence of some foreign moieties or molecules in system led to either the increase or decrease of film stability, depending on thickness [11, 57]. For example, the stability of 5 nm thick film increases significantly when 5 mol% of chloromethylstyrene groups is chemically incorporated into PS chain [11]. The increase of film thickness to 22 nm, however, causes an opposite result. This mainly arises from surface anchoring effect of the

foreign group, which diminishes upon increasing the film thickness. In the relatively thick film, the incompatibility between different moieties drives the dewetting process. Here, we investigate the efficiency of HBA1 as a dewetting inhibitor upon increasing PS11K film thickness to 23 nm. The nucleation process of holes in the 23 nm thick film is quite different from that of the 7 nm thick film. AFM measurement reveals that a number of holes detected in an early stage of the dewetting are much lesser in the thicker film. This discrepancy is attributed to an interfacial effect, which becomes more pronounced upon decreasing film thickness. In the 7 nm thick film, slight difference of surface energies on solid substrate may lead to the nucleation of holes while it requires higher magnitude of the perturbation in the thicker film.

Figure 5.4 shows OM images of the 23 nm thick films containing different concentrations of HBA1. Dewetting rates of these films are much slower than those of the 7 nm thick films. Total dewetting of pure PS11K film occurs at 12 h of the annealing at 120 °C. Similar to the system of 7 nm thick film, the addition of HBA1 results in systematic increase of the film stability. It is clearly observed from OM images recorded at 6 h of the annealing where the dimension and number of holes changes with HBA1 concentration. Our results are further illustrated by plotting the dewetting area as a function of annealing time as shown in Figure 5.5. Slopes of the plots systematically decrease upon increasing the HBA1 concentration. An increase of annealing time to 24 h still does not cause total dewetting of the film containing 5 wt.% of HBA1. These results show that the HBA1 can also be used as a dewetting inhibitor for the 23 nm thick film. This further supports our earlier hypothesis that the improvement of PS film stability arises from the increase of physical cross-linking within the system. This effect persists upon increasing the film thickness. The change of interfacial interaction due to the presence of HBA1 is expected to play lesser role. It is worthwhile to note that the formation of circular hills is also detected in the films containing 5 wt.% of HBA1. However, their number density is much smaller compared to the 7 nm thick film.

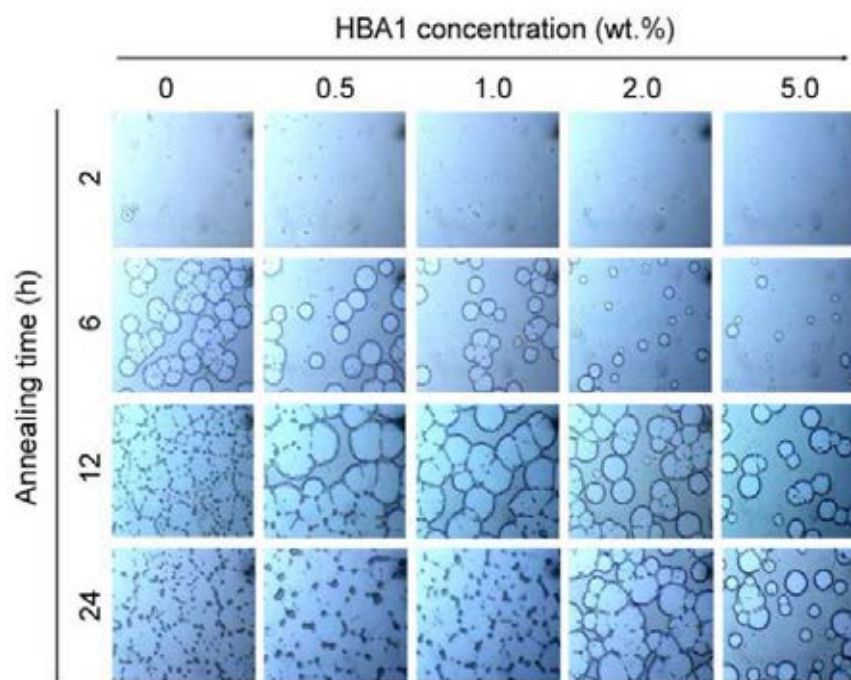


Figure 5.4 Optical micrographs of 23 nm thick PS11K films containing different concentrations of HBA1 annealed at 120 °C for 2, 6, 12 and 24 h. Size of each image is 100 μm x 100 μm .

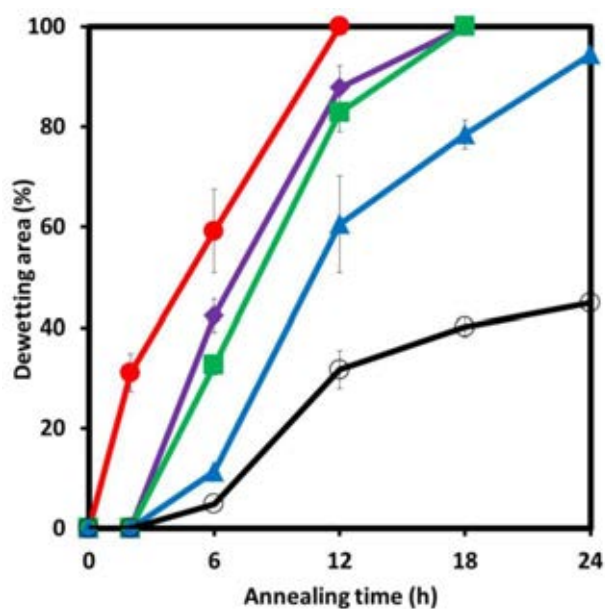


Figure 5.5 Dewetting area versus annealing time of 23 nm thick PS11K films annealed at 120 °C. Concentrations of HBA1 are (●) 0 wt.%, (◆) 0.5 wt.%, (■) 1.0 wt.%, (▲) 2.0 wt.% and (○) 5.0 wt.%.

5.1.3 EFFECT OF PS MOLECULAR WEIGHT

It is known that the entanglement of PS chains occurs when their molecular weights are increased above 18K [77, 78]. Therefore, the PS11K chains, investigated in the previous sections, behave as a simple liquid in the melt state. This allows us to observe significant improvement of film stability upon the addition of HBA1 into the system. An increase of PS molecular weight above 18K leads to chain entanglement, which in turn causes an increase of its viscosity [77, 78]. The increase of film stability upon increasing molecular weight is similar to the influence of HBA1 additive. In this section, the effectiveness of HBA1 as a dewetting inhibitor is compared to the increase of PS chain entanglement. Thin films of PS33K with thickness of 7 nm and 23 nm are prepared in a similar fashion. The concentration of HBA1 within the films is varied from 0 to 5 wt.%. The efficiency of HBA1 as a dewetting inhibitor for these films is also investigated.

Morphological changes revealed by AFM of the 7 nm thick films upon increasing the annealing time are shown in Figure 5.6. Dewetting mechanism of the PS33K films is similar to that of the PS11K films [11]. Hole sizes decrease upon increasing HBA1 concentration, as shown in Table 5.2. The dewetting rate, however, is much slower. This is illustrated in the plots of dewetting area versus annealing time in Figure 5.7. The annealing of pure PS33K film at 120 °C for 2 h causes about 30% of the dewetting. At this condition, total dewetting already occurs in the system of pure PS11K film (see Figure 5.1 and Figure 5.2 (a)). To reach total dewetting state of pure PS33K film, it requires about 9 h of the annealing. The addition of 0.5 and 1 wt.% HBA1 into PS11K films causes the increase of film stability. However, their dewetting rates are still faster than that of pure PS33K film. When the concentration of HBA1 is increased to 2 wt.% the dewetting rate of PS11K film is comparable to that of the pure PS33K film. At this condition, the influence of HBA1 is comparable to the increase of chain entanglement upon increasing molecular weight from 11K to 33K.

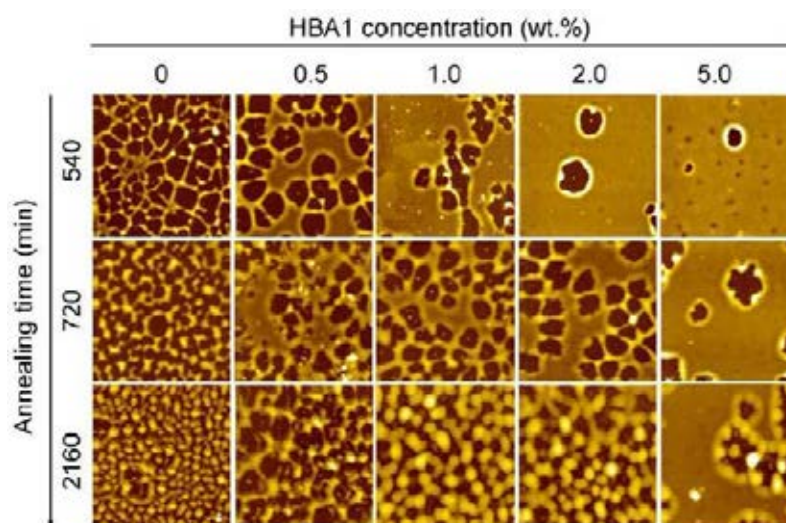


Figure 5.6 AFM topography images of 7 nm thick PS33K films containing different concentration of HBA1 annealed at 120 °C for 540, 720 and 2160 min. Size of each image is 10 μm x 10 μm .

Table 5.2 Hole depth and hole width of 7 nm-PS33K films containing different concentration of HBA1 annealed at 120 °C for 120 min

HBA1 conc.	0 wt.%	0.5 wt.%	1.0 wt.%	2.0 wt.%	5.0 wt.%
Hole depth (nm)	3.69 ± 0.18	3.64 ± 0.10	2.82 ± 0.38	2.47 ± 0.63	1.16 ± 0.25
Hole width (nm)	964.8 ± 91.9	741.1 ± 98.1	630.5 ± 97.6	396.7 ± 35.8	311.3 ± 17.1

Similar to PS11K system, the addition of HBA1 into PS33K films results in the improvement of film stability. The dewetting rates systematically decrease upon increasing HBA1 concentration. The investigation of 23 nm films shows consistent results. In this system, the annealing temperature at 120 °C causes rather slow dewetting rate. To accelerate the process, the annealing temperature is increased to 165 °C. It is worthwhile to note that the improvement of film stability is more obvious in the system of PS11K films. The separation of lines in the plots between dewetting area and annealing time (see Figure 5.2 (a) and Figure 5.7 (a)) reflects the change of dewetting rate upon addition of the HBA1 into PS films. It is clear that the magnitude of stability improvement is higher in the PS11K films. This is attributed to the increase of chain entanglement within PS33K system, which obscures the influence of HBA1 as a

dewetting inhibitor. Therefore, the HBA1 is a more effective dewetting inhibitor when the molecular weight of PS is decreased. We also note that sizes of the PS33K droplets are smaller than those of the PS11K (see Figure 5.3 and Figure 5.6). This is attributed to the increase of film viscosity, which in turn retards the coalescence of small droplets in the PS33K system [3].

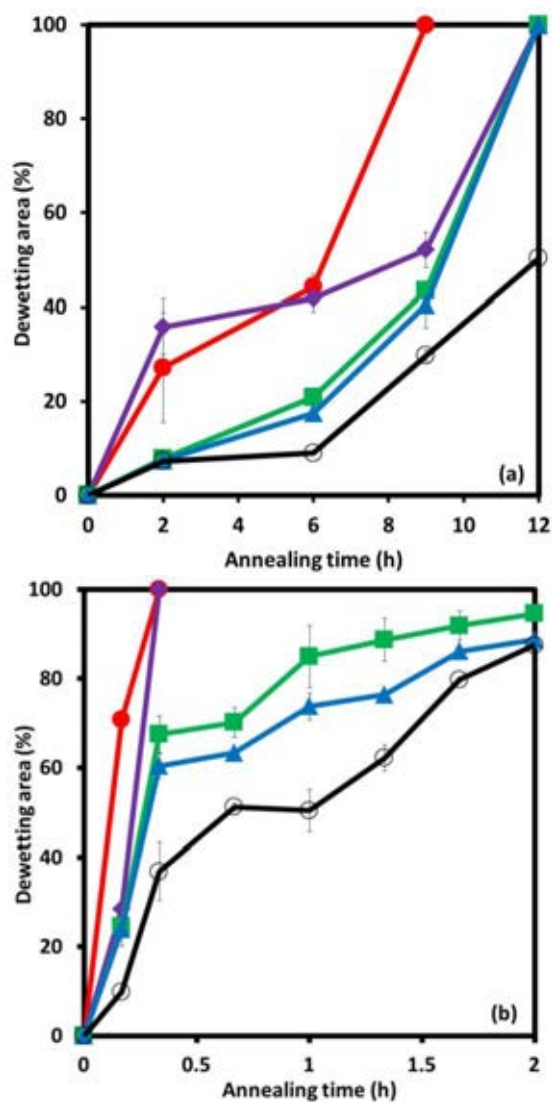


Figure 5.7 (a) Dewetting area versus annealing time of 7 nm thick PS33K films annealed at 120 °C. (b) Dewetting area versus annealing time of 23 nm thick PS33K films annealed at 165 °C. Concentrations of HBA1 are (●) 0 wt.%, (◆) 0.5 wt.%, (■) 1.0 wt.%, (▲) 2.0 wt.% and (○) 5.0 wt.%.

5.1.4 EFFECT OF HBA STRUCTURE

In this section, the effects of HBA molecular structure are investigated. The structure of HBA2 shown in Figure 1.1 constitutes of different type of aromatic core. The T_g of HBA2 is about 185 °C [71], which is much higher than those of HBA1 and PS. These discrepancies may affect the strength of intermolecular interactions and segmental dynamics within the system leading to the variation of dewetting behaviour. PS11K films with thickness of 23 nm are prepared by using HBA1 and HBA2 as dewetting inhibitors. The concentrations of both HBA1 and HBA2 are controlled to be the same. All films are annealed simultaneously at 120 °C. OM images show that the dewetting mechanisms of both systems are similar. The dewetting areas measured as a function of annealing time are plotted in Figure 5.8. Similar to the system of HBA1, the addition of HBA2 into PS11K films results in systematic improvement of film stability. The dewetting rate of the PS11K film containing 5 wt.% of HBA2 significant decreases compared to that of pure PS11K film. The annealing of this film for 48 h still does not induce total dewetting. The effects of HBA1 and HBA2 on dewetting dynamics of PS11K films are comparable. Therefore, the slight difference of their molecular structures does not affect the intermolecular interactions with PS matrix. This result further confirms that this new class of highly branched aromatic molecules can be utilized as dewetting inhibitors of PS film. We also perform similar annealing experiments at 140 °C and 190 °C, which are above T_g of HBA1 and HBA2, respectively. The PS11K films containing 5 wt.% of HBA1 and HBA2 are used. These annealing temperatures are expected to induce different segmental dynamics of the HBA1 and HBA2 molecules due to the difference of their T_g . However, the results in Figure 5.9 show that dewetting rates of the two systems are still comparable at those annealing temperatures. We suggest that the systems of HBA1 and HBA2 in PS11K matrix behave as a dilute solution. The PS11K in melt state behaves as a simple liquid. Therefore, segmental dynamics of the HBA1 and HBA2 are expected to increase significantly when the PS11K films are annealed above its T_g , about 93 °C [11].

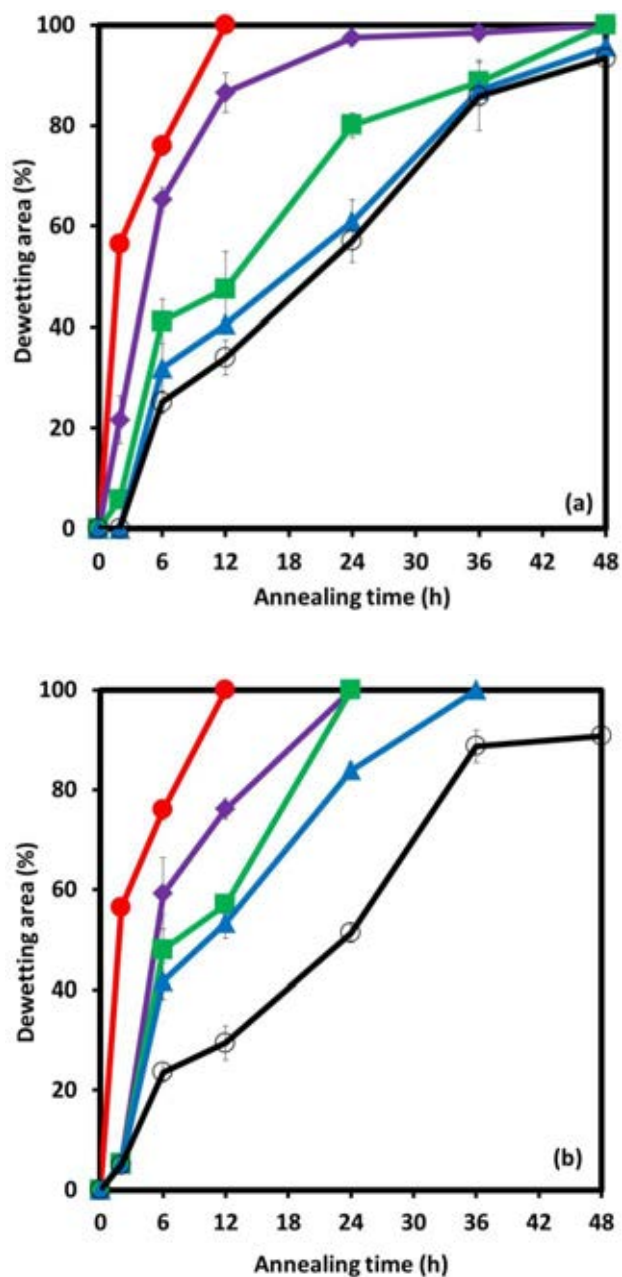


Figure 5.8 Dewetting area versus annealing time of 23 nm thick PS11K films containing (a) HBA1 and (b) HBA2 annealed at 120 °C. Concentrations of HBA1 and HBA2 are (●) 0 wt.%, (◆) 0.5 wt.%, (■) 1.0 wt.%, (▲) 2.0 wt.% and (○) 5.0 wt.%.

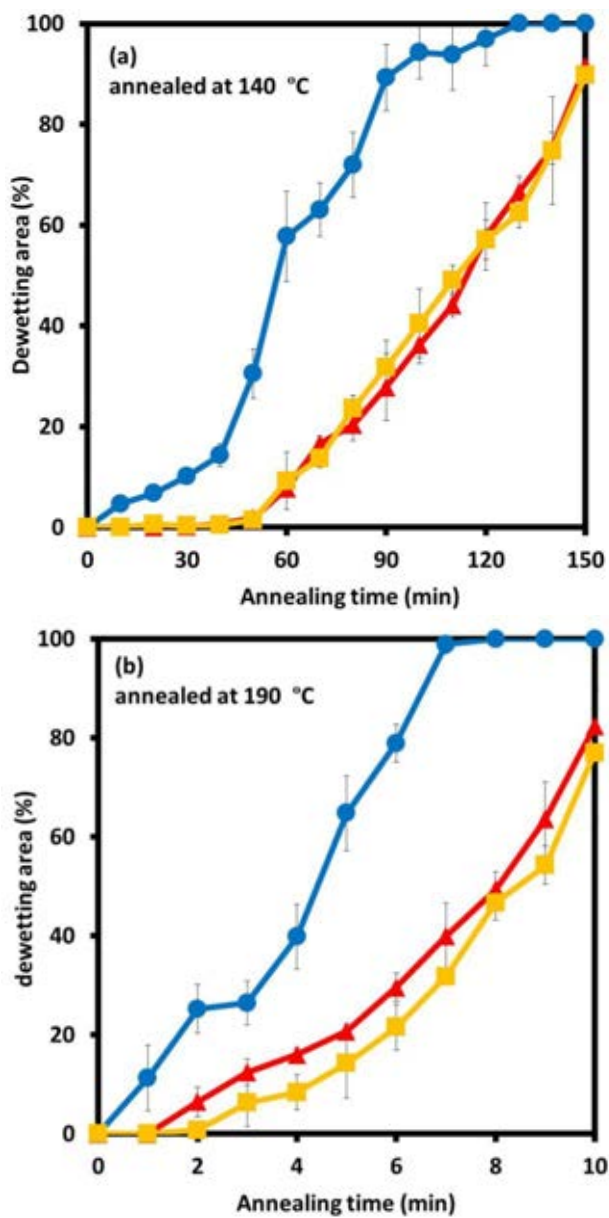


Figure 5.9 Dewetting area versus annealing time of 23 nm thick (●) pure PS11K films and the PS11K films containing 5 wt.% of (▲) HBA1 and (■) HBA2 annealed at (a) 140 °C and (b) 190 °C.

5.2 THREE-ARM POLYSTYRENE

From literature, the presence of cross-linking produces a strong interaction inside the polymeric film [7, 46-48, 79]. Addition of chemical or physical cross-linker to the polymer film increases macromolecule network, which reduces the film mobility. Therefore, the film viscosity is enhanced and the dewetting process is inhibited. Chemical cross-linking can be generated by irradiation or addition of cross-linking agent [47, 79]. However, addition of physical cross-linking additive to improve the film stability has not been studied yet. In this section, we focus on the effects of three-arm polystyrene (TA-PS) on the stability of PS thin films. The chemical structure of TA-PS additive is shown in Figure 1.2. Since of the TA-PS branches and surface energy are similar to the PS matrix (see Table 4.3), interaction between them in the mixed polymeric films are expected to be favourable. Moreover, the films are expected to show greater chain entanglements, which increase the film viscosity. By the kinetic mechanism, reducing film mobility generally improves thermal stability of polymer film. Therefore, the physical cross-linker TA-PS should act as a dewetting inhibitor in PS film. In addition, effects of the molecular weight of TA-PS branches, molecular weight of PS and the film thickness on thin film stability are investigated.

PS, TA-PS19 and TA-PS110 films are prepared by spin-casting from 1 wt.% solutions to investigate their surface energies. All films are left in vacuum oven at room temperature for several hours to confirm the completely evaporation of toluene solvent. Water and diiodomethane are dropped on the sample surface. The contact angles of each film are recorded and used to calculate the surface energy. As shown in Table 4.3, PS, TA-PS19 and TA-PS110 films present similar values of surface energy. Thus, both TA-PS are expected to distribute randomly in PS matrix as illustrated in Figure 1.2.

5.2.1 EFFECT OF TA-PS19 IN PS11K FILMS

PS11K and TA-PS19 are chosen for matrix and additive in the first system. Since the entanglement of PS chains generally occurs when their molecular weight are higher than 18K [77, 78], PS11K film acts as a liquid when melt. Thus, the role of TA-PS on improvement of film stability can be clearly observed. The concentrations of TA-PS are varied from 0 to 100 wt.% in PS films. The thicknesses of all films, measuring by ellipsometer and AFM, are about 23 nm. OM images reveal smooth surface of all as-cast films. Annealing thin films at 120 °C, which is above the glass transition temperature (T_g) of PS11K [11], for 12 h induces the dewetting behavior. All films are annealed at the same time in vacuum oven to diminish experimental errors. As shown in Figure 5.10, pure PS film exhibits some tiny holes; however, all the mixed films still completely spread over the substrate. Increasing annealing time to 36 h, a few holes can be observed in 2 wt.% mixed film, corresponding to an early stage of dewetting. Dewetting process in this film is around 3 times slower than the pure PS system. By annealing for 60 h, small holes are detected in 5 and 10 wt.% mixed films. These holes are expanded by increasing annealing time. After heating for 120 h, the dewetting area of pure PS film reaches about 70% (see Figure 5.11.(a)). Addition of 2, 5, 10 and 20 wt.% TA-PS19 additive causes the drop of the dewetting area to about 45%, 15%, 10% and 0%, respectively.

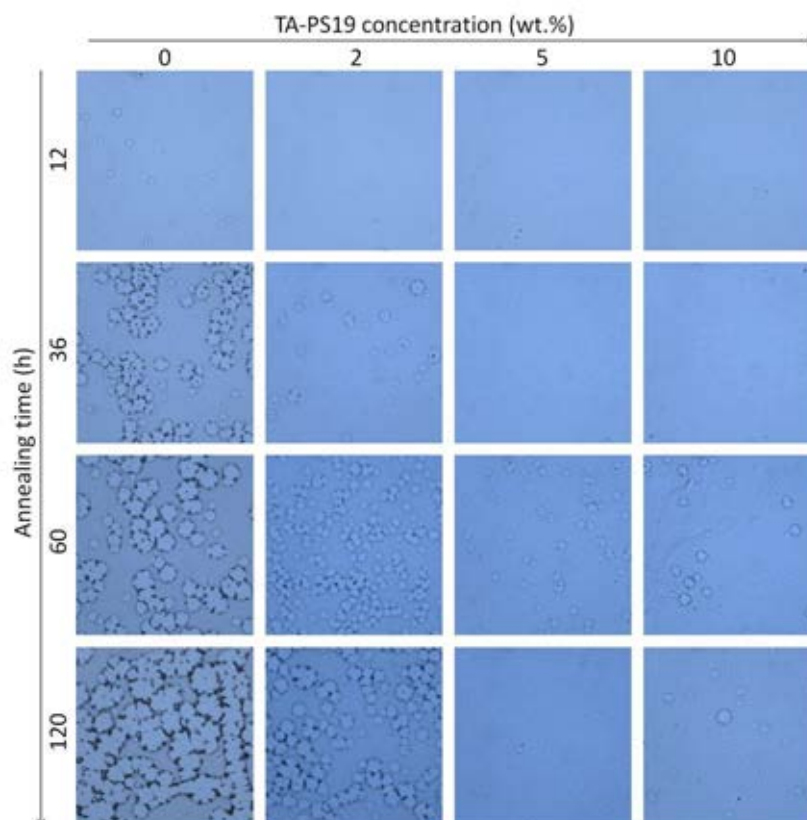


Figure 5.10 Optical micrographs of 23 nm thick PS11K films containing different concentrations of TA-PS19 annealed at 120 °C for 12, 36, 60 and 120 h. Size of each image is 100 μm x 100 μm .

Figure 5.11 (a) shows the plot between percent dewetting area versus annealing time. The dewetting rates of each systems are described by the slopes of these plots. By annealing all the films at 120 °C for 120 h, the dewetting rates of pure PS film and 2 wt.% mix film are almost the same. The mixed films containing 5 and 10 wt.% of TA-PS19 shows significantly lower dewetting rates. Figure 5.11 (b) presents the plots between percentage of dewetting area versus the concentration of TA-PS19. These results indicate that addition of TA-PS19 cross-linker in 23 nm thick PS11K film can suppress dewetting actions. Moreover, increasing amount of TA-PS19 significantly increases the stability of the films. Because of the insignificant variation of surface energy between PS11K and TA-PS19, we believe that the major reason for the improvement in thermal stability of the films is chain entanglement.

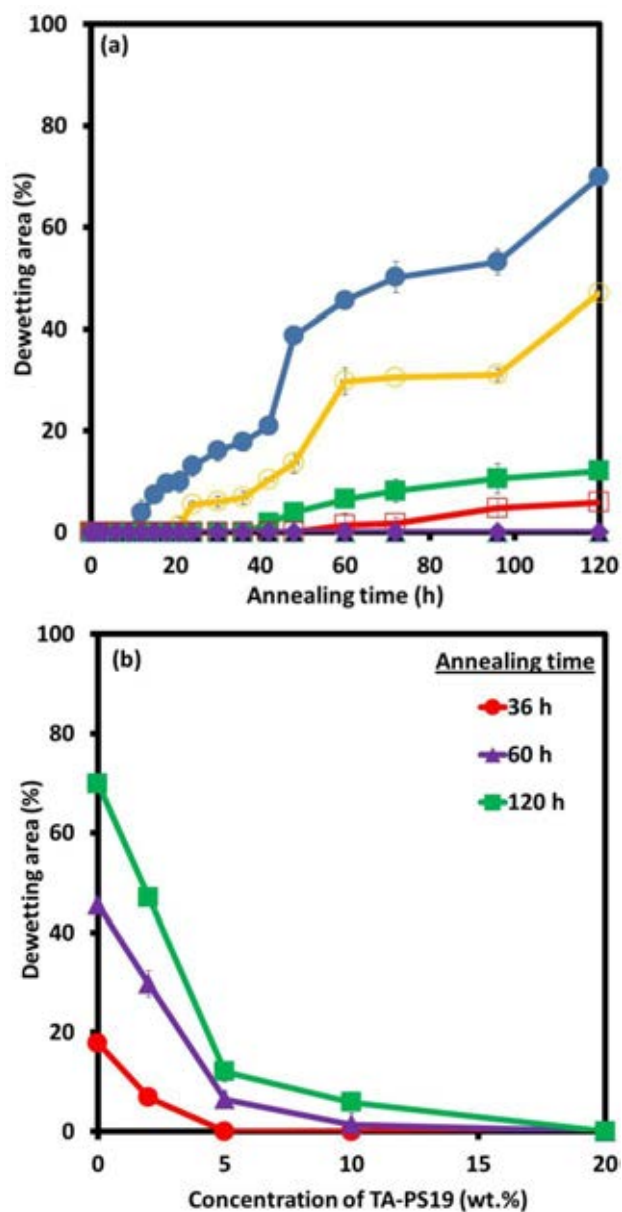


Figure 5.11 (a) Dewetting area versus annealing time of 23 nm thick PS11K films annealed at 120 °C. Concentrations of TA-PS19 are (●) 0 wt.%, (○) 2 wt.%, (■) 5 wt.%, (□) 10 wt.% and (▲) 20 wt.%. (b) Dewetting area of PS/TA-PS19 films versus TA-PS19 concentration.

5.2.2 EFFECT OF MOLECULAR WEIGHT OF TA-PS BRANCH

To study the effects of molecular weight of additives, TA-PS19 and TA-PS110 are used as cross-linkers for PS films. PS33K which has a higher degree of an entanglement is used as a matrix, so that the dewetting process can be followed more clearly. The concentrations of TA-PS19 and TA-PS110 are varied from 0 to 100 wt.% in PS33K films. Thin films with thickness about 23 nm are prepared using the same method as stated above. The as-cast films at room temperature are continuously spread over the substrate. Heating the films at 120 °C cannot induce the dewetting process because of their relatively high molecular weight. Therefore, all films are annealed at 165 °C with the different periods of time. Optical micrographs of PS33K films adding with TA-PS19 and TA-PS110 cross-linkers are shown in Figure 5.12 (a) and (b), respectively. Annealing the films at 165 °C causes dewetting structure. Many holes detected in the films are expanded after annealing for 30 min. Pure PS33K film becomes totally dewet and mixed films containing 2 and 5 wt.% of TA-PS19 show a number of holes which merge into each other. Annealing for 60 min promotes the final stage of dewetting process on TA-PS19/PS33 films. On the other hand, a slower dewetting process is observed in TA-PS110/PS33K films, as shown in Figure 5.12 (b). By annealing the films for 60 min, 2 wt.% TA-PS110 film transforms to hemispherical droplet. Mixed films with 5 and 20 wt.% TA-PS110 exhibit large holes which expand as a function of annealing time until 120 min.

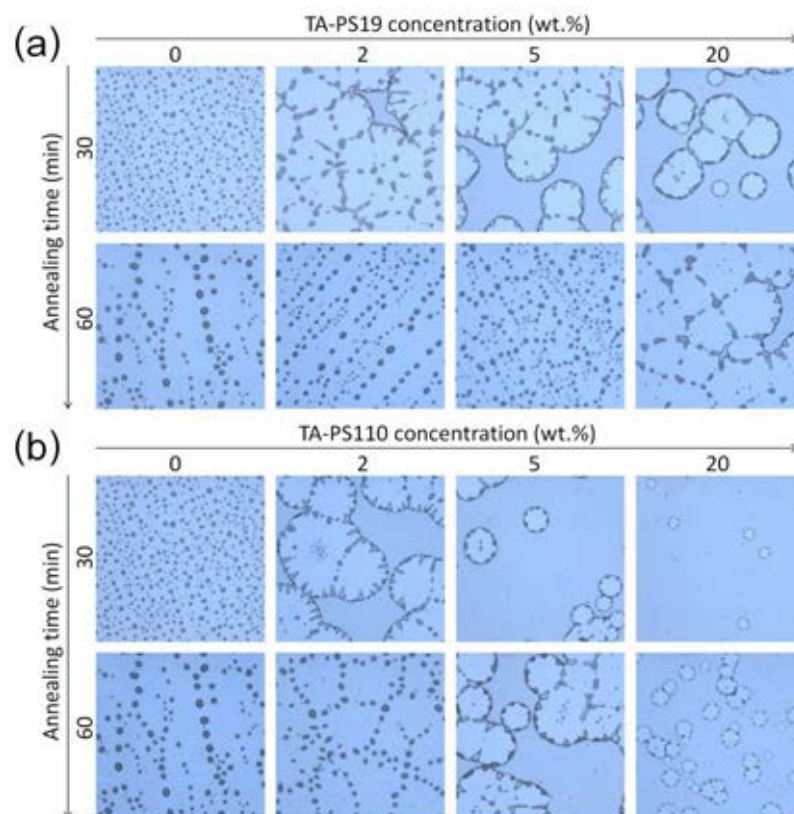


Figure 5.12 Optical micrographs of 23 nm thick PS33K films containing different concentrations of (a) TA-PS19 and (b) TA-PS110 annealed at 165 °C for 30 and 60 min.

Size of each image is 100 μm x 100 μm .

TA-PS19/PS33K film illustrates a relatively high dewetting rate as can be seen from the slopes in Figure 5.13 (a). The pure PS and mixed films with 2, 5 and 10 wt.% of TA-PS19 exhibit similar dewetting rate. Mixed films with 20 and 40 wt.% TA-PS19 show lower dewetting rate. The pure TA-PS19 film also exhibits dewetting, though at significantly lower rate than the others. The TA-PS110 cross-linker with longer branch chains shows higher ability to suppress dewetting process. The mixed film with 2 wt.% TA-PS110 dewets at higher rate compared to films with 5 wt.%, 10 wt.% and 20 wt.% of TA-PS110. Therefore, increasing TA-PS110 concentration reduces the dewetting rate as expected. Comparing to TA-PS19, the longer branch chain TA-PS110 shows higher efficiency as a dewetting inhibitor. At annealing time of 60 min, TA-PS19 for 20 wt.% can suppress dewetting behavior, while only 5 wt.% TA-PS110, is required as shown in

Figure 5.12. From the results, we conclude that the stability of the mixed films can be improved with increasing the molecular weight of branch chains of TA-PS cross-linker.

Similar results are detected in PS11K system also, as shown in Figure 5.14. The effects of molecular weight of TA-PS branch on the thermal stability are clearly observed in PS11K system because of their liquid behavior. Addition of TA-PS110 only 2 wt.% can retard the dewetting up to 48 h annealing time and the dewetting rate is significantly lower than mixed films with TA-PS19. As we found in optical micrographs (not shown), there are no dewetting area in 5 wt.% TA-PS110/PS11K films. Consequently, TA-PS110 with the long branch chains is a good inhibitor against dewetting process. The higher effectiveness of TA-PS110 to stabilize polymer thin films is due to its longer branch chains compared to TA-PS19. With increasing of molecular weight of branch of cross-linker additive. The formation of chain entanglements inside polymer film increases. The film mobility is reduced and then the stability of thin film increase.

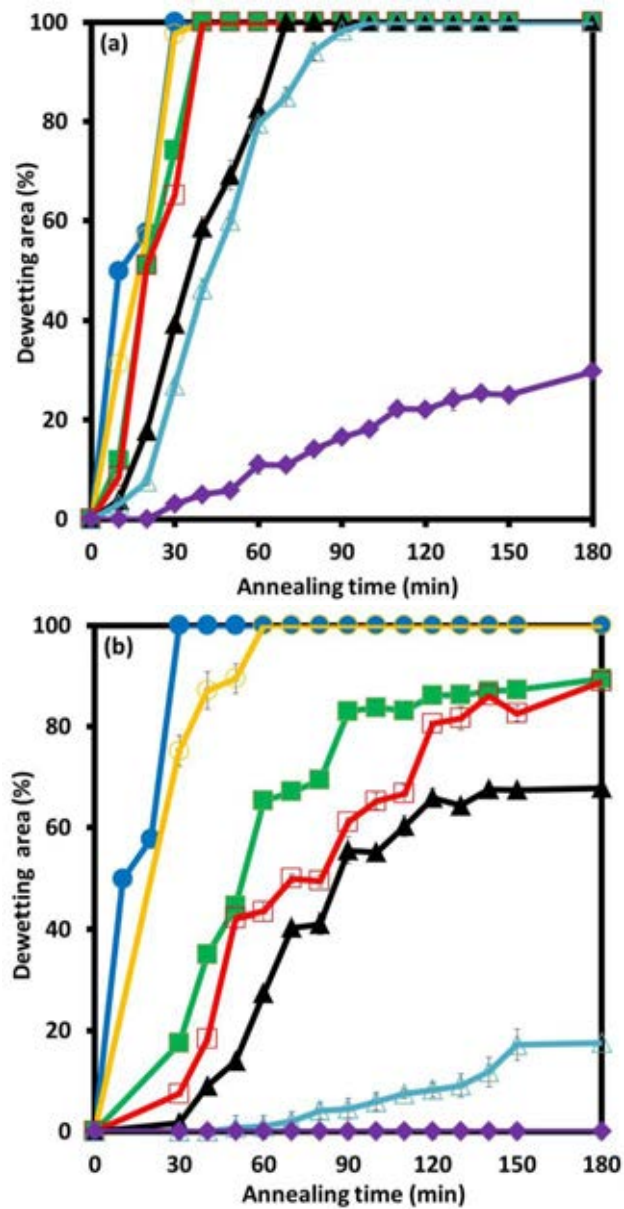


Figure 5.13 Dewetting area versus annealing time of 23 nm thick PS33K films annealed at 165 °C. Concentrations of (a) TA-PS19 and (b) TA-PS110 are (●) 0 wt.%, (○) 2 wt.%, (■) 5 wt.%, (□) 10 wt.%, (▲) 20 wt.%, (△) 40 wt.% and (◆) 100 wt.%.

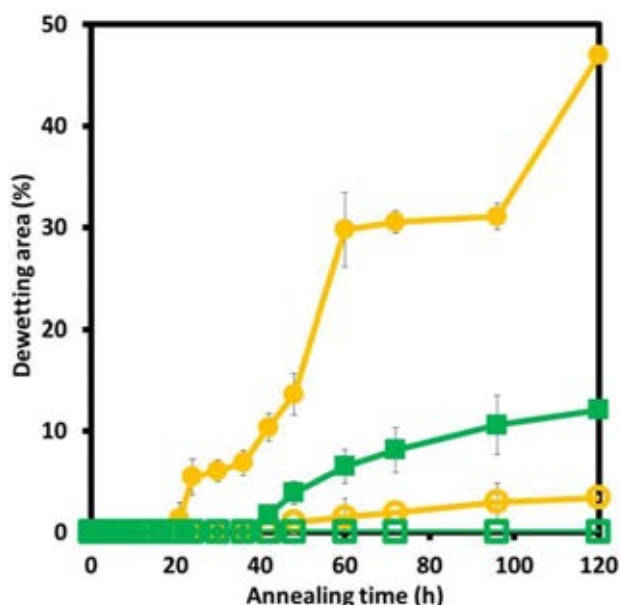


Figure 5.14 Dewetting area versus annealing time of 23 nm thick PS11K films annealed at 120 °C. Concentrations of TA-PS19 are (●) 2 wt.% and (■) 5 wt.% and concentrations of TA-PS110 are (○) 2 wt.% and (□) 5 wt.%.

5.2.3 EFFECT OF FILM THICKNESS

The previous work of our research group showed that the effect of some foreign molecules on the film stability depends on film thickness [11, 57]. Generally, there are 2 mechanisms improving stability of polymer film i.e., changing interfacial interaction and increasing viscosity [7]. In thin film system, effect of interfacial interaction is predominant. On the other hand, effect of film mobility is predominant in thicker film. To confirm the major mechanism controlling wetting property in TA-PS/PS system, effect of TA-PS on the stability of thin films (~7 nm) are investigated and compared with the 23 nm film system. PS33K is used as a matrix and TA-PS19 and TA-PS110 are used as fillers at concentrations range from 0 to 100 wt.%. All as-cast films show the homogeneous surfaces. A number of tiny holes are detected in 2 wt.%, 5 wt.% and 20 wt.% TA-PS19 films when heating at 115 °C for 120 min (see in Figure 5.15 (a)). Increasing annealing time to 300 min, the mixed films with 2 wt.% and 5wt.% of TA-PS19

additive show final stage of dewetting. For TA-PS110/PS33K system, annealing at 115 °C for 120 min causes the mixed films containing 2 and 5 wt.% TA-PS110 to transform from continuous film to dewetting structure, as shown in Figure 5.15(b). When increasing heating time to 300 min, the 2 and 5 wt.% TA-PS110 reach 100% dewetting area, while 20 wt.% of TA-PS110 exhibits some small holes.

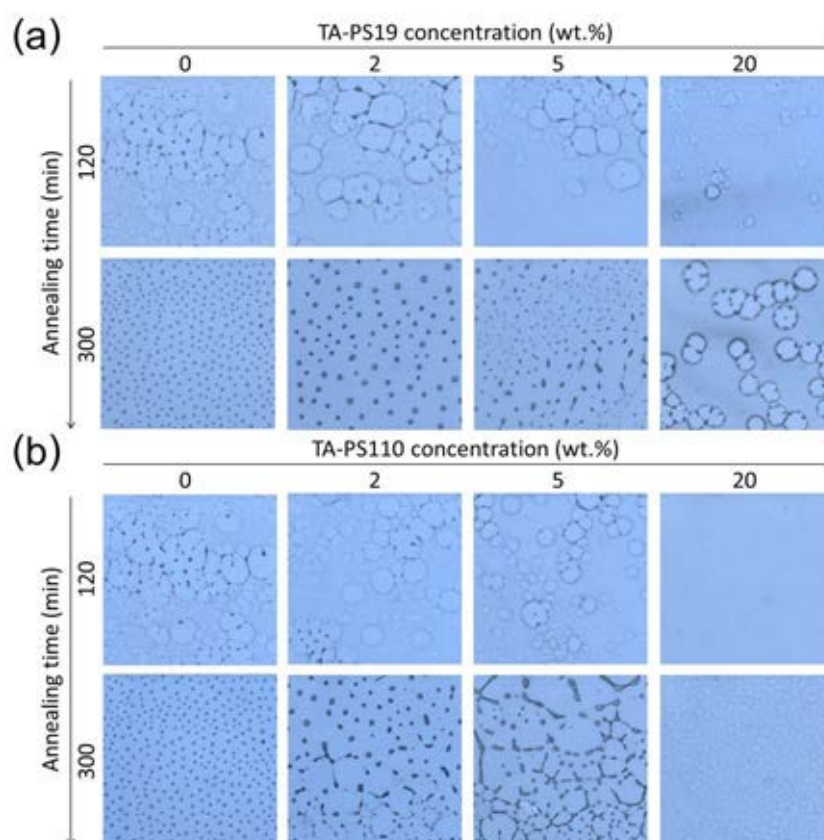


Figure 5.15 Optical micrographs of 7 nm thick PS33K films containing different concentrations of (a) TA-PS19 and (b) TA-PS110 annealed at 115 °C for 120 and 300 min. Size of each image is 50 μm x 50 μm .

AFM topography images (see in Figure 5.16) confirm that the local structures of the mixed films with 10, 20 and 40 wt.% additive correspond to structures as shown in optical micrographs. No phase separation is observed in this system. The holes detected in all films shows the same morphology. Since the holes distributions in annealed films are randomly, the dewetting process is likely to occur by heterogeneous

nucleation mechanism. Percentages of dewetting area as a function of annealing time of TA-PS19/PS33K and TA-PS110/PS33K systems are shown in Figure 5.17. All films exhibit high slope, indicating high dewetting rate. The dewetting areas of pure PS33K and 2 wt.% TA-PS19/PS33K film are rapidly reach 100 % after heating for 180 min (see Figure 5.17 (a)). The dewetting rate of 5, 10, 20 and 40 wt.% TA-PS19 films are almost the same and show than the pure PS33K and 2 wt.% TA-PS19 films. For TA-PS110/PS33K films, 2 and 5 wt.% TA-PS110 illustrate steep dewetting slope, as shown in Figure 5.17 (b). The films reach 100 % of dewetting area when annealing at 115 °C for 240 and 300 min, respectively. The mixed films with 10, 20 and 40 wt.% TA-PS110 indicate slower dewetting rate. The pure TA-PS films, however, exhibit no dewetting at this annealing condition.

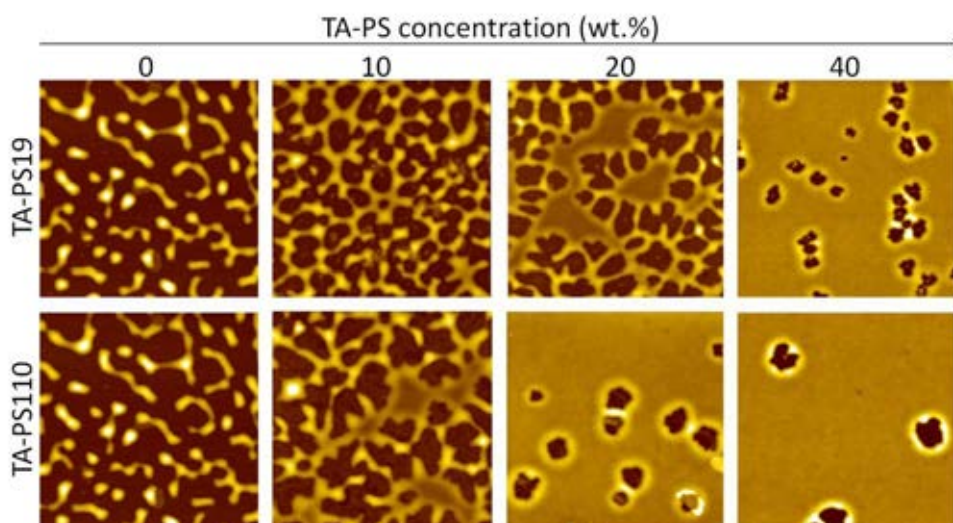


Figure 5.16 AFM topography images of 7 nm thick PS33K films containing different concentration of TA-PS19 and TA-PS110 annealed at 115 °C for 300 min. Size of the images are 10 μm x 10 μm .

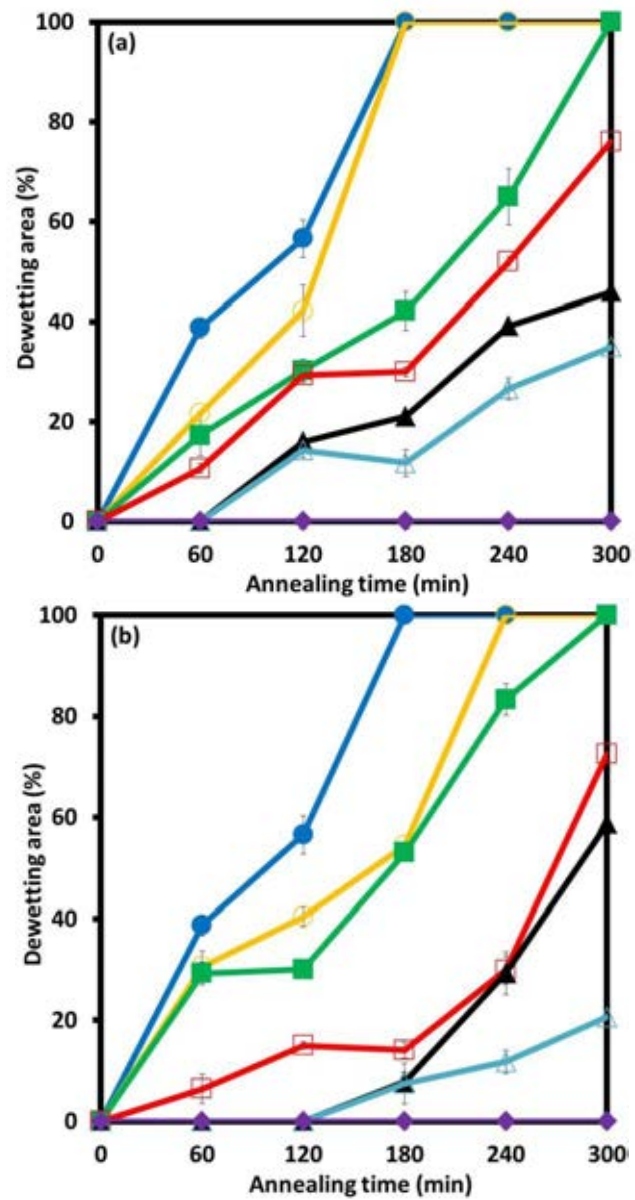


Figure 5.17 Dewetting area versus annealing time of 7 nm thick PS33K films annealed at 115 °C. Concentrations of (a) TA-PS19 and (b) TA-PS110 are (●) 0 wt.%, (○) 2 wt.%, (■) 5 wt.%, (□) 10 wt.%, (▲) 20 wt.%, (△) 40 wt.% and (◆) 100 wt.%.

From the results, we can conclude that addition of TA-PS19 and TA-PS110 in PS33K matrix inhibit dewetting process in 7 nm films, as in the previous system. The quantity of TA-PS additives obviously affects the stability of the mixed films. Increasing amount of the additives significantly increases the ability to inhibit dewetting behavior. TA-PS with higher molecular weight of branch, TA-PS110, shows higher capability to prevent the mixed films against dewetting. Increasing amount of the filler up to 40 wt.%, the 7 nm film finally become stable. In addition, the effectiveness of both TA-PS additive to improve polymer films stability is confirmed in the extremely thin PS films. However, by comparing between 7 nm and 23 nm film systems, TA-PS additives show higher efficiency in 23 nm film system. At the annealing conditions that the pure PS films are totally dewet, i.e. 180 min for 7 nm and 30 min for 23 nm, 40 wt.% TA-PS110 cannot prevent dewetting of 7 nm film (Figure 5.13 (b)). The result suggests that chain entanglement is a major reason for improving film stability in TA-PS/PS system instead of phase separation from polarity of the additive. As shown in previous researches [47, 80, 81], effect of reduction of film mobility or the presence of chain entanglement is predominant in thick film system. Because, in ultrathin film, it is difficult to form an entanglement. Then, addition of cross-linker additive is not sufficient to prevent dewetting behaviour in ultrathin film. The entanglement density is drastically reduced by decreasing the film thickness. Our hypothesis corresponds with AFM result which illustrates no phase separation occur in polymer film.

5.3 EFFECTS OF NANOPARTICLES

Effects of nanoparticle fillers on dewetting retardation were first reported by Barnes et al. [43]. A significant increase in stability of polystyrene (PS) and polybutadiene thin films was observed when small amounts of C_{60} fullerene nanoparticles were added. Fullerenes were found to segregate to the film-solid substrate interface, which altered the interfacial chemistry and geometry. Proposed mechanisms for suppression of dewetting via nanoparticles included contact line pinning and increasing in film-substrate interaction due to interfacial roughness. In addition to organic nanofillers, inorganic additives i.e., metal and metal oxide nanoparticles were also found to improve film stability. Mukherjee et al. [31] studied stability of PS film with Au nanoparticle additive. With increasing Au concentrations, the polymer films changed from complete dewetting to complete stability. Sharma et al. [53] incorporated silica into PS film and found that dewetting was inhibited by the contact line pinning.

In this study, we investigate titanium dioxide (TiO_2) and zinc oxide (ZnO) nanoparticles as dewetting inhibitors for PS films. Effects of nanoparticle concentration and film thickness on the film stability are examined. TiO_2 is of interest due to its high corrosion resistance and excellent optical transparency in the visible light, which are useful for anti-reflection coatings in optical devices [82]. ZnO is a well-known inorganic filler with unique properties, i.e. strong UV absorption combined with good transparency in visible light. Thus, Polymer/ZnO composite is used as UV-shielding [83]. TiO_2 and ZnO nanoparticles used in this research are commercial ones and used without further modification. Thus, the nanoparticles exhibit size distribution and a chance of agglomeration. This is different from the previous studies that often employ the synthesized nanoparticles and some with surface modification. In addition, to our knowledge, the dewetting behavior and stability of the PS film containing TiO_2 and ZnO nanoparticles have not yet been studied.

5.3.1 TiO₂ NANOPARTICLES

Effects of TiO₂ nanoparticles on thermal stability of thin PS52K films (~30 nm) are illustrated, as shown in Figure 5.19. The pure PS and PS/TiO₂ films undergo the dewetting process when annealing time increases from 10 to 60 min. Holes are observed in all films at annealing time of 10 min with remarkably larger diameter in the pure PS films than in the PS/TiO₂ films. Increasing annealing time results in expansion and merging of the holes. At annealing time of 60 min, the pure PS film reaches the final stage of dewetting, showing droplets of polymer. In contrast, at the same annealing time, the PS/TiO₂ films are in the intermediate stage of the dewetting process. Percentage of dewetting as a function of annealing time is shown in Figure 5.19. It is obvious that adding TiO₂ nanoparticles can retard the dewetting process in the PS film even at a very low concentration of 0.05 wt.%. The results also demonstrate that an increase in concentration of TiO₂ nanoparticles significantly improves the stability of the PS thin film.

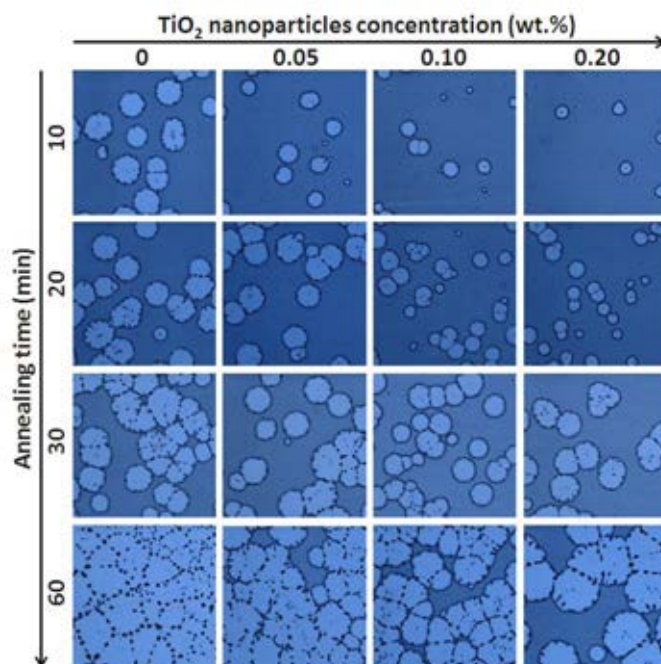


Figure 5.18 Optical micrographs illustrate dewetting pattern of PS films containing TiO_2 nanoparticles at 0-0.02 wt.%. Film thickness is ~ 30 nm. All films are annealed at 180°C .

Image size is $300\ \mu\text{m} \times 300\ \mu\text{m}$.

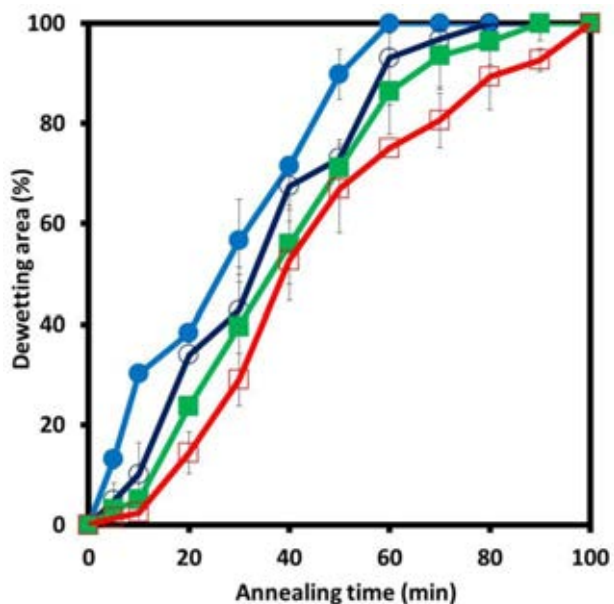


Figure 5.19 The %dewetting area versus annealing time of 30 nm-films

(● PS, ○ 0.05 wt.% TiO_2 , ■ 0.10 wt.% TiO_2 and □ 0.20 wt.% TiO_2).

Next, dewetting behaviors of the pure PS and PS/TiO₂ films with thickness ~100 nm are investigated at annealing temperature of 190°C. Results from optical microscopy (see Figure 5.20) are similar to those of 30 nm-films i.e., TiO₂ nanoparticles suppress dewetting of the PS films and increasing in the TiO₂ concentration enhances the film stability. Dewetting areas determined from the optical micrographs are plotted as a function of annealing time and shown in Figure 5.19 and Figure 5.21 for films with thicknesses of 30 and 100 nm, respectively. In films with both thin and moderate thicknesses, %dewetting area of the PS/TiO₂ films are lower than that of the pure PS films, as shown in Figure 5.22 (a) and (b). The dewetting inhibition could result from segregation of nanoparticles at the polymer-substrate interface as proposed by Barnes et al. [43]. Since TiO₂ nanoparticles favor the polar SiO_x/Si substrate, the nanoparticles separate from the polymer matrix toward the substrate interface. Increasing in surface roughness by nanoparticles alters surface energy and increases wettability of the substrate. In addition, the 100 nm-film with 0.20 wt.% exhibits a constant dewetting area after annealing for 16 h (see Figure 5.21), indicating that hole growth is subdued by contact line pinning [43]. The nanoparticles affect the kinetic of hole growth by segregating at the contact line between dry area (inside the holes) and hole rim. Therefore, the contact line cannot move and the hole growth is restricted. It has also been reported that pinning effect depends on nanoparticle concentration [22, 31, 43]. Thus, as shown in the results, the film stability is enhanced by increasing amounts of TiO₂ nanoparticles.

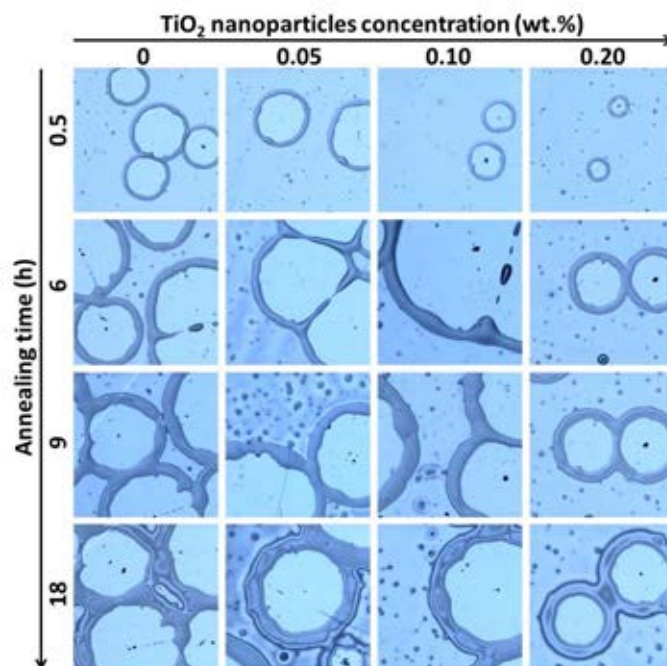


Figure 5.20 Optical micrographs illustrate dewetting pattern of PS films containing TiO₂ nanoparticles at 0-0.02 wt.%. Film thickness is ~100 nm. All films are annealed at 190°C.

Image size is 500 μm \times 500 μm .

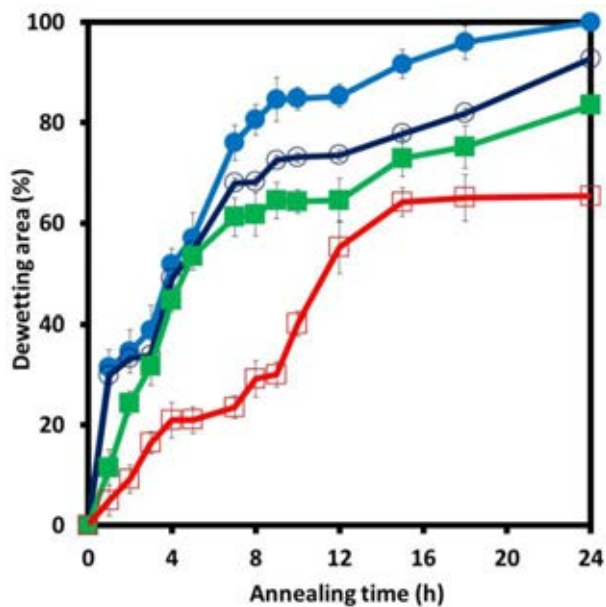


Figure 5.21 The %dewetting area versus annealing time of 100 nm-films

(● PS, ○ 0.05 wt.% TiO₂, ■ 0.10 wt.% TiO₂ and □ 0.20 wt.% TiO₂).

Dewetting rate can be determined by the slope of the %dewetting versus annealing time curve. For the 30 nm-films, the dewetting rate of the pure PS and the PS/TiO₂ films are similar. On the other hand, the dewetting rate of the 100 nm-films with 0.2 wt.% TiO₂ is significantly lower than that of the pure PS of the same thickness. The results suggest higher efficiency of TiO₂ nanoparticles to promote film stability in the 100 nm-films than in the 30 nm-films. This could result from the difference in surface morphology of the as-cast films with 0.2 wt.% TiO₂ nanoparticles as illustrated by AFM topographs in Figure 5.23. Bright spots are detected on the surface of the 30 nm-film, corresponding to protrusion of the nanoparticles from the film (Figure 5.23 (a)). Conversely, the 100 nm-film exhibits smooth surface (Figure 5.23 (b)). The roughness of 30 nm- and 100 nm-films are 0.3 ± 0.1 nm and 0.07 ± 0.01 nm, respectively. The nanoparticles that are not covered with polymer could act as initial points of dewetting. Therefore, adding TiO₂ nanoparticles as a dewetting inhibitor is less effective in the 30 nm-films.

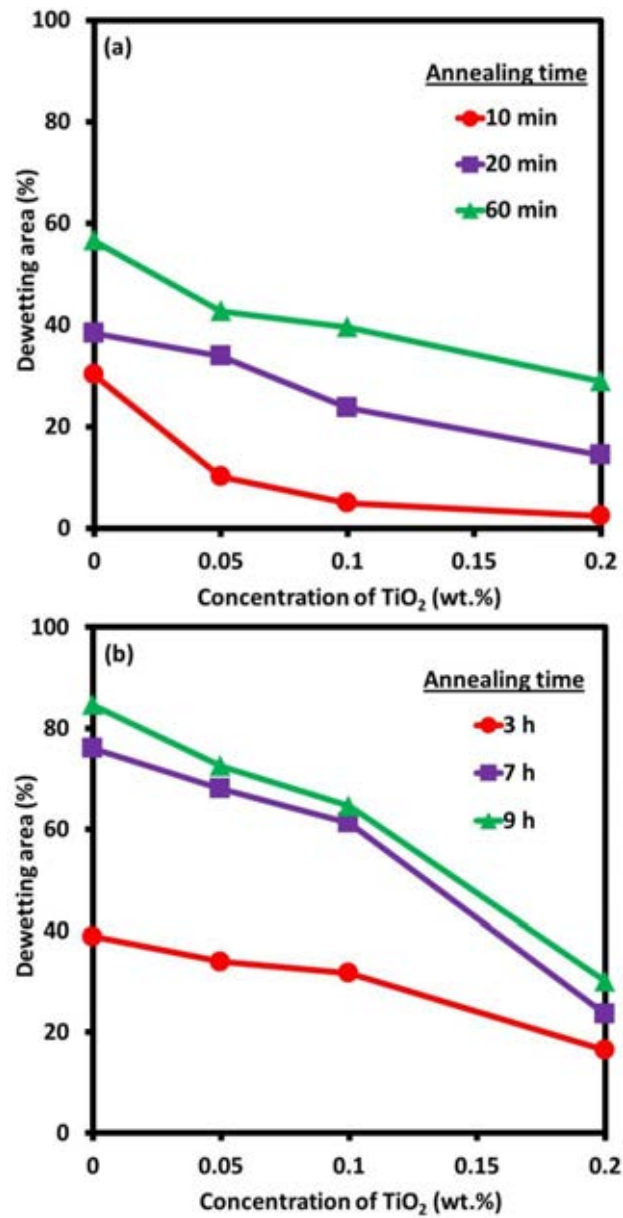


Figure 5.22 The %dewetting area versus Ratio of TiO₂ nanoparticles with thickness about (a) 30 nm-films and (b) 100 nm-films.

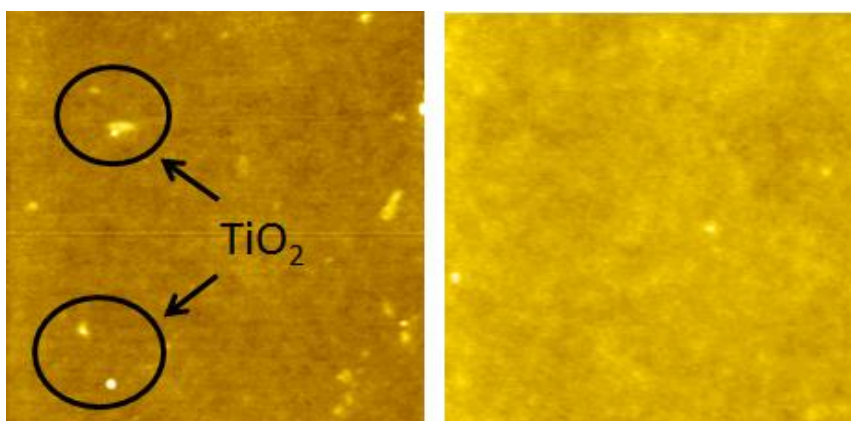


Figure 5.23 AFM topographs of the as-cast films with 0.2 wt.% TiO_2 (a) 30 nm-films and (b) 100 nm-films. Image size is $10\ \mu\text{m} \times 10\ \mu\text{m}$.

To further study the effects of the film thickness, dewetting behavior of the films with thickness of 265 nm is investigated. OM images are shown in Figure 5.24. All films are annealed at 190°C and %dewetting as a function of annealing time is shown in Figure 5.25. All PS/ TiO_2 films exhibit higher dewetting area comparing to the pure PS film at the same annealing time. Moreover, increasing TiO_2 nanoparticles significantly enhances the dewetting area. Dewetting occurs in the film with 0.20 wt.% TiO_2 nanoparticles at annealing time of 3 h, and the dewetting area reaches $\sim 50\%$ at annealing time of 12 h. The pure PS film, on the other hand, is still stable at 12 h. It is obvious that addition of TiO_2 nanoparticles to the 265 nm-films enhances the dewetting instead of suppressing the process.

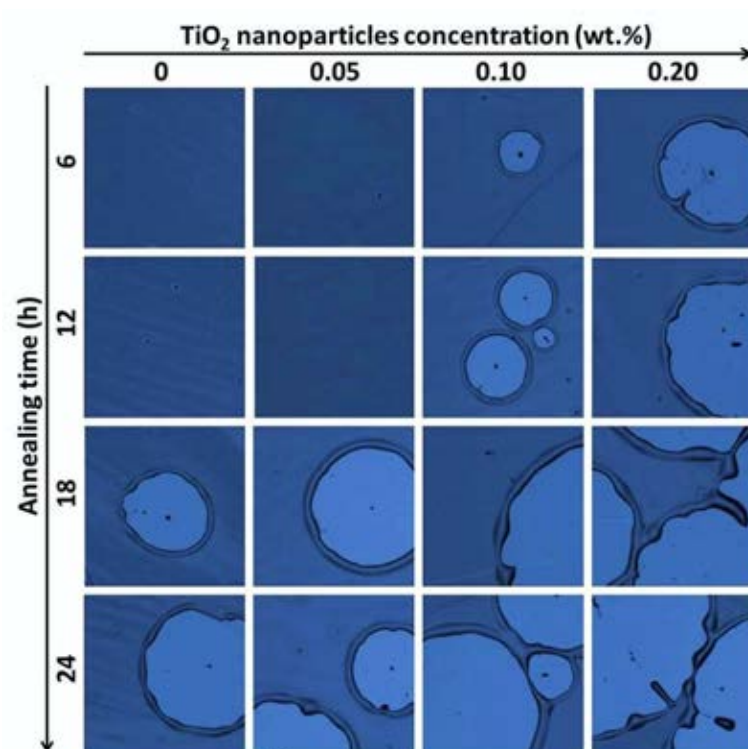


Figure 5.24 Optical micrographs illustrate dewetting pattern of PS films containing TiO_2 nanoparticles at 0-0.02 wt.%. Film thickness is ~ 265 nm. All films are annealed at 190°C .

Image size is $1000\ \mu\text{m} \times 1000\ \mu\text{m}$.

Hosaka et al. [30] reported that segregation of nanoparticles on polymer-air interface and/or polymer-substrate interfaces leads to dewetting retardation. However, particles homogeneously dispersed in polymer films result in dewetting. Our results suggest that there are TiO_2 nanoparticles dispersed in the 265 nm-film since segregation of the nanoparticles to the polymer-substrate interface could be difficult with this film thickness. Heterogeneity between particles and polymer induces stress in the film, leading to the dewetting. There is also a chance that some nanoparticles could segregate to the substrate, which increase interface roughness and interfacial interaction. This interaction, however, is short-length and applicable only within 100 nm [30]. The phase separation to film-air interface can be negligible as confirmed by AFM.

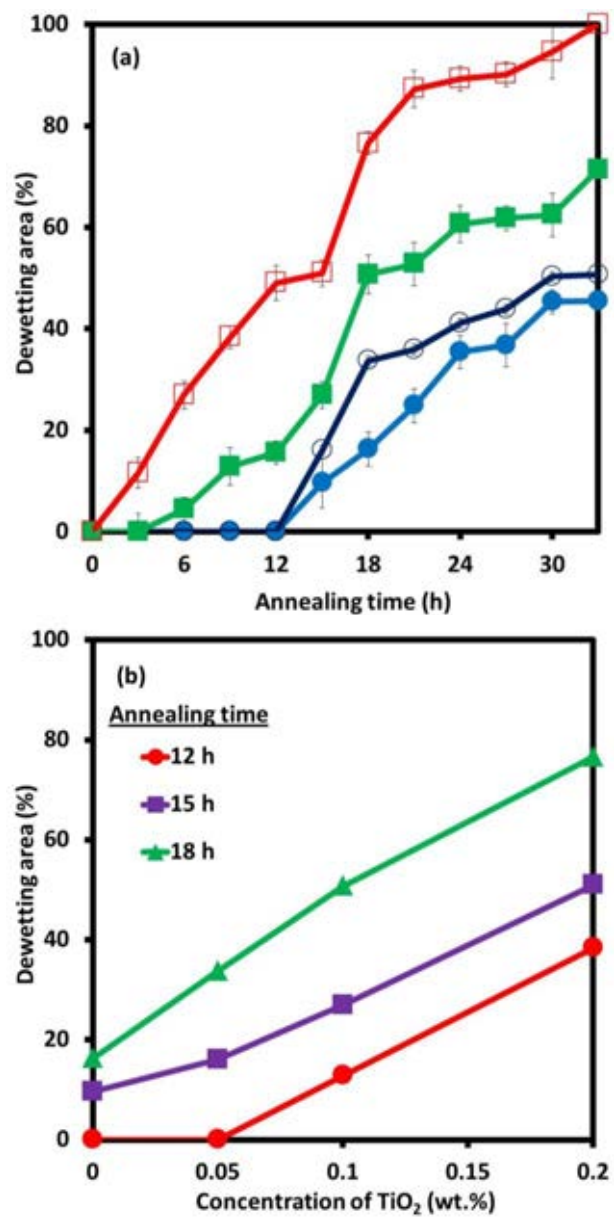


Figure 5.25 (a) The %dewetting area versus annealing time of 256 nm-films

(● PS, ○ 0.05 wt.% TiO₂, ■ 0.10 wt.% TiO₂ and □ 0.20 wt.% TiO₂).

(b) %dewetting area versus Ratio of TiO₂ nanoparticles.

5.3.2 ZnO NANOPARTICLES

Thermal stability of PS/ZnO films with the thickness about 30 nm are investigated. PS52K is used as a matrix. Figure 5.26 shows dewetting structure in all films by heating at 180 °C for different periods of time. The PS film is destroyed and demonstrates some large holes after annealing for 10 min, while only small holes are detected in all mixed films. Increasing annealing time results in expansion and merging of the holes. Finally, the PS film become completely dewet when increasing annealing time to 60 min. All PS/ZnO films, however, indicate the slower dewetting process and exhibit intermediate stage of the dewetting. Percentage of dewetting area as a function of annealing time is shown in Figure 5.27. It is obvious that adding ZnO nanoparticles can retard the dewetting process in the PS film even at a very low concentration of 0.05 wt.% (see Figure 5.27) and the concentrations of ZnO nanoparticles affect the film stability improvement.

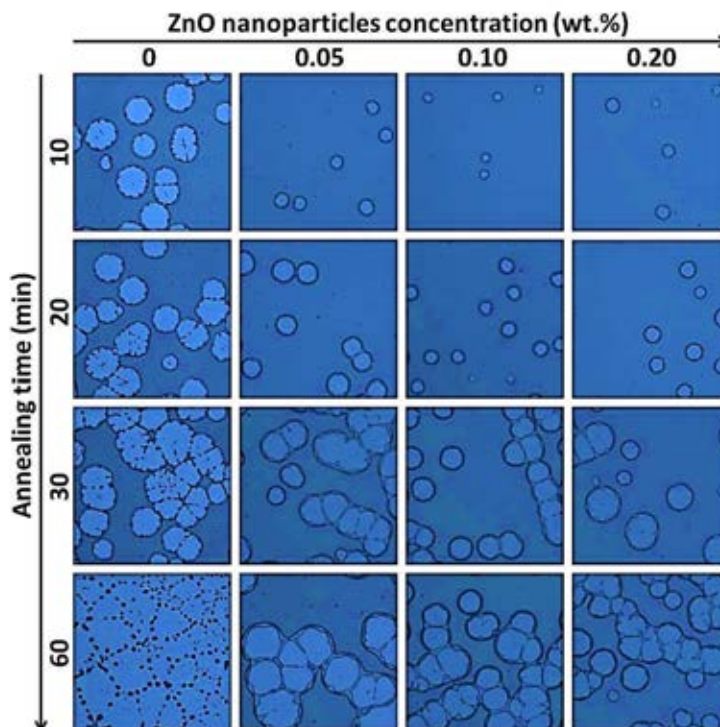


Figure 5.26 Optical micrographs illustrate dewetting pattern of PS films containing ZnO nanoparticles at 0 to 0.20 wt.%. Film thickness is ~30 nm. All films are annealed at 180°C. Image size is 300 μm x 300 μm .

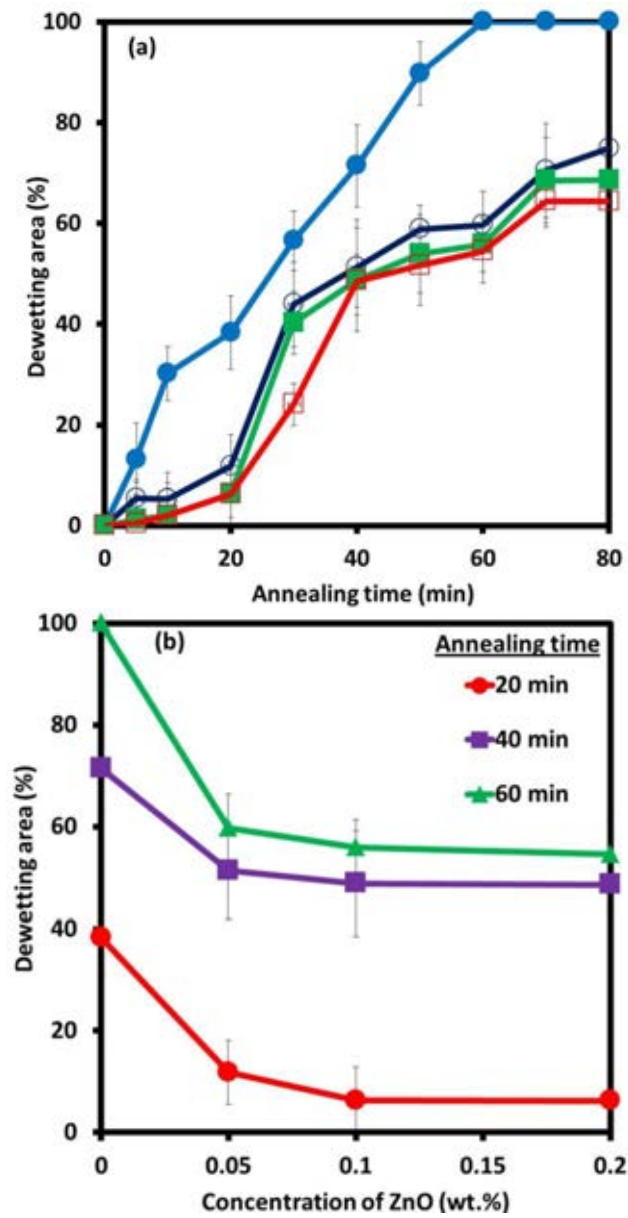


Figure 5.27 (a) The %dewetting area versus annealing time of 30 nm-films

(● PS, ○0.05 wt.% ZnO, ■0.10 wt.% ZnO and □0.20 wt.% ZnO).

(b) %dewetting area versus Ratio of ZnO nanoparticles at different annealing time.

The dewetting behaviors of the pure PS and PS/ZnO films with thickness ~ 100 nm are also investigated. All films are annealed at 190°C to accelerate the dewetting process. As same as in 30 nm thick film, results from optical microscopy reveal that addition of ZnO nanoparticles suppress dewetting of the PS films and increasing in the ZnO concentration enhances the film stability (Figure 5.28). We note that, the holes detected in 0.20 wt.% of ZnO film are very small and are not expanded after heating for a long time. Dewetting areas determined from the optical micrographs are plotted as a function of annealing time and shown in Figure 5.29. The percentage of dewetting area of all mixed films are significantly lower than that of the pure PS film. By increasing annealing time, dewetting area of PS/ZnO films are less than 50 %. The film stability is enhanced by increasing amounts of nanoparticles. Expectially, 0.20 wt.% ZnO film exhibits a constant of percent dewetting area (< 5 %), though the annealing time is increased to 24 h. The result indicates that the hole growth is subdued by contact line pinning effect [43]. The nanoparticles segregate to the contact line and then the hole growth is restricted, as described in previous report [22, 31, 43]. Furthermore, the dewetting inhibition could result from segregation of nanoparticles at polymer-substrate interface. ZnO nanoparticles favored the polar substrate separate from the polymer matrix toward the substrate interface. Then, film stability is improved by increasing in surface roughness.

The presence of ZnO nanoparticles in PS films causes a similar effect as in PS/TiO₂ film system. Both nanoparticles plays role as a dewetting inhibitor in thin PS film (less than 100 nm). Additions of the nanoparticles improve thermal stability of PS films and increasing nanoparticle concentrations decreases the dewetting action. The segregation of nanoparticles at the interface and the pinning contact line effect are the reasons of dewetting retardation. In addition, results suggest that, ZnO nanoparticle exhibits higher efficiency to suppress dewetting comparing to PS/TiO₂ system. As shown in Figure 5.20 and Figure 5.28, the holes detected in 0.20 wt.% ZnO film is much smaller than the holes detected in 0.20 wt.% TiO₂ film. Moreover, addition of small amount of

ZnO (only 0.20 wt.%) greatly prevent the destruction of thin PS film. This could results from the different in surface property between ZnO and TiO₂ nanoparticles, which requires further investigation.

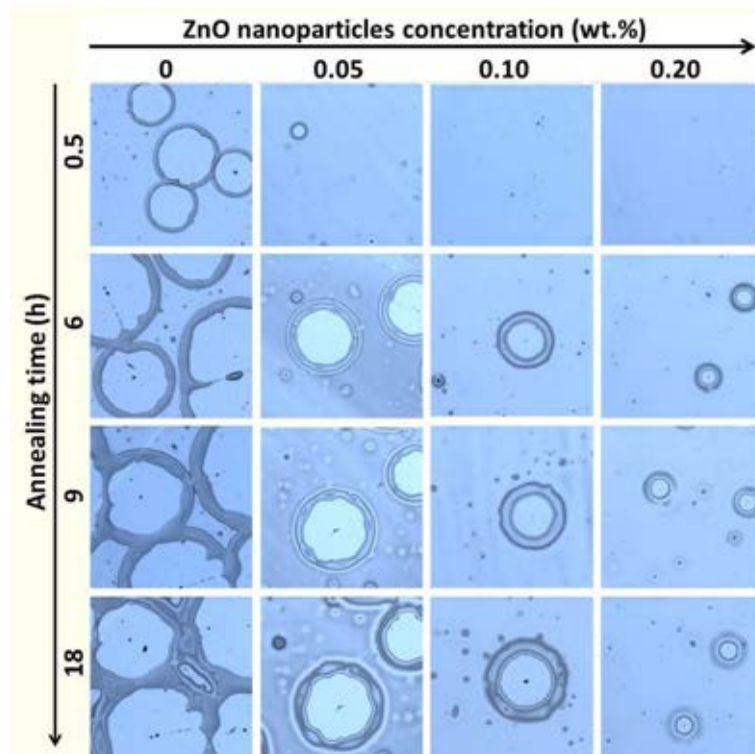


Figure 5.28 Optical micrographs illustrate dewetting pattern of PS films containing ZnO nanoparticles at 0 - 0.20 wt.%. Film thickness is ~ 100 nm. All films are annealed at 190°C . Image size is $500\ \mu\text{m} \times 500\ \mu\text{m}$.

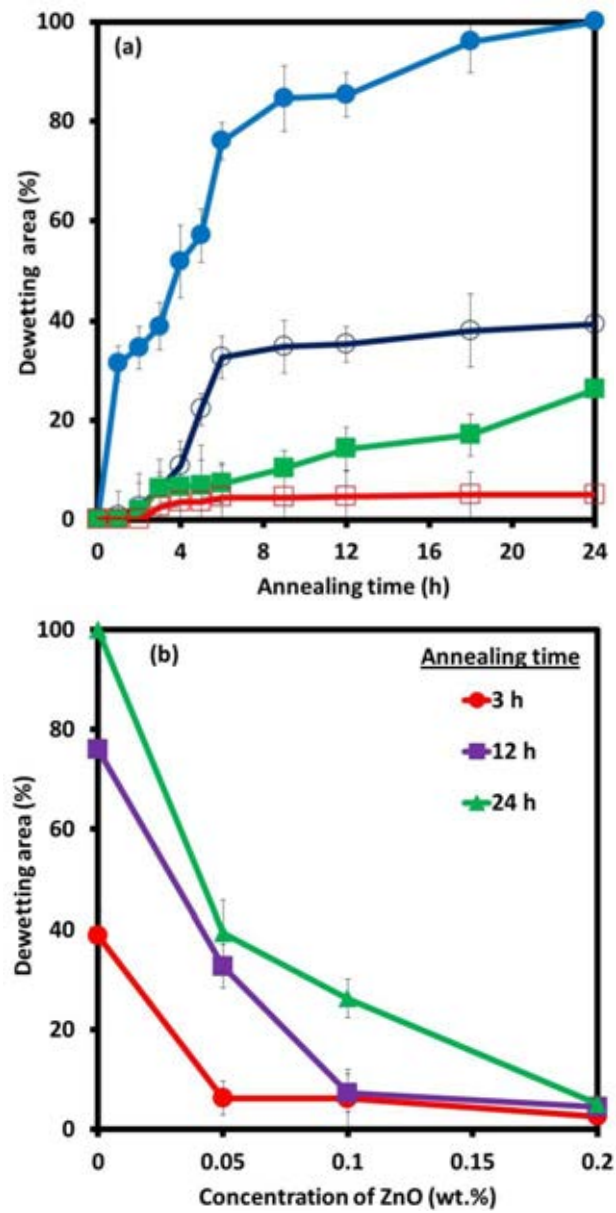


Figure 5.29 (a) The %dewetting area versus annealing time of 100 nm-films (● PS, ○ 0.05 wt.% ZnO, ■ 0.10 wt.% ZnO and □ 0.20 wt.% ZnO).
 (b) %dewetting area versus Ratio of ZnO nanoparticles.

CHAPTER VI

CONCLUSIONS

We demonstrate that HBA molecules can be used as dewetting inhibitors for PS ultrathin films. Thermal stability of the PS films is improved significantly when a small amount of HBA is added. Structure of the HBA constitutes a large number of aromatic groups and alkyl moieties, which enhances the $\pi - \pi$ and dispersive interactions with PS chains. Therefore, these HBA molecules behave as physical cross-linking points for PS chains. The effect of HBA additives persists upon increasing film thickness from 7 to 23 nm. The HBA can be used as a dewetting inhibitor for PS with molecular weight of 11K and 33K. However, its efficiency is more pronounced in thin films of PS with smaller molecular weight.

Secondly, effect of TA-PS cross-linkers on the thermal stability of PS film is investigated. TA-PS, whose chemical structures similar to polymer matrix, play role as a physical cross-linker by inducing an entanglement inside the PS film. Addition of both TA-PS19 and TA-PS110 improves the wetting property in 7 and 23 nm film systems. Increasing quantity of TA-PS significantly increases the film stability. Moreover, the longer branch chain of TA-PS110 exhibits greater efficiency to suppress dewetting process comparing with TA-PS19. The mechanism controlling wetting property in PS/TA-PS system is chain entanglement corresponding with the insignificant difference of their surface tension. The entanglement density is drastically reduced by decreasing the film thickness. Hence, TA-PS shows a higher efficiency in 23 nm thick film system.

Lastly, the presence of ZnO and TiO₂ nanoparticles in PS films is found to be able to inhibit dewetting behavior. Addition of the fillers improves wetting property in polymer thin film (less than 100 nm) and increasing nanoparticles concentration obviously decreases the dewetting process. The segregation of nanoparticles to the interface and

the pinning contact line effect are the mechanisms improving film stability. ZnO nanoparticle is found to exhibit higher efficiency than TiO_2 in order to suppress the dewetting. This could result from the different in surface property.

RECOMMENDED FUTURE WORK

This research clearly presents that TiO_2 and ZnO nanoparticles can be used as dewetting inhibitor in PS films. However, ZnO nanoparticles exhibit higher efficiency to suppress the dewetting. Addition of small amount of ZnO greatly prevents the destruction of the PS thin film. The property of nanoparticles that causes the variation in suppressing the dewetting should be further investigated. Moreover the critical concentration of TiO_2 and ZnO nanoparticles to stabilize PS film need to be studied.

REFERENCES

- [1] Wyart, F.B., and Daillant, J. Drying of solids wetted by thin liquid films. Canadian Journal of Physics 68 (1990): 1084-1088.
- [2] Reiter, G. Dewetting of thin polymer films. Physical Review Letters 68 (1992): 75-78.
- [3] Reiter, G. Unstable thin polymer films: rupture and dewetting processes. Langmuir 9 (1993): 1344-1351.
- [4] Xie, R., Karim, A., Douglas, J.F., Han, C.C., and Weiss, R.A. Spinodal Dewetting of Thin Polymer Films. Physical Review Letters 81 (1998): 1251-1254.
- [5] Meredith, J.C., Smith, A.P., Karim, A., and Amis, E.J. Combinatorial Materials Science for Polymer Thin-Film Dewetting. Macromolecules 33 (2000): 9747-9756.
- [6] Shull, K.R., and Karis, T.E. Dewetting dynamics for large equilibrium contact angles. Langmuir 10 (1994): 334-339.
- [7] Xue, L., and Han, Y. Inhibition of dewetting of thin polymer films. Progress in Materials Science 57 (2012): 947-979.
- [8] Yuan, C., Ouyang, M., and Koberstein, J.T. Effects of Low-Energy End Groups on the Dewetting Dynamics of Poly(styrene) Films on Poly(methyl methacrylate) Substrates. Macromolecules 32 (1999): 2329-2333.
- [9] Ashley, K.M., Raghavan, D., Douglas, J.F., and Karim, A. Wetting-dewetting transition line in thin polymer films. Langmuir 21 (2005): 9518-9523.
- [10] Choi, S.H., and Zhang Newby, B.M. Suppress polystyrene thin film dewetting by modifying substrate surface with aminopropyltriethoxysilane. Surface Science 600 (2006): 1391-1404.
- [11] Traiphol, R. Influences of chain heterogeneity on instability of polymeric thin films: dewetting of polystyrenes, polychloromethylstyrenes and its copolymers. Journal of Colloid and Interface Science 310 (2007): 217-228.

- [12] Zhai, X., and Weiss, R.A. Wetting behavior of lightly sulfonated polystyrene ionomers on silica surfaces. Langmuir 24 (2008): 12928-12935.
- [13] Feng, Y., Karim, A., Weiss, R.A., Douglas, J.F., and Han, C.C. Control of Polystyrene Film Dewetting through Sulfonation and Metal Complexation. Macromolecules 31 (1998): 484-493.
- [14] Tucker, R.T., Han, C.C., Dobrynin, A.V., and Weiss, R.A. Small-Angle Neutron Scattering Analysis of Blends with Very Strong Intermolecular Interactions: Polyamide/Ionomer Blends. Macromolecules 36 (2003): 4404-4410.
- [15] Wunnicke, O., Müller-Buschbaum, P., Wolkenhauer, M., Lorenz-Haas, C., Cubitt, R., Leiner, V., and Stamm, M. Stabilization of Thin Polymeric Bilayer Films on Top of Semiconductor Surfaces. Langmuir 19 (2003): 8511-8520.
- [16] Hamley, I.W., Connell, S.D., and Collins, S. In Situ Atomic Force Microscopy Imaging of Adsorbed Block Copolymer Micelles. Macromolecules 37 (2004): 5337-5351.
- [17] Wei, B., Genzer, J., and Spontak, R.J. Dewetting behavior of a block copolymer/homopolymer thin film on an immiscible homopolymer substrate. Langmuir 20 (2004): 8659-8667.
- [18] An, N., Li, Y., Yang, Y., Yu, F., and Dong, L. Stabilization of Polymer Bilayers by Introducing Crosslinking at the Interface. Macromolecular Rapid Communications 27 (2006): 955-960.
- [19] Miyamoto, K., Hosaka, N., Kobayashi, M., Otsuka, H., Yamada, N., Torikai, N., and Takahara, A. Dewetting Inhibition and Interfacial Structures of Silsesquioxane-terminated Polystyrene Thin Films. Polymer Journal 39 (2007): 1247-1252.
- [20] Han, X., Luo, C., Dai, Y., and Liu, H. Effect of Polymer-Substrate Interactions on the Surface Morphology of Polymer Blend Thin Films. Journal of Macromolecular Science, Part B 47 (2008): 1050-1061.
- [21] Henn, G., Bucknall, D.G., Stamm, M., Vanhoorne, P., and Jérôme, R. Chain End Effects and Dewetting in Thin Polymer Films. Macromolecules 29 (1996): 4305-4313.

- [22] Barnes, K.A., Douglas, J.F., Liu, D.W., and Karim, A. Influence of nanoparticles and polymer branching on the dewetting of polymer films. Advances in Colloid and Interface Science 94 (2001): 83-104.
- [23] Mackay, M.E., Hong, Y., Jeong, M., Hong, S., Russell, T.P., Hawker, C.J., Vestberg, R., and Douglas, J.F. Influence of Dendrimer Additives on the Dewetting of Thin Polystyrene Films. Langmuir 18 (2002): 1877-1882.
- [24] Besancon, B.M., and Green, P.F. Polystyrene-Based Single-Walled Carbon Nanotube Nanocomposite Thin Films: Dynamics of Structural Instabilities. Macromolecules 38 (2004): 110-115.
- [25] Krishnan, R.S., Mackay, M.E., Hawker, C.J., and Van Horn, B. Influence of molecular architecture on the dewetting of thin polystyrene films. Langmuir 21 (2005): 5770-5776.
- [26] Chung, H.J., Ohno, K., Fukuda, T., and Composto, R.J. Internal Phase Separation Drives Dewetting in Polymer Blend and Nanocomposite Films. Macromolecules 40 (2006): 384-388.
- [27] Kropka, J.M., and Green, P.F. Control of Interfacial Instabilities in Thin Polymer Films with the Addition of a Miscible Component. Macromolecules 39 (2006): 8758-8762.
- [28] Xavier, J.H., and others. Effect of Nanoscopic Fillers on Dewetting Dynamics. Macromolecules 39 (2006): 2972-2980.
- [29] Krishnan, R.S., and others. Self-Assembled Multilayers of Nanocomponents. Nano Letters 7 (2007): 484-489.
- [30] Hosaka, N., Otsuka, H., Hino, M., and Takahara, A. Control of dispersion state of silsesquioxane nanofillers for stabilization of polystyrene thin films. Langmuir 24 (2008): 5766-5772.
- [31] Mukherjee, R., Das, S., Das, A., Sharma, S.K., Raychaudhuri, A.K., and Sharma, A. Stability and dewetting of metal nanoparticle filled thin polymer films: control of instability length scale and dynamics. ACS Nano 4 (2010): 3709-3724.

- [32] Seemann, R., Herminghaus, S., and Jacobs, K. Dewetting Patterns and Molecular Forces: A Reconciliation. Physical Review Letters 86 (2001): 5534-5537.
- [33] Erbil, H.Y. Surface Chemistry of solid and liquid interfaces. Blackwell Publishing Ltd, 2006.
- [34] Ruckenstein, E., and Jain, R.K. Spontaneous rupture of thin liquid films. Journal of the Chemical Society, Faraday Transactions 2: Molecular and Chemical Physics 70 (1974): 132-147.
- [35] Mitlin, V.S. Dewetting of Solid Surface: Analogy with Spinodal Decomposition. Journal of Colloid and Interface Science 156 (1993): 491-497.
- [36] Mitlin, V.S. On dewetting conditions. Colloids and Surfaces A: Physicochemical and Engineering Aspects 89 (1994): 97-101.
- [37] Reiter, G., and de Gennes, P.G. Spin-cast, thin, glassy polymer films: Highly metastable forms of matter. The European Physical Journal E 6 (2001): 25-28.
- [38] Reiter, G., and others. Residual stresses in thin polymer films cause rupture and dominate early stages of dewetting. Nature Materials 4 (2005): 754-758.
- [39] Vix, A.B.E., Müller-Buschbaum, P., Stocker, W., Stamm, M., and Rabe, J.P. Crossover between Dewetting and Stabilization of Ultrathin Liquid Crystalline Polymer Films. Langmuir 16 (2000): 10456-10462.
- [40] Stephan Herminghaus, K.J., Klaus Mecke, Jorg Bischof, Andreas Fery, Mohammed Ibn-elhaj, Stefan Schlagowski. Spinodal Dewetting in Liquid Crystal and Liquid Metal Films. Science 282 (1998): 916-919.
- [41] Wei, B., Lam, P.G., Braunfeld, M.B., Agard, D.A., Genzer, J., and Spontak, R.J. Tunable instability mechanisms of polymer thin films by molecular self-assembly. Langmuir 22 (2006): 8642-8645.
- [42] Raczkowska, J., and others. Structure Evolution in Layers of Polymer Blend Nanoparticles. Langmuir 23 (2007): 7235-7240.
- [43] Barnes, K.A., Karim, A., Douglas, J.F., Nakatani, A.I., Gruell, H., and Amis, E.J. Suppression of Dewetting in Nanoparticle-Filled Polymer Films. Macromolecules 33 (2000): 4177-4185.

- [44] Yerushalmi-Rozen, R., and Klein, J. Stabilization of Nonwetting Thin Liquid Films on a Solid Substrate by Polymeric Additives. Langmuir 11 (1995): 2806-2814.
- [45] Kerle, T., Yerushalmi-Rozen, R., Klein, J., and Fetters, L.J. van der Waals stable thin liquid films: Correlated undulations and ultimate dewetting. Europhysics Letters 44 (1998): 484.
- [46] Kerle, T., Yerushalmi-Rozen, R., and Klein, J. Cross-link-induced autophobicity in polymer melts: A re-entrant wetting transition. Europhysics Letters 38 (1997): 207.
- [47] Carroll, G.T., Sojka, M.E., Lei, X., Turro, N.J., and Koberstein, J.T. Photoactive additives for cross-linking polymer films: Inhibition of dewetting in thin polymer films. Langmuir 22 (2006): 7748-7754.
- [48] Akhrass, S.A., and others. Design of crosslinked hybrid multilayer thin films from azido-functionalized polystyrenes and platinum nanoparticles. Soft Matter 5 (2009): 586-592.
- [49] Akhrass, S.A., Ostaci, R.V., Grohens, Y., Drockenmuller, E., and Reiter, G. Influence of progressive cross-linking on dewetting of polystyrene thin films. Langmuir 24 (2008): 1884-1890.
- [50] Hugh R. Brown, T.P.R. Entanglements at Polymer Surfaces and Interfaces. Macromolecules 29 (1996): 798-800.
- [51] Gabriele, S., Damman, P., Sclavons, S., Desprez, S., Coppée, S., and Reiter, G. Viscoelastic dewetting of constrained polymer thin films. Journal of Polymer Science Part B: Polymer Physics 44 (2006): 3022-3030.
- [52] Cole, D.H., Shull, K.R., Baldo, P., and Rehn, L. Dynamic Properties of a Model Polymer/Metal Nanocomposite: Gold Particles in Poly(tert-butyl acrylate). Macromolecules 32 (1999): 771-779.
- [53] Sharma, S., Rafailovich, M.H., Peiffer, D., and Sokolov, J. Control of Dewetting Dynamics by Adding Nanoparticle Fillers. Nano Letters 1 (2001): 511-514.
- [54] Li, X., Han, Y., and An, L. Inhibition of thin polystyrene film dewetting via phase separation. Polymer 44 (2003): 5833-5841.

- [55] Li, X., Han, Y., and An, L. Surface morphology control of immiscible polymer-blend thin films. Polymer 44 (2003): 8155-8165.
- [56] Sangjan, S., Traiphol, N., and Traiphol, R. Improvement of ultrathin polystyrene film stability by addition of poly(styrene-stat-chloromethylstyrene) copolymer: An atomic force microscopy study. Thin Solid Films 518 (2010): 4879-4883.
- [57] Sangjan, S., Traiphol, N., and Traiphol, R. Influences of poly[(styrene)_x-stat-(chloromethylstyrene)_y]s additives on dewetting behaviors of polystyrene thin films: effects of polar group ratio and film thickness. Thin Solid Films 520 (2012): 4921-4928.
- [58] Murphy, D.B., and Davidson, M.W. Fundamentals of Light Microscopy. In Fundamentals of Light Microscopy and Electronic Imaging, pp. 1-19:John Wiley & Sons, Inc., 2012.
- [59] Barrett, C.J. Nanotechnology: A Brief Overview
- [60] Bullen, R.A.W.a.H.A. Introduction to Scanning Probe Microscopy (SPM). In Basic Theory Atomic Force Microscopy (AFM), pp. 8.
- [61] Yuan, Y., and Lee, T.R. Contact Angle and Wetting Properties. Surface Science Techniques 51 (2013): 3-34.
- [62] Erbil, H.Y. Surface Chemistry of Solid and Liquid Interfaces.Wiley-Blackwell, 2006.
- [63] Zenkiewicz, M. Methods for the calculation of surface free energy of solids. journal of Achievements in Materials and Manufacturing Engineering 24 (2007): 137-145.
- [64] Jesper Jung, J.B., Tobias Holmgaard, Niels Anker Kortbek. Ellipsometry. In, pp. 138.
- [65] Rancourt, J.D. Optical Thin Films - User Handbook.SPIE
- [66] Zoran Stojanovic, S.M. Determination of particle size distributions by laser diffraction. Technics-New materials 21 (2012): 11-20.
- [67] Particle Size Distribution Calculation Method [Online]. Available from : <http://www.shimadzu.com/an/powder/support/practice/p01/lesson22.html>
[2013, August 21]

- [68] Dynamic Light Scattering (DLS).NBTC Zetasizer User Instructions
- [69] A guidebook to particle size analysis.HORIBA Instruments, Inc.
- [70] Leng, Y. Transmission Electron Microscopy. In Materials Characterization, pp. 79-119:John Wiley & Sons (Asia) Pte Ltd, 2008.
- [71] Promarak, V., Ichikawa, M., Meunmart, D., Sudyoadsuk, T., Saengsuwan, S., and Keawin, T. Synthesis and properties of stable amorphous hole-transporting molecules for electroluminescent devices. Tetrahedron Letters 47 (2006): 8949-8952.
- [72] Xu, L., Yu, X., Shi, T., and An, L. Investigation of the dewetting inhibition mechanism of thin polymer films. Soft Matter 5 (2009): 2109.
- [73] Kwok, D.Y., and Neumann, A.W. Contact angle measurement and contact angle interpretation. Advances in Colloid and Interface Science 81 (1999): 167-249.
- [74] Bucknall, D.G. Influence of interfaces on thin polymer film behaviour. Progress in Materials Science 49 (2004): 713-786.
- [75] Mounghai, S., Pham, T.C.H., Rajaendran, A.A., and Stein, G.E. Ordered arrays of polymer droplets with triangular, circular, and rod-like shapes. Soft Matter 8 (2012): 10026-10031.
- [76] Xue, L., and Han, Y. Pattern formation by dewetting of polymer thin film. Progress in Polymer Science 36 (2011): 269-293.
- [77] Montfort, J.P., Marin, G., and Monge, P. Effects of constraint release on the dynamics of entangled linear polymer melts. Macromolecules 17 (1984): 1551-1560.
- [78] Watanabe, H., Sakamoto, T., and Kotaka, T. Entanglements in linear polystyrenes. Macromolecules 18 (1985): 1436-1442.
- [79] Xu, L., Yu, X., Shi, T., and An, L. Dewetting of Linear Polymer/Star Polymer Blend Film. Macromolecules 41 (2007): 21-24.
- [80] Brown, H.R., and Russell, T.P. Entanglements at Polymer Surfaces and Interfaces. Macromolecules 29 (1996): 798-800.

- [81] Bodiguel, H., and Fretigny, C. Viscoelastic dewetting of a polymer film on a liquid substrate. Eur Phys J E Soft Matter 19 (2006): 185-193.
- [82] Madani, M., Sharifi-Sanjani, N., Hasan-Kaviar, A., Choghazardi, M., Faridi-Majidi, R., and Hamouda, A.S. PS/TiO₂(polystyrene/titanium dioxide) composite nanofibers with higher surface-to-volume ratio prepared by electrospinning: Morphology and thermal properties. Polymer Engineering & Science (2013): 1-6.
- [83] Ge, J., Zeng, X., Tao, X., Li, X., Shen, Z., Yun, J., and Chen, J. Preparation and characterization of PS-PMMA/ZnO nanocomposite films with novel properties of high transparency and UV-shielding capacity. Journal of Applied Polymer Science (2010): 1507-1512.

BIOGRAPHY

Name : Nampueng Pangpaiboon
Date Of Birth : 07/10/1983
Nationality : Thai
Address : 121/86 Sangchuto Banpong Ratchaburi Thailand
E-mail : nampuengp@hotmail.com

ACADEMIC PROFILE

2001-2005 B.S. in Physics, Silpakorn University, Nakornpratom, Thailand
[Solving the Eigenvalue problems of coupled harmonic oscillators]
2005-2006 Diploma of Teaching Science (Graduate Studies), Mahidol University,
Bangkok, Thailand
2006-2008 M.S. in Materials Science (Ceramic Technology), Chulalongkorn
University, Thailand
[Utilization of aluminum oxynitride thin film as membrane of ion sensitive
field effect transistor for pH measurement]

JOURNAL PUBLICATIONS

1. Nampueng Pangpaiboon, Nisanart Traiphol*, Vinich Promarak, Rakchart Traiphol*, "Retardation the dewetting dynamics of ultrathin polystyrene films using highly branched aromatic molecules as additives," Thin Solid Films, accepted.
2. Nampueng Pangpaiboon, Nisanart Traiphol*, "Enhancement of thermal stability of polystyrene thin film using titanium dioxide nanoparticles," submitted.